Spring 5-2018

Single-Stage, Venturi-Driven Desalination System

Brandon Proetto
Old Dominion University, bproe001@odu.edu

SINGLE-STAGE, VENTURI-DRIVEN DESALINATION SYSTEM

by

Brandon Proetto
B.S. May 2015, Rutgers University

A Thesis Submitted to the Faculty of
Old Dominion University in Partial Fulfillment of the
Requirements for the Degree of

MASTER OF SCIENCE

MECHANICAL ENGINEERING

OLD DOMINION UNIVERSITY

May 2018

SINGLE-STAGE VENTURI-DRIVEN DESALINATION SYSTEM

By

Brandon Proetto

B.S. May 2015, Rutgers University

A Thesis Submitted to the Faculty of Old Dominion University in Partial Fulfillment of the Requirement for the Degree of

MASTER OF SCIENCE

in

MECHANICAL ENGINEERING

OLD DOMINION UNIVERSITY

May 2018

Approved by:

Xiaoyu Zhang (Director)

Arthur Taylor (Member)

Shizhi Qian (Member)

ABSTRACT

Water demand is increasing at a rapid pace due to population increase, industrial expansion, and agricultural development. The use of desalination technology to meet the high water demands has increased global online desalination capacity from 47 million m^3/d in 2007 to 92.5 million m^3/d as of June 2017 [49]. Membrane and thermal processes are the two mainstream desalination categories used worldwide for desalination plants. Reverse Osmosis (RO) is the most widely used membrane process and it has become the dominant technology for building desalination plants over recent decades. Thermal distillation, however, has become less and less competitive due to its high production costs, mainly due to a reliance on increasing fuel prices and large thermal energy requirements. Although heat recuperation is commonly used, it adds investment cost and increases complexity of the system.

The concept of Single-Stage Venturi-driven (SSV) Desalination, a single-stage, thermal desalination system, using a Multifunctional Venturi Water Ejector (Venturi system), is proposed, analyzed, and demonstrated. The system requires only low-grade solar heat (< 60 °C) mainly to supplement the heat loss during operation. As compared to the conventional methods of solar desalination, the proposed system has the following intellectual novelties: First, the novel multifunctional water ejector integrates a vacuum pump for steam production, a compressor for condensation, and a starter for heat recuperation. Second, only residential-grade solar water heating is needed for the heat demand which greatly reduces the production cost of solar desalination, as compared to those systems using concentrated solar power (CSP). Third, the proposed system is operated standalone based solely on solar energy.

The main objective of this research is to accurately analyze and model the SSV system, and achieve an estimated levelized cost of water (LCOW) close to the DOE target of \$0.50/m^3 (DE-FOA-0001778) [55]. Additionally, prototypes, operating at about 0.1 bar, were built to prove the concept that very low-grade heat sources can be utilized with the system. While similar to other thermal methods, such as MSF (multi-stage flash desalination), MED (multi-effect desalination), and VC (vapor compression desalination), the SSV system utilizes a unique water ejector to reduce vapor pressure in a "boiler" and operate at lower temperatures, thereby increasing the heat regeneration efficiency and decreasing the heat input temperature requirements. The concept, as well as the scalability, of the system is proven in the results. The performance of the Venturi System was simulated using Comsol Multiphysics. The simulation results were compared to both the theoretical and experimental results. The lowest experimental vacuum pressure achieved during operation was 0.07 bar, equating to a boiling point of 40 ℃. High-performance, customized Venturi water ejector designs are projected to further lower vacuum pressures. In this study, a thermo-economic analysis was performed as a theoretical baseline for the performance of the novel technology. In the future, the baseline results should be compared to experimental results of a pilot or operational SSV desalination plant. The resulting energy requirements of the system are calculated as 40.6 kWh/m^3 for thermal and 0.23 kWh/m^3 for electrical energy requirements. The performance ratio and exergy efficiency are calculated as 15.4 and 39%, respectively. Using all three modes of analysis, theoretical, experimental, and computer simulation, the system makes a strong case as a cost competitive desalination solution. Ultimately, the Thermo-Economic model estimated the LCOW at \$0.67/m^3, achieving a lower price point than most commercialized solar desalination technologies.

ACKNOWLEDGEMENTS

I would like to thank my advisor, Dr. Xiaoyu Zhang, for all his support, determination, guidance, and creativity throughout the research performed in this paper. During my time as a graduate student at ODU, Xiaoyu has acted as a model professor. From the first day I met him, Professor Zhang kept an open door whenever I needed assistance, supported my ambitions, fed my innovative spirit, and guided me down a path of success as a graduate student and young professional. There is nothing more influential than great mentor.

I would like to thank Steve Nelson for his relentless pursuit of innovation and hard work that made the research in this paper possible. Steve and I spent many days and nights in the lab running the experimental tests necessary to obtain the results in this paper.

I would like to thank my girlfriend, Nicole, for all her support and encouragement.

I would like to thank my committee members, Dr. Arthur Taylor and Dr. Shizhi Qian, for the support and additional guidance they provided me in the development of this Master's Thesis.

I would like to thank all the great scientists who came before me and set the foundation that made this research possible. "If I have seen further than others, it is by standing upon the shoulders of giants." -Isaac Newton

Lastly, I would like to thank the Old Dominion University staff and Engineering Department.

NOMENCLATURE

S	Flow stream identifier
T	Temperature (°C)
$\dot{m}$	Mass flow rate (kg/s)
H	Enthalpy (kJ)
h	Specific Enthalpy (kJ/kg)
E	Exergy (kJ)
e	Specific exergy (kJ/kg)
C	Cost ($)
$\dot{Q}$	Heat rate (kW)
mf_s	Mass fraction of salt
mf_w	Mass fraction of water
τ	Rate of transmission of solar collector cover
α	Rate of absorption of solar collector absorber
$\dot{W}$	Power (kW)
V	Velocity
s	Specific entropy (kJ/kg*K)
A	Area (m^2)
ρ	Density (kg/m^3)
B	Volumetric Flow rate (m^3/s)
P	Pressure (Pa)
c_P	Specific Heat (kJ/kg*K)

Subscripts:

b	boiler
bp	Boiling point
1	Location 1 in SSV system
2	Location 2 in SSV system
3	Location 3 in SSV system
P1	Primary water without steam
P2	Primary water with steam
br	Brine flow
dist	Distillate flow
sys	System
o	Out of control volume
i	Into control volume
HX	Heat exchanger
f	Final
0	Reference or dead state
sw	Seawater
in	Seawater into the boiler

Abbreviations:

MSF	Multi-Stage Flash Desalination
RO	Reverse Osmosis
ME	Multi-Effect Distillation
VC	Vapor Compressrion
IRR	Internal Rate of Return
PV	Present Value
SSV	Single-Stage, Venturi-Driven

Table of Contents

Chapter Page

LIST OF TABLES

LIST OF FIGURES

Figure Page

Figure Page

Figure Page

I. CHAPTER 1:

INTRODUCTION

A. Problem Background

Fresh water demand continues to rise each year due to increased population, GDP and industrial growth, and agricultural development. Water, an essential aspect of human existence, is one of the most abundant resources on earth, coving three-fourths of our planet's surface. About 97% of the earth's water is salt water in the oceans and 3% is fresh water contained in the poles (in the form of ice), groundwater, lakes, and rivers, which supply most of human and animal needs [3]. In many arid regions of the world, fresh water sources have become extremely limited and these areas are already heavily dependent on desalination technologies to supply their growing demand for potable water.

Currently, there are more than 18,000 desalination plants in operation worldwide producing several billion gallons of water per day [49]. Over 50% are in the Middle East where large-scale conventional heat and power plants are among the region's most important commercial processes. They play a crucial role in providing fresh water for many communal and industrial sectors, especially in areas with a high density of population [9]. Qatar and Kuwait rely 100% on desalinated water for domestic and industrial supplies [12].

The use of desalination technology to meet the high water demands has increased global online desalination capacity from 47 million m^3/d in 2007 to 92.5 million m^3/d as of June 2017 [49]. Figure 1 shows the global online desalination capacity and capacity added each year since 1980.

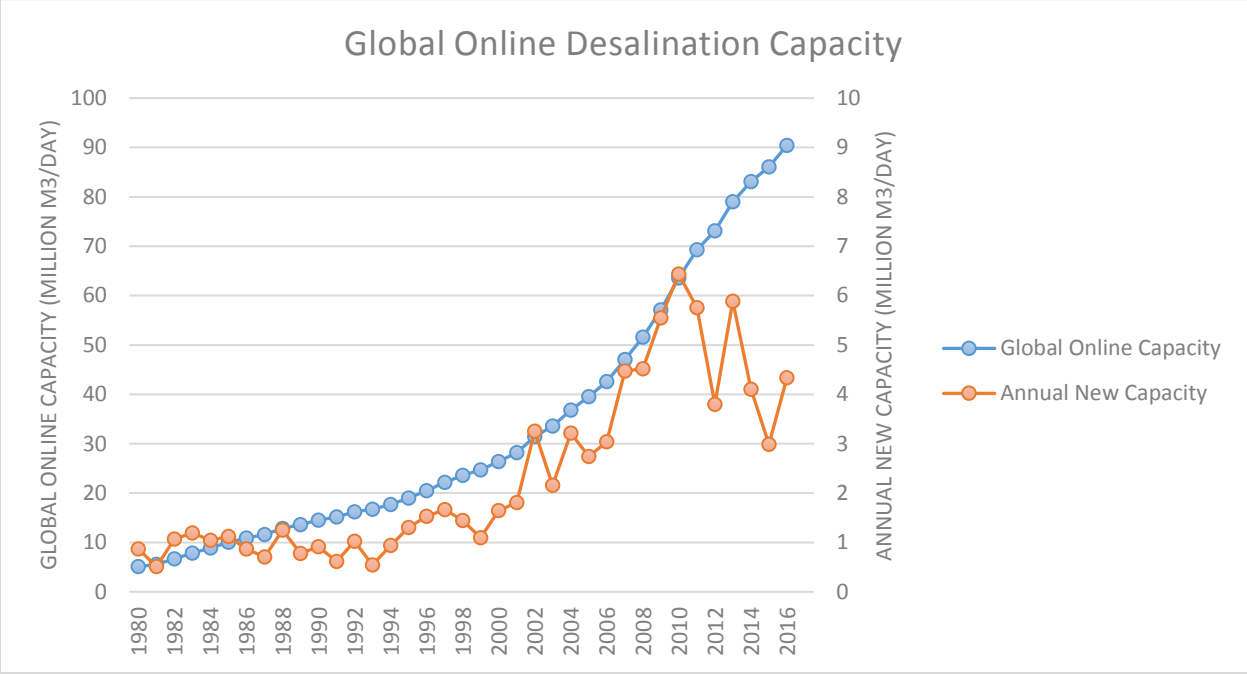

Figure 1: Global Online Desalination Capacity and Annual New Capacity since 1980 [49].

B. Desalination Industry Overview

The mainstream desalination technologies can be divided into two main categories: Thermal and Membrane technologies. Other types of desalination categories include absorption and chemical processes. Thermal desalination methods have been around for much longer than Membrane technologies, which were not commercialized until the 1970s [8]. Figure 2 shows a classification of desalination categories and current technologies.

Thermal desalination methods involve heating salt water until it evaporates from a salt solution, and then recovering the heat in the water vapor by condensing it back into liquid water. Thermal

desalination systems include: multi-stage flash distillation (MSF), multi-effect distillation (MED), vapor compression (VC), humidification-dehumidification (HDH), and solar distillation (SD). Freezing (Frz) distillation is considered a thermal desalination system but produces clean water from freezing the liquid water. Membrane technologies utilize a semi-permeable membrane and a driving mechanism to force the liquid water through the membrane but leave other solid contaminants behind. The driving force is supplied through various methods, such as mechanical pressure, electrical potential, or a concentration gradient. Membrane desalination systems include: Reverse Osmosis (RO), Forward Osmosis (FO), Electro-dyalysis (ED), and nanofiltration (NF). Some chemical desalination technologies include: ion-exchange (I.Ex), liquid-liquid extraction (LLE) and gas hydrate (G.Hyd). Recently, absorption technology (Ads) has been investigated for desalination application [17].

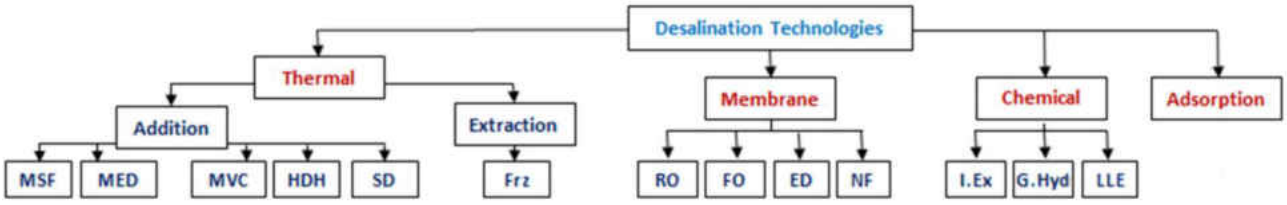

Figure 2: Classification of desalination technologies [17].

In 2012, the total installed capacity was 66.4 million m^3/day, and 59.85% came from the Seawater Reverse Osmosis (RO), the most popular membrane technology [12]. Multi-Stage Flash (MSF) and Multi-Effect Desalination (MED or MEB) are the most widely used thermal technologies on the market (Figure 3).

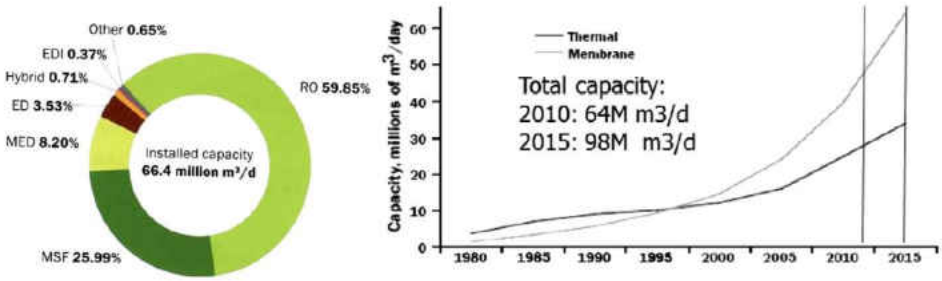

Figure 3: Installed (left) and forecasted (right) desalination capacities by technology (as of first quarter of 2012) [12].

Desalination technologies, mainly MSF, MED, and RO, have made great strides in reducing cost. As the price points become more competitive, and as the demand for fresh water resources expands, the utilization of these technologies in plant-scale systems has increased. Today, the specific, equivalent electrical consumption of mainstream desalination methods ranges from 4 to 20 kWh/m^3 (Table 1). The electrical energy equivalent of thermal energy is based on power plant efficiency of 30%.

Table 1: Energy consumption of the main desalination processes [3].

Properties	MSF	MED	MVC	TVC	SWRO	BWRO	ED
Typical unit size (m^3/day)	50,000–70,000	5,000–15,000	100–3,000	10,000–30,000	Up to 128,000	Up to 98,000	2–145,000
Electrical energy consumption (kW h/m^3)	2.5–5	2–2.5	7–12	1.8–1.6	4–6 with energy recovery	1.5–2.5	2.64–5.5
Thermal energy consumption (MJ/m^3)	190–282	145–230	None	227	None	None	None
Equivalent electrical to thermal energy (kW h/m^3)	15.83–23.5	12.2–19.1	None	14.5	None	None	None
Total electricity consumption (kW h/m^3)	19.58–27.25	14.45–21.35	7–12	16.26	4–6	1.5–2.5	2.64–5.5, 0.7–2.5 at low TDS
Product water quality (ppm)	≈ 10	≈ 10	≈ 10	≈ 10	400–500	200–500	150–500

Table 2: Average water production cost of the main desalination processes [10].

Type of process	Type of water	Cost of water (US$/m^3)
MSF	Seawater	
23,000–528,000 m^3/day		0.56 to 1.75
MED	Seawater	
91,000–320,000 m^3/day		0.52–1.01
		0.95–1.5
12,000–55,000 m^3/day		2.0–8.0
Less than 100 m^3/day		
VC	Seawater	
30,000 m^3/day		0.87–0.95
1,000 m^3/day		2.0–2.6
RO	Seawater	
100,000–320,000 m^3/day		0.45–0.66
15,000–60,000 m^3/day		0.48–1.62
1,000–4,800 m^3/day		0.7–1.72
RO	Brackish water	
Large capacity: 40,000 m^3/day		0.26–0.54
Medium: 20–1,200 m^3/day		0.78–1.33
Very small: few m^3/day		0.56–12.99
ED	Brackish water	
Large capacity		0.6
Small capacity		1.05

Reverse Osmosis is the most dominant technology in the desalination market today. Over 50% of the total desalination investments each year are for RO projects mainly due to its lower investment and total water cost compared to other technologies [12]. However, for highly saline seawater, RO is inefficient and sometime incapable of producing high-quality, desalinated water. In these environments, thermal desalination methods involving vaporization are the optimal technology. According to World Health Organization (WHO) guidelines, the permissible limit of salinity in drinking water is 500 ppm and for special cases up to 1000 ppm. RO also produces high levels of brine discharge, which have a strong potential to detrimentally impact both the physicochemical and ecological attributes of receiving environments [9].

For popular thermal desalination methods, mainly MSF, MED, and VC, the high quality of clean water production comes at a price. In these traditional technologies, high energy requirements for boiling water are combated with high temperature heat inputs and complex designs for efficient heat recuperation. The disadvantages of such designs are increased costs (energy input and investment costs), increased construction time, and decreased location flexibility. MSF and MED traditionally require either a nearby power plant to extract residual steam or an established delivery route for fossil fuels. The high-temperature heat source requirement limits the application of the technologies. Also, the designs are too complex and large-scale to be made as a portable, modular system. The remainder of this paper will focus of thermal desalination technologies to compare the novel SSV system to other similar thermal desalination systems in the market today.

C. Thermal Desalination Technologies

This paper presents further detail of the three mainstream thermal desalination technologies, MSF, MED, VC, followed by an introduction to solar desalination. The performance of MSF and MED can be used as a baseline comparison for the SSV system presented in this paper. MSF and MED require both thermal and electrical energy input. The efficiency of heat input for each thermal system is described using two equivalent parameters: (1) the gain output ratio (GOR), which is a measure of how much thermal energy is consumed in the desalination process, and is defined as the ratio of the mass distillate (kg) to the mass (kg) or the input steam, and (2) the performance ratio (PR), which is the mass of distillate (kg) per 2326 kJ, the heat of vaporization of 1 kg of liquid water. Since the SSV system presented in this paper does not require input

steam, the performance ratio and energy requirements will be used to compare performance between thermal desalination systems. In the Solar Desalination section, direct and indirect solar desalination systems will be introduced, and further detail will be provided about the solar still, solar MSF, and solar MED technologies.

Multi-Stage Flash Desalination:

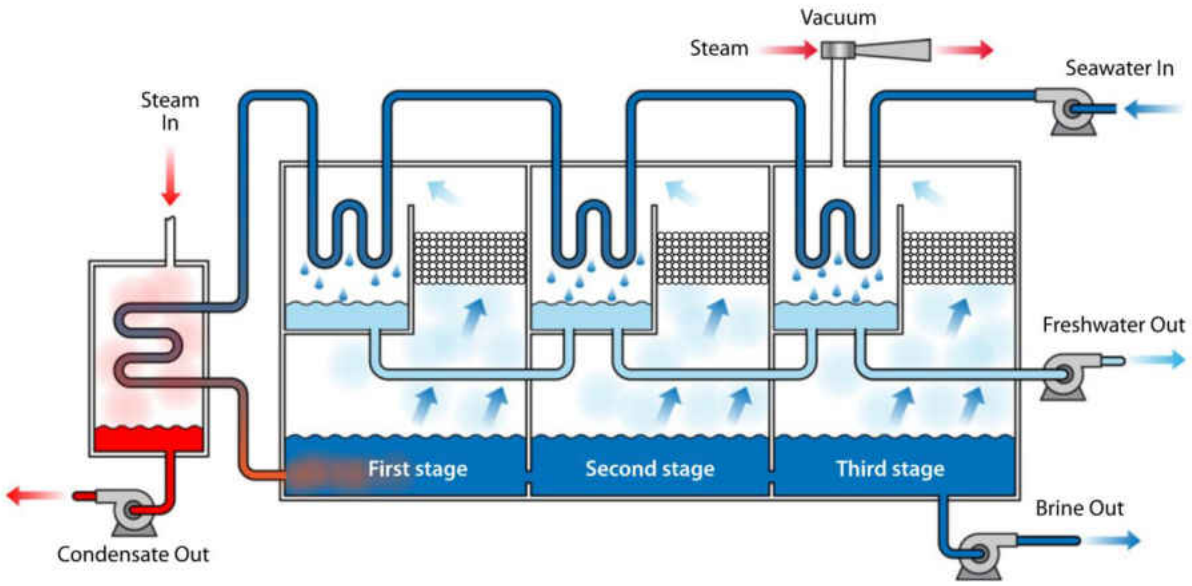

Figure 4: Schematic diagram of a typical MSF unit [10].

MSF is currently the second-most installed desalination process worldwide after the RO process. The thermal energy is in the form of low-pressure bleed steam (1 to 3 bars) for the feed-brine heating, and medium pressure steam for the ejectors to generate the required vacuum in different sections of the unit. The dependence of MSF on a steam source reduces the number of

applications and locations of use. MSF units consist of a series of stages, ranging from 4 to 40 each, with successively lower temperature and pressure that cause flash evaporation of the hot brine followed by the condensation as fresh water. If steam is not available, a separate boiler is necessary to produce the steam for the first stage. External heat from fossil fuel boilers, power plant waste heat, nuclear reactor, renewable energy, and any other heating source is supplied to the intake brine temperature of 90°C to 110°C. The high intake brine temperature limits the use of low-cost, low temperature heat sources, such as geothermal and non-concentrating solar, with the MSF system. Flashing of the steam forms scales and deposits on the tubes, so periodic cleaning and removal is required [10]. If we use the manufacturers' values, then the thermal energy consumption of an MSF plant ranges between 53.78 kWh/m^3 (GOR=12) and 78.33 kWh/m^3 (GOR=8). The electricity consumption of the pumps ranges between 2.5 and 5 $kWhe/m^3$. Therefore, the total equivalent electrical energy consumption of the MSF unit ranges between 19.58 and 27.25 $kWhe/m^3$ [10].

Multi-Effect Distillation:

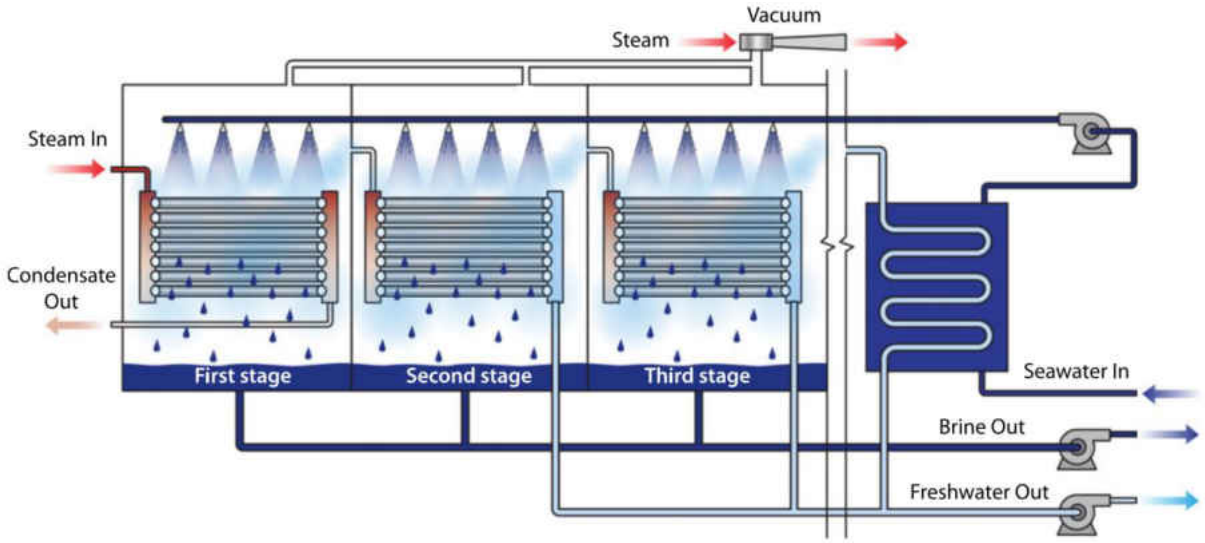

Figure 5: Schematic diagram of a typical MED unit [10].

The MED process consists of a series of stages (usually from 2 to 16) that are maintained at decreasing levels of pressure. The MED system has a top brine temperature around 70°C, increasing thermal efficiencies and decreases the cost of external heat input. External steam is used to evaporate some of the brine inside the stage that is kept at low pressure. The water vapor produced from the stage is transferred inside a tube to the next stage for boiling additional seawater, which produces water vapor in a series fashion [10].

Unlike an MSF plant, the MED process usually operates as a once through system without a large mass of brine recirculating around the plant. This design reduces both pumping requirements and scaling tendencies [39]. Additionally, the performance ratio for an MED plant

is more rigidly linked to and cannot exceed a limit set by the number of effects in the plant. For instance, a plant with 13 effects might typically have a PR of 10. However, an MSF plant with a PR of 10 could have 13-35 stages depending on the design. MED plants commonly have performance ratios as high as 12-14 [26]. Typical Arab Gulf countries' MED plants operate at GOR values of 8 to 12, slightly lower than manufacturer ratings [10]. The main difference between this process and the MSF is that the steam of each effect just travels to the following effect, where it is immediately used for preheating the feed. This process requires more complicated circuit equipment than the MSF [3].

Like MSF, MED also uses steam for both the heat input and to drive steam ejectors. Steam ejectors are necessary to produce vacuum pressures in each effect but lead to thermal inefficiencies. This paper offers an alternative method to produce vacuum pressures using a water ejector. Typically, both MSF and MED require a large number of pumping units, including pumps for seawater intake, distillate product, brine blowdown, and chemical dosing. If we use the manufacturers' values, then the thermal energy consumption of MED plants ranges between 40.28 kWh/m^3 (GOR=16) to 63.89 kWh/m^3 (GOR=10). The electrical energy consumption of the pumps ranges from 2.0 to 2.5 kWhe/m^3. Therefore, the total equivalent electrical energy consumption of the MED units ranges from 14.45 to 21.35 kWhe/m^3 [10].

Vapor Compression:

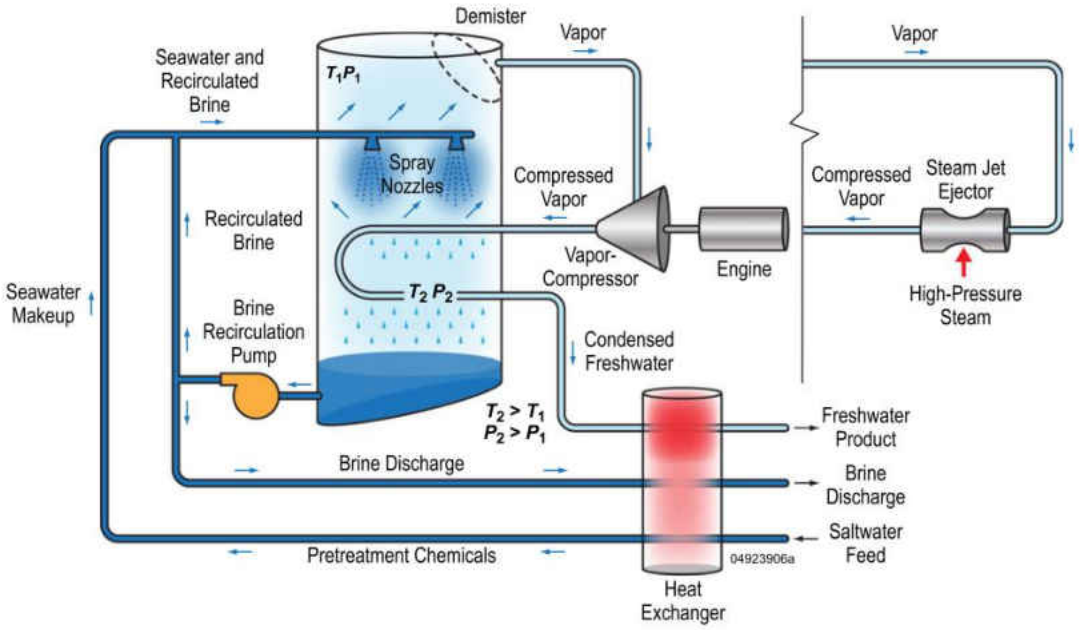

Figure 6: Schematic diagram of typical VC (MVC and TVC) units [10].

Distillation plants using vapor compression rely on the heat generated by the compression and subsequent condensation of water vapor to evaporate salt water, and two methods are employed – mechanical vapor compression (MVC) and thermal vapor compression (TVC). The feed water enters the VC process through a heat exchanger, and vapor is generated in the evaporator and compresses by mechanical (MVC) or thermal (TVC) means. Compressing the vapor raises its temperature by a sufficient amount to serve as the heat source. The concentrated brine is removed from the evaporator vessel by the Brine Recirculation Pump. This flow is then split, and a portion is mixed with the incoming feed and the remainder is pumped to the waste [10]. MVC

uses electricity to drive the compressor, whereas in TVC a stream jet creates the lower pressure via a thermocompressor. Using a thermocompressor, or steam ejector, in TVC requires a steady steam supply to operate. A steam ejector will have substantial energy losses due to shock waves. Many modern MED plant are combined with TVC technology. MVC, like RO, needs electrical or mechanical energy only. It operates at a maximum TBT around 74 °C, with electrical energy consumption ranging from 7 to 12 kWhe/m^3. For TVS, both low-temperature heat (steam) and electricity are needed. At TBT ranges from 63 °C to 70 °C, thermal energy requirements are approximately 63.1388 kWh/m^3, electricity consumption is about 1.6-1.8 kWhe/m^3, and total equivalent electrical energy consumption of the TVC process is about 16.26 kWhe/m^3 [10].

D. Solar Desalination

Thermal desalination requires a large amount of thermal energy, making solar thermal energy a great alternative heat source to conventional fossil fuels and residual power plant heat. Unfortunately, as the temperature of the heat input increases, the cost of the solar thermal system increases and the efficiency decreases. The high cost of CSP greatly diminishes the original financial advantage of using abundant solar thermal energy. At low temperatures, Flat Plate solar collectors may be used. This section reviews the operating principle of solar thermal systems and compares various types of solar collectors.

In solar desalination, two types of solar collection methods are included: direct and indirect. The representative example of direct collection systems is the solar still. Indirect collection systems employ two subsystems: one for collection of renewable energy and one for desalination [3]. Figure 7 presents different methods of solar desalination that have been investigated on a lab or

commercial scale [43]. All three thermal desalination technologies (MSF, MED, and VC) utilize indirect solar collection methods. When

Table 2 and Table 3 are compared, it is obvious that adding renewable energy significantly increasing the production cost of every desalination technology. Coupling solar CSP with MED increases the cost of water production from an estimated $\$0.5/m^3$ to $\$2.4/m^3$. A list of solar desalination plants implemented worldwide can be seen in Figure 11.

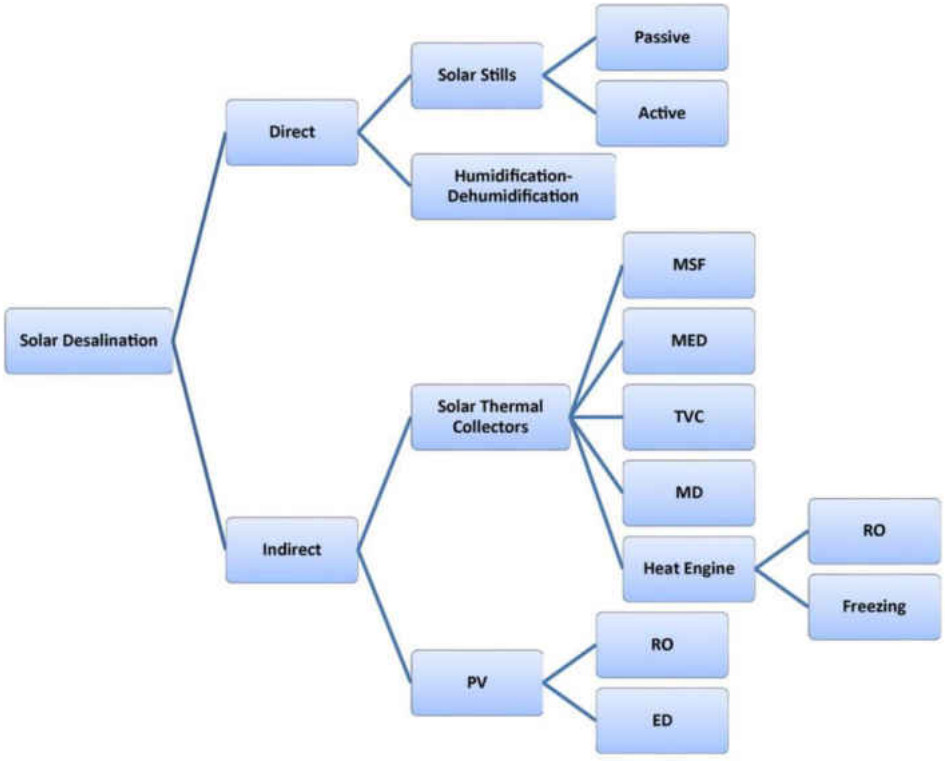

Figure 7: Pilot tested solar desalination technologies [43].

Table 3: Energy consumption and water production of common Renewable Energy-coupled desalination [10].

RE-desalination process	Typical capacity (m^3/day)	Energy demand (kW he/m^3)	Water production cost (US$/$m^3$)
Solar still	< 100	Solar passive	1.3–6.5
Solar MEH	1–100	Thermal: 29.6 Electrical: 1.5	2.6–6.5
Solar MD	0.15–10	45–59	10.5–19.5
Solar pond/MED	20,000–200,000	Thermal: 12.4–24.1 Electrical: 2–3	0.71–0.89
Solar pond/RO	20,000–200,000	Seawater: 4–6 Brackish water: 1.5–4	0.66–0.77
Solar CSP/MED	> 5,000	Thermal: 12.4–24.1 Electrical: 2–3	2.4–2.8
Solar PV/RO	< 100	Seawater: 4–6 Brackish water: 1.5–4	11.7–15.6 6.5–9.1
Solar PV/EDR	< 100	1.5–4	10.4–11.7
Wind/RO	50–2,000	Seawater: 4–6 Brackish water:1.5–4	6.6–9.0 small capacity 1.95–5.2 for 1000 m^3/d
Wind/MVC	< 100	7–12	5.2–7.8
Geothermal/MED	80	Thermal: 12.4–24.1 Electrical: 2–3	2–2.8

Solar Thermal Collectors

Solar thermal energy collectors are a special kind of heat exchanger that transforms solar radiation to internal energy of the transport medium. The major component of any solar system is the solar collector. This is a device, which absorbs the incoming solar radiation, converts it into heat, and transfers this heat to a fluid (usually air, water, or oil) flowing through the collector [3]. Typically, the circulating fluid must be put through an additional heat exchanger to extract the solar energy, leading to further inefficiencies and complexity. The SSV system bypasses the additional heat exchanger by using the inlet seawater both as the collector circulating fluid and heat input fluid for the desalination system.

There are basically two types of solar collectors: non-concentrating or stationary and concentrating. A non-concentrating collector has the same area for intercepting and for absorbing solar radiation, whereas a sun-tracking concentrating solar collector usually has a concave

reflecting surfaces to intercept and focus the sun's beam radiation to a smaller receiving area, thereby increasing the radiation flux [3]. A list of common solar collectors is presented in Table 4. A comprehensive review of various types of collectors currently available is presented in [33] and may not be repeated here.

As collector temperatures increase, cost and complexity of the solar collector system increase while the efficiency decreases. For most solar MSF and MED plants, a parabolic collector is typically used as seen in Galvan *et al.* [40], S.M.A. Moustafa *et al.* [28], and Eduardo Zarza *et al.* [30]. Some modern desalination plants do, however, use evacuated tube collectors, such as A.M. El-Nashar *et al.* [31].

Table 4: Types of solar thermal energy collectors [21].

Solar energy collectors

Motion	Collector type	Absorber type	Concentration ratio	Indicative temperature range (°C)
Stationary	Flat plate collector (FPC)	Flat	1	30–80
	Evacuated tube collector (ETC)	Flat	1	50–200
	Compound parabolic collector (CPC)	Tubular	1–5	60–240
Single-axis tracking	Compound parabolic collector (CPC)	Tubular	5–15	60–300
	Linear Fresnel reflector (LFR)	Tubular	10–40	60–250
	Parabolic trough collector (PTC)	Tubular	15–45	60–300
	Cylindrical trough collector (CTC)	Tubular	10–50	60–300
Two-axes tracking	Parabolic dish reflector (PDR)	Point	100–1000	100–500
	Heliostat field collector (HFC)	Point	100–1500	150–2000

Note: Concentration ratio is defined as the aperture area divided by the receiver/absorber area of the collector.

Flat plate Solar Collector:

The flat plate solar collector system was used in this study as the heat source in the thermo-economic model. Flat plate collectors are the most common solar collector for solar water-heating systems in homes and solar space heating. A typical flat plate collector (Figure 8) is an insulated metal box with a glass or plastic cover (called the glazing) and a dark-colored absorber plate. These collectors heat liquid or air at temperatures less than 80 °C [21].

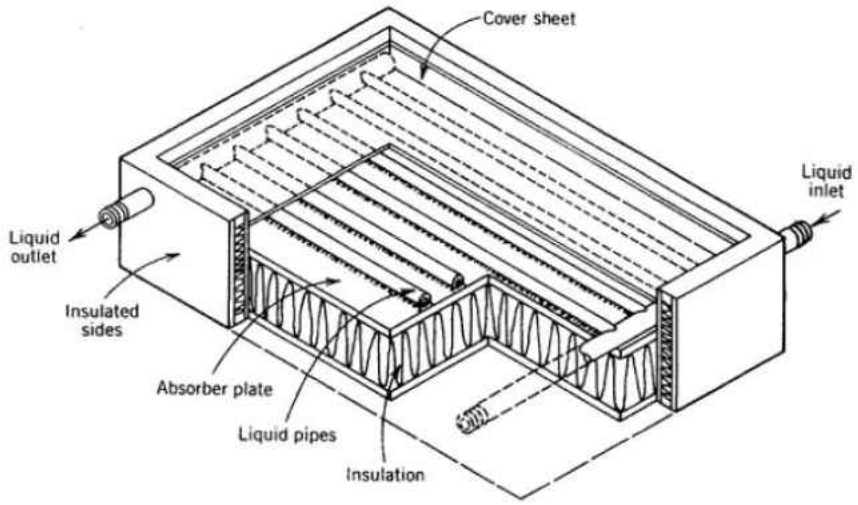

Figure 8: A typical liquid Flat Plate Collector [21].

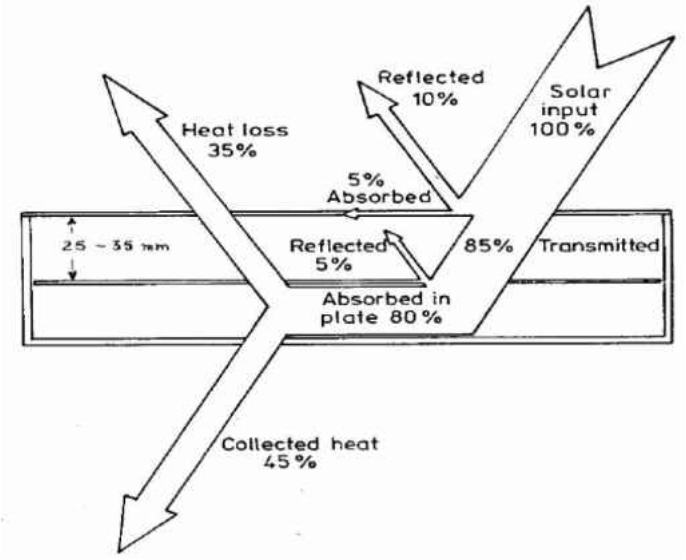

Figure 9: Example Heat flow through a Flat Plate solar collector [21].

As shown in Figure 9 , a part of the radiation is reflected back to the environment, another component is absorbed by the glazing, and the rest is transmitted through the glazing and reaches the absorber plate as short-wave radiation. Therefore, the conversion factor indicates the percentage of solar rays penetrating the transparent cover of the collector (transmission) and the percentage being absorbed. Basically, it is the product of the rate of transmission of the cover and the absorption rate of the absorber [21].

Direct Solar Desalination Systems

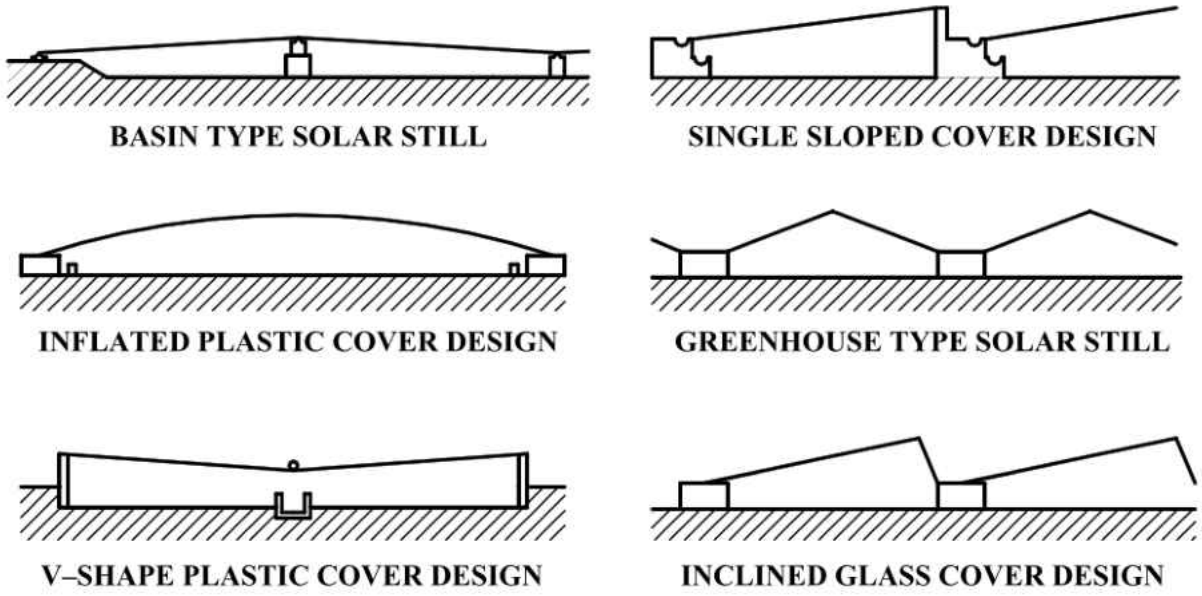

Figure 10: Common designs of solar stills [3].

Solar Still:

A conventional solar still uses the greenhouse effect to evaporate salty water. It consists of a basin, in which a constant amount of seawater is enclosed in a 'V'-shaped glass envelope. The sun's rays pass through the glass roof and are absorbed by the blackened bottom of the basin. As water is heated, its vapor pressure is increased. The resultant water vapor is condensed on the underside of the roof and runs down into the troughs, which conduct the distilled water to the reservoir. The still acts as a heat trap because the roof is transparent to the incoming sunlight, but it is opaque to the infrared radiation emitted by the hot water (greenhouse effect). The roof

encloses all of the vapor, prevents losses, and keeps the wind from reaching and cooling the salty water [3].

The still requires frequent flushing, which is usually done during the night. Flushing is performed to prevent salt precipitation [24]. Design problems encountered with stills are brine depth, vapor tightness of the enclosure, distillate leakage, and cover slope, shape, and material [24; 25]. A typical still efficiency, defined as the ratio of energy utilized in vaporizing the water in the still to the energy incident on the glass cover, is 35% (maximum) and daily still production is about 3-4 L/m^2 [26].

Indirect Solar Desalination Systems

Project	Capacity (m^3/day)	Process
Margarita de Savoya, Italy	50–60	MSF
Islands of Cape Verde	300	Atlantis 'Autoflash'
Tunisia	0.2	MSF
El Paso, Texas, USA	19	MSF
University of Ancona, Italy	30	MEB
Dead Sea, Jordan	3000	MEB
Safat, Kuwait	10	MSF
Takami Island, Japan	16	ME-16 effects
Abu Dhabi, UAE	120	ME-18 effects
Al-Ain, UAE	500	ME-55 stages, MSF-75 stages
Arabian Gulf	6000	MEB
Al Azhar University, Palestine	0.2	MSF 4 stages
Almeria, Spain	72	MED-TVC 14 effects
Berken, Germany	10	MSF
Hzag, Tunisia	0.1–0.35	Distillation
Gran Canaria, Spain	10	MSF
La Desired Island, France	40	ME-14 effects
Lampedusa Island, Italy	0.3	MSF
Kuwait	100	MSF
La Paz, Mexico	10	MSF 10-stages

Figure 11: List of solar thermal desalination plants implemented in the world [47].

Solar MSF:

In MSF, the solar collector is used in place of a conventional brine heater to heat the feed saline water above the saturation temperature and is made to flash in the vessel where low pressure is maintained. Because the input seawater is heated above 100 °C, concentrated solar power (CSP) is typically required. A disadvantage of MSF is that precise pressure levels are required in the different stages and therefore some transient time is required to establish the normal running operation of the plant. This feature makes the MSF relatively unsuitable for solar energy applications unless a storage tank is used for thermal buffering [27].

S.M.A. Moustafa *et al.* [28] report on the performance of a 10 m^3/day solar MSF desalination system tested in Kuwait. The system consisted of a 220 m^2 parabolic trough collectors, 7000 L of thermal storage and a 12-stage MSF desalination system. The thermal storage system was used to level off the thermal energy supply and allowed the production of fresh water to continue during periods of low radiation and night-time. The output of the system is reported to be over 10 times the output of solar stills for the same collector area [3].

Solar MED:

MED has advantages when coupled with solar thermal energy collectors because of its stable operation between virtually 0 and 100% output even when sudden changes are made and its ability to follow a varying steam supply [29].

E. Energy and Exergy Analysis of Desalination Systems

It is common to analyze thermal desalination systems using an energy balance on both the entire process and each subsystem. Most of the thermodynamic analysis performed on desalination systems is based on the first law of thermodynamics [34; 35; 36]. Although the first law is an important tool in evaluating the overall performance of a desalination plant, such analysis does not take into account the quality of energy transferred. This is an issue of particular importance when both thermal and mechanical energy are employed, as they are in thermal desalination plants. First-law analysis cannot show where the maximum loss of available energy takes place. Second-law (exergy) analysis is needed to place all energy interactions on the same basis and to give relevant guidance for process improvement [3]. Analysis of exergetic flows helps engineers and analysts to identify source, magnitude, and importance of thermodynamic inefficiencies [2]. Normally, an exergy analysis will be performed on an existing desalination system as an analysis tool. In this study, a theoretical exergy and energy analysis was performed as a theoretical baseline for the performance of a novel technology, SSV desalination. In the future, the baseline results should be compared to experimental results of a pilot or operational SSV desalination plant.

MED Exergy Analysis:

Exergy analysis, based on actual measured data of the Multi-Effect Stacked (MES) plant installed in the solar plant near Abu Dhabi, is presented by Ali M. El-Nashar *et al.* [32]. The exergy destruction was calculated for each source of irreversibility. The major exergy destruction was found to be caused by irreversibilities in the different pumps with the vacuum pump representing the main source of destruction.

Major exergy losses are associated with the effluent streams of distillate, brine blow-down and seawater. Exergy destruction due to heat transfer and pressure drop in the different effects, in the preheaters and in the final condenser, and in the flashing of brine and distillate between the successive effects represents an important contribution to the total amount of exergy destruction in the evaporator [3].

Vapor Compression Exergy Analysis:

Exergy analysis reveals that the thermal vapor compression desalination plant (TVC) is the most exergy efficient when compared with mechanical vapor compression (MVC) and multi-effect distillation (MED) plants [3]. The SSV system presented in this paper utilizes a similar Venturi device as the focal point of the system with promise of high exergy efficiencies.

The sub-system most responsible for exergy destruction in all three desalination systems investigated is the first effect, because of the high temperature of its heat input. In the TVC system, this amounts to 39%, with the second highest exergy defect being that of the thermocompressor, equal to 17% [3]. As stated previously, lowering the temperature of the heat input has grand implications. At lower temperature heat transfer, the exergy destruction in the boiler is decreased.

Exergy losses can be significantly reduced by increasing the thermo-compressor entrainment ratio (vapor taken from evaporate and compressed by ejector), or by decreasing the top brine and first-effect heat input temperature [3].

F. Economic and Cost Analysis of Desalination Systems

Economic models for desalination systems account for the cost of components, including maintenance, and the cost of fuel consumption. Most economic studies of MED and MSF break down the cost into capital costs, fuel costs, and operating and maintenance (O&M) costs [2]. Almar water solutions produced a report in 2016 on the cost of desalination in the Middle East and North Africa (MENA) region. Almar water solutions is a desalination plant manager and operator in more than 30 different countries in the region. MENA is one of the largest regional consumers of desalination technologies, containing over 50% of worldwide desalination plants [9]. The average capital and O&M costs of the desalination in the MENA are shown in Figure 12. While the costs in the report represent real desalination project costs in the MENA region, the average capital and O&M costs vary significantly from source to source and tend to be dramatically lower than the costs referenced by Almar. In Ali M. El-Nashar *et al.* [44], the average MED capital and O&M costs were estimated 22% and 28% lower, respectively. In this paper, a conservative and appropriate approach is taken by using the average capital costs and O&M costs reference in this paper. The capital cost and O&M cost breakdown for thermal desalination and RO projects are shown in Figure 13 and Figure 14. In the O&M cost average, the electrical energy cost and thermal energy, or fuel, costs are included.

Desalination Plant Type	Capital Cost (Million US$/MLD)		O&M Cost (US$/ m^3)		Cost of Water Production (US$/ m3)	
	Range	Average	Range	Average	Range	Average
MSF	1.7-3.1	2.1	0.22-0.30	0.26	1.02-1.74	1.44
MED-TVC	1.2-2.3	1.4	0.11-0.25	0.14	1.12-1.50	1.39
SWRO Mediterranean Sea	0.8-2.2	1.2	0.25-0.74	0.35	0.64-1.62	0.98
SWRO Arabian Gulf	1.2-1.8	1.5	0.36-1.01	0.64	0.96-1.92	1.35
SWRO Red Sea	1.2-2.3	1.5	0.41-0.96	0.51	1.14-1.70	1.38
Hybrid MSF/MED	1.5-2.2	1.8	0.14-0.25	0.23	0.95-1.37	1.15
Hybrid SWRO	1.2-2.4	1.3	0.29-0.44	0.35	0.85-1.12	1.03

Figure 12: Summary of Desalination Costs in the MENA Region [14].

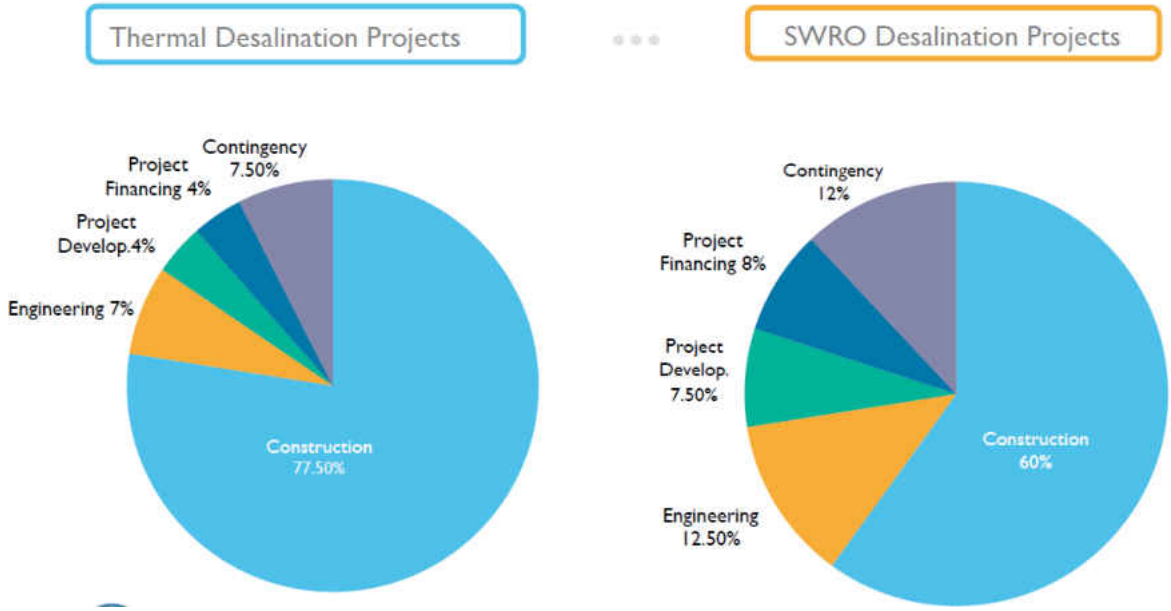

Figure 13: Average Capital Cost Breakdown of Desal Projects in MENA Region [14].

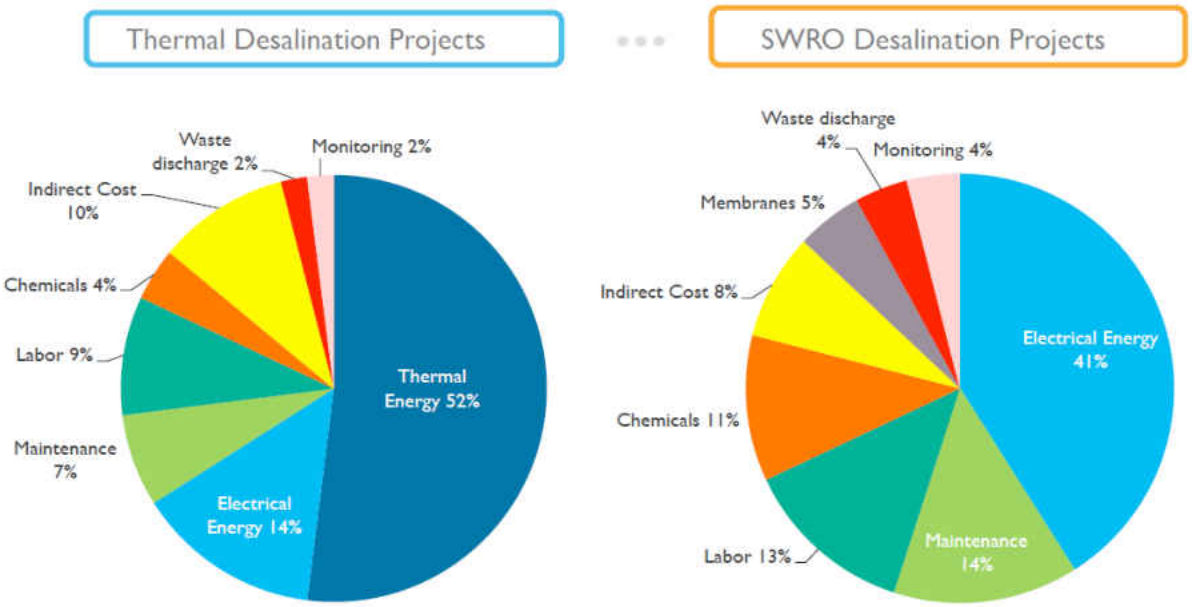

Figure 14: Average O&M Cost Breakdown of Desalination Projects in MENA Region [14].

The interest rate used in economic studies also varies significantly. For this study, the interest rate on initial investment will be assumed zero. Without determining the financing structure, it would be inappropriate to assume 100% of the investment cost will be in the form of debt financing with a fixed interest rate. It is likely that equity financing or government grants will make up the bulk of the project funds.

A Discounted Cash Flow (DCF) analysis is a valuation method used to estimate the attractiveness of an investment opportunity. DCF analyses uses future free cash flow projections and discounts them, using a required discount rate to arrive at the present value of the estimates [50]. The internal rate of return (IRR) is a metric used in capital budgeting to estimate the

profitability of potential investments. Internal rate of return is a discount rate that makes the net present value (NPV) of all cash flows from a particular project equal to zero [50]. In the Economic Analysis section, the IRR of a theoretical SSV Plant project was determined using cash flow tables with different prices for the production of clean water.

II. CHAPTER 2:

Project Idea, Technical Approach, and System Design

Project Idea

In this thesis, we proposed the concept of Single-Stage Venturi-driven (SSV) Desalination, a single-stage, thermal desalination system using a multifunctional Venturi water ejector (Venturi System). The system only requires low-grade solar heat (< 60 ºC) mainly to supplement the heat loss during operation. As compared to the conventional methods of solar desalination, the proposed system has the following intellectual novelties: **First,** the novel Multifunctional Venturi Water Ejector (Venturi System) integrates a vacuum pump for steam production, a compressor for condensation, heat transfer device, and a starter for heat recuperation. **Second**, only residential-grade solar water heating is needed for the heat demand which greatly reduces the production cost of desalination, as compared to those systems using concentrated solar power (CSP). **Third**, the proposed system is operated standalone based solely on solar energy. It can be modularized and easily scaled up due to its simplicity.

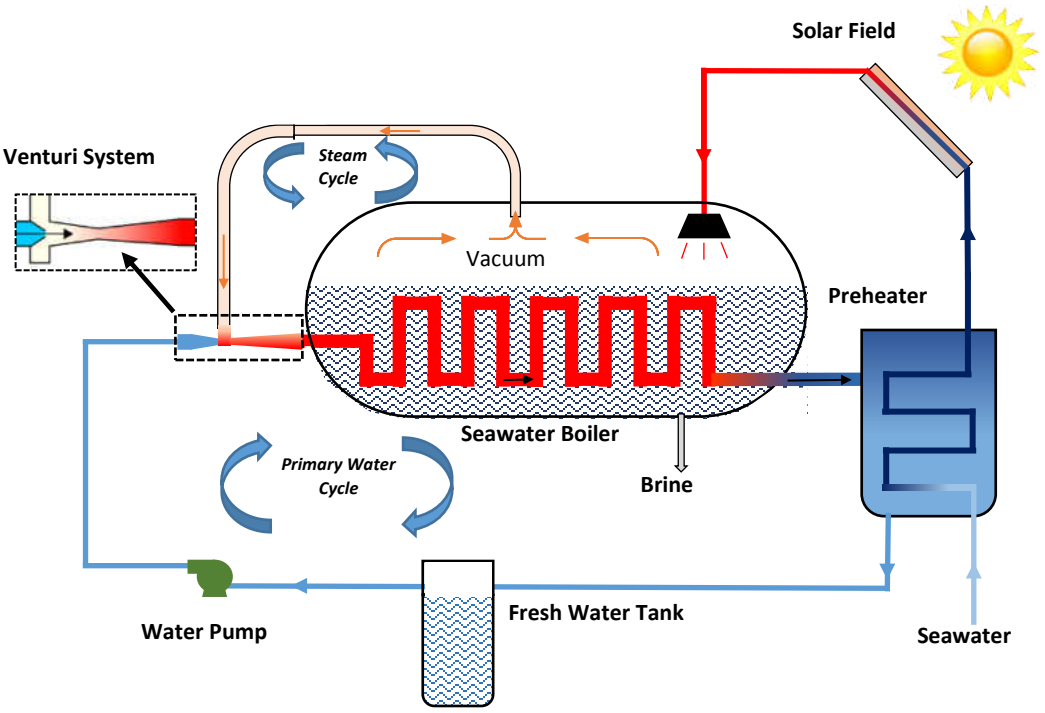

Figure 15: Schematic of Single-Stage Venturi-Driven Desalination.

Figure 15 shows a schematic diagram of the proposed desalination system. It is comprised of two interactive thermofluidic cycles: Primary water and steam cycle. In the steam cycle, steam is produced through boiling saline water at vacuum pressure (< 0.1 bar) and relatively low temperature (< 45 ºC). The Multifunctional Venturi Water Ejector is used to create a vacuum to pump out steam from the boiling vessel. Steam is then condensed back into fresh water within the boiler via a heat exchanger. During steam condensation, latent heat is released and recuperated back into the boiling tank. In the Primary water cycle, fresh water, or primary water, is circulated by a water pump, mainly to drive the Multifunctional Venturi Water Ejector. Fresh

water coming from steam condensation is collected continuously by a fresh water tank during circulation.

Both MSF and MED have complex heat recuperation systems, which reduce thermal energy losses, but increase the installation and maintenance costs of the systems. SSV solves these issues by utilizing a simple, single-stage design with extremely low operating temperatures and a Venturi system with no moving parts.

Venturi Devices:

The Multifunctional Venturi Water Ejector (Venturi System) is a liquid-gas steam ejector and is the keystone to the SSV system. A steam ejector, like a thermocompressor, is a type of Venturi device. To understand its usefulness, the operating principle of the Venturi nozzle must be discussed. A Venturi nozzle is a converging, diverging nozzle. When a fluid is pumped through the Venturi, it travels first in a section of decreasing cross-sectional area (converging), then reaches a section of minimum cross-sectional area (neck), and finally exits the nozzle through a section of increasing cross sectional area (diverging). The inlet and outlet cross sectional areas are typically equal. In the converging section, the pressure is reduced and velocity increases. This concept is derived from Bernoulli's Principle. The fluid will reach a minimum pressure at the neck, or throat, of the Venturi nozzle, the section with the minimum cross-sectional area. The pressure will increase and velocity will decrease again as the fluid flows through the diverging portion of the Venturi nozzle. When a container or tank is connected to the neck of the Venturi, the nozzle will act like an ejector, or vacuum pump, and uses jet action of a high-pressure motive fluid to entrain a secondary fluid. The Multifunctional Venturi Water Ejector allows boiling

water at a lower pressure, and therefore lower boiling temperature. The entrainment ratio is the mass ratio between the primary, motive fluid and secondary, entrained fluid.

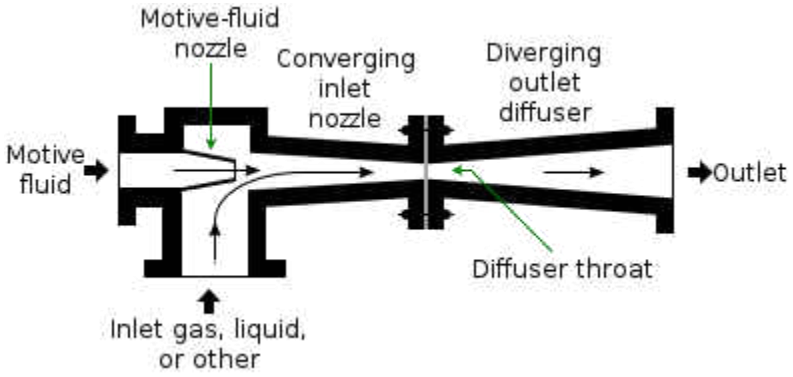

Figure 16: Operation of Liquid Jet Ejector [57].

Vapor Pressure:

A unique challenge to the SSV system is that water is used as the motive fluid in the Venturi system. Most MED plants utilize a similar Venturi device but integrate a thermocompressor design that uses steam as the motive fluid [36]. When using water as the motive fluid, water vapor (steam) pressure buildup must be considered. The temperature of the liquid water entering the Venturi System must be below the boiling point temperature corresponding to the target vacuum pressure in Table 16, found in the Appendix. Figure 17 shows the correlation between saturated vapor pressure and the boiling point temperature of water. In this study, vapor pressure issues complicated the heat transfer process in the preliminary experiments. Ultimately, the vapor pressure issues caused the preliminary experiments to be performed without analyzing the heat transfer characteristics of the system.

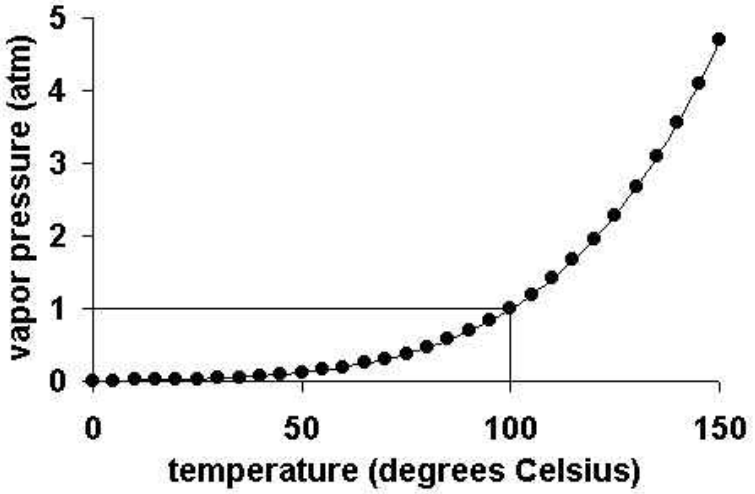

Figure 17: Saturated vapor pressure of water at different temperatures [51].

System Design and Components

The SSV system is comprised two cycles or systems: the primary water system and steam system (See Figure 15). The primary system contains freshwater, circulating continuously in a closed loop. In the closed loop, the water passes through a circulating pump, Venturi System, boiler heat exchanger, and preheater heat exchanger. The boiler heat exchanger consists of a coiled tube inside a boiler tank and is similar to a shell (boiler tank) and tube (coiled tube) heat exchanger. After steam is injected into the primary flow stream via the Venturi System, the stream enters the coiled tube and transfers heat back into the boiler as the steam condenses. The steam system operates at a constant boiling point temperature, and any heat added to the system will be converted into steam generation. As the saline water in the boiler is heated from the primary flow stream and turned into water vapor, it is injected into the primary flow stream via the Venturi

System. The diverging section of the Venturi System is placed inside the heat exchanger to prevent the water vapor from condensing beforehand. As the water vapor condenses inside the heat exchanger, the latent heat is directly transferred through the walls of the heat exchanger into the boiler.

The amount of steam produced in the boiler tank is equal to the rate of clean water production of the system. The system works efficiently because of the use of the Venturi system. The Venturi system reduces the vapor pressure, and therefore boiling point temperature inside the boiler. Thus, the temperature in the primary flow stream is always above the temperature in the boiler and can be used as an effective heat exchanger. The reduction in boiling point of the saline water in the boiler allows the entire system to run at a very low overall temperature and reduce heat losses to the environment. The system aims to eventually be able to operate under ambient temperatures (~20°C) so there will be effectively no heat loss to the environment or need for insulation. In fact, there can be heat addition from the environment.

Technology advantages:

Low-temperature, solar SSV desalination solves the issues of cost, fossil fuel reliance, and location flexibility. When compared other thermal desalination methods, there are a few stark differences. SSV desalination operates in a closed loop design requiring a single circulating pump, uses fresh (primary) water as the motive fluid for steam injection and vacuum pressure generation, operates at lower temperatures in a single boiling stage, and does not require steam input as the heat source or motive fluid. The SSV System utilizes clean, low-cost solar thermal energy, and has a simple design that can operate in remote, off-grid regions.

Fossil Fuel Independence:

Since many thermal desalination plants burn fossil fuels to supply heat, MED and MSF plants are becoming very expensive to run and the environmental pollution they produce is increasingly recognized as very harmful to the globe [9]. Nearly 10,000 tons of oil is required every year to produce 1000 m^3/day of desalination water [8]. Additionally, carbon taxes may increase prices further. Wagner and Rubin [47] state that a price of $US 153 per ton CO_2 or higher could make concentrated solar thermal power competitive with coal electricity. To combat high fossil fuel prices and power plant dependence, solar-assisted desalination plants have emerged over the past decade. SSV desalination provides a highly cost competitive solution to produce water without the need of fossil fuels.

Low-grade solar heat input:

Many desalination plants, including RO, MED, and MSF, are becoming integrated with solar thermal energy sources, but require expensive CSP systems to achieve higher temperature heat or to produce steam. Widespread deployment of CSP plants has been hindered by cost and intermittency issues [47]. Without the high-grade heat or steam input requirement, SSV desalination will not require CSP, and other solar thermal collectors with lower costs and higher efficiencies can be utilized. Additionally, other sources of low-grade heat, such as geothermal or process heat, can be easily integrated with the SSV system.

Simple Design:

The simple, single-stage design has many advantages to the complex MSF and MED systems. The SSV desalination system can be scaled down to a modular design for quick deployment and

off-grid operations in emergency situations. For larger, plant-sized SSV systems, decreased construction times, installation costs, and O&M costs can all be expected when compared to MSF and MED. This advantage should not be overlooked. Many desalination projects discourage private investors because of the long and complex construction process. Longer, riskier, and more complex construction projects require higher return on investment (ROI) and interest rates.

Electrical Power Requirements:

The electrical power demand is also significantly decreased due to the use of a single, circulating pump. As a comparison, MSF typically require recycle pumps, cooling water pumps, distillate product pumps, brine blow down pumps, condensate pumps, and chemical dosing pumps [10]. This decreases both the construction and maintenance costs.

Zero Liquid Discharge:

Due to the open loop design, RO, MED, and MSF discharge highly saline brine water, which has harmful environmental impacts. The SSV design uses a closed loop design and can potentially operate in over-saturated concentrations to discharge pure solid salt and achieve true Zero-Liquid Discharge, a goal of the DOE in DE-FOA-0001778 [55]. At the higher temperatures of the MSF and MED first few stages and effects, the high salt concentrations will accelerate scaling and corrosion. The SSV system may be able to operate at low enough temperatures to prevent such issues. An alternative design is proposed here, where the solid salt particles will accumulate at the bottom of the boiler and be removed either continuously or periodically.

Corrosion:

Since the SSV desalination system operates at lower temperatures than both MED and MSF, there is less corrosion and pitting issues. This further reduces the water pretreatment and O&M costs of the SSV desalination system.

III. CHAPTER 3:

OBJECTIVES

The main goal of this study is to introduce, analyze the performance of, and estimate the cost of a novel desalination technology, Single-Stage, Venturi-driven desalination. In doing so, system components, mainly the Venturi System, needed to be further analyzed. CFD simulations, using Comsol Multiphysics, and experimental tests were performed to verify the proof of concept and scalability of using a water-jet ejector to achieve vacuum pressures and heat transfer simultaneously. The minimum vacuum pressure achieved in the experimental results was used in later analysis. The above-mentioned simulations were also performed to analyze the effect of certain geometric, flow, and heat transfer characteristics on the performance of the Venturi system. A thermo-economic model was created to estimate the performance of the entire system and compare the performance and cost to other common desalination technologies and commercially operating plants. Ultimately, the goal of the research was to perform an accurate thermo-economic analysis of the system and achieve an estimated levelized cost of water (LCOW) below the DOE target of $\$0.50/m^3$ (DE-FOA-0001778) [55].

Each of the three modes of analysis, CFD simulations, experimental tests, and thermo-economic analysis, had unique objectives. Initially, the Venturi system was analyzed using the results from experiments and CFD simulations. The CFD simulation provided baseline performance results for the Venturi System operation. Additionally, heat and mass transfer were simulated as a guideline for future experiments, which were difficult to conduct with an extremely limited budget. Using Comsol Multiphysics, the simulations were carried out by varying different parameters, including geometry, flow rate, pressure, and heat transfer coefficients. The

simulation results were analyzed to recognize the effect of the parameters used in the SSV system, such as inlet velocity and entrainment ratio. Venturi nozzles of different sizes were experimentally tested under constant flow conditions to compare with the simulation results. Scalability was a main objective to extrapolate small-scale model results to large-scale plant performance. Experimental tests were performed to validate the CFD results, where possible. A prototype test was further developed to provide proof of concept in an experimental setting. Also, the prototype was used to determine the achievable vacuum pressure, or boiling point temperature, to use later in the study.

The thermo-economic analysis focused on the entire SSV system. To achieve the main objectives of this paper, an accurate and comprehensive estimate of both the performance and cost of the entire system was necessary. The thermo-economic analysis consisted of two separate studies: a thermodynamic analysis and economic analysis. The thermodynamic study can be further broken down into an energy and mass balance and an exergy analysis. From the energy and mass balance, common desalination performance metrics could be calculated, such as performance ratio, thermal energy requirement, and thermal efficiency. An exergy analysis is commonly performed on commercially operating desalination plants using operating data. The exergy analysis in this paper is used as a theoretical baseline estimate to compare the exergy destruction and efficiency calculated to other operational desalination technologies and an operational SSV plant in the future. The economic analysis used inputs from the energy and exergy analysis to estimate various costs to construct and operate a theoretical SSV desalination plant rated at 100 m^3/day. The economic analysis results were used to compare SSV desalination to other commercial desalination technologies in terms of cost. A discounted cash flow (DCF) analysis

was performed to show the unit cost of water ($/m^3) in scenarios with different ROI and interest rates.

IV. CHAPTER 4:

CFD SIMULATIONS

A. Method: Simulating the Venturi system

Comsol Multiphysics was used to create the geometry and run simulations of the Venturi System. The Venturi nozzle was modeled in 2-D to analyze flow characteristics and heat transfer behavior. Two sets of simulations were run in Comsol. First, (CFD Simulation Set 1) simulations were performed to determine the flow characteristics of the Venturi System. The heat transfer module was incorporated into the Comsol model, but not the heat exchanger itself. The purpose of the flow simulations was to determine how scale, pump pressure, and area ratio effect the minimum vacuum pressure and entrainment ratio. A main objective of this set of simulations was to validate the scalability of the SSV system. The results of the simulation were later compared to the experimental results for validation. The next set of simulations (CFD Simulation Set 2) incorporated a fixed length of heat exchanger and was used to analyze heat transfer behavior. The simulations were performed to determine the effect of primary flow rate, entrainment ratio, boiling point, and heat transfer coefficient on heat exchanger efficiency and final temperature. In both models, similar flow assumptions were used. Since the motive fluid used in this research is water as the primary fluid, the assumption of incompressible flow is appropriate [38].The standard k-ὲ with high Reynolds number was selected to govern the turbulence characteristics [38]. Due to complications with two-phase flow simulations, liquid water was used as the secondary, or entrained fluid. The simulations assume that steam has condensed before entering the Venturi System. The temperature of the secondary liquid water is elevated to account for the latent heat released during condensation.

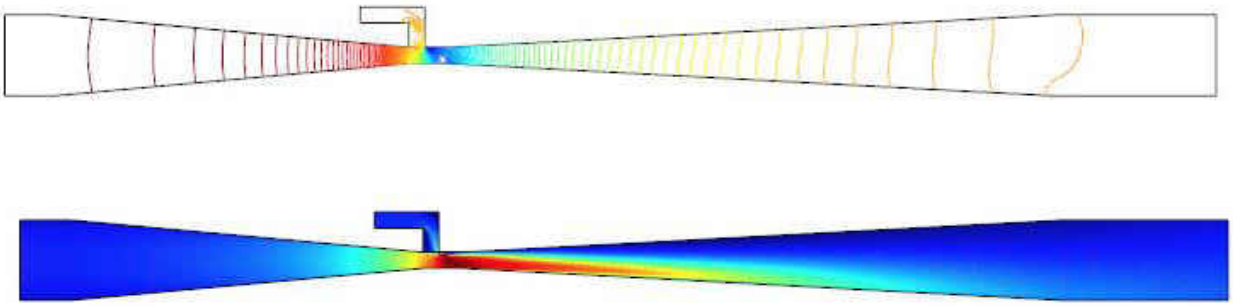

Figure 18: Pressure (above) and Velocity (below) profile example for CFD Simulation Set 1.

CFD Simulation Set 1: Venturi Flow Characteristics

The geometry of the 2D model was built to replicate a simple Venturi nozzle with an inlet at the neck of the nozzle. In the Venturi System model, the two faces, primary inlet and vacuum inlet, were set as independent variables to pressure conditions. While the Primary inlet pressure represented the pump pressure and varied throughout the experiment, the vacuum inlet pressure remained constant at atmospheric pressure. The discharge was set to an outlet condition at atmospheric pressure. The temperatures of each of the two faces were set as independent variables and remained constant throughout the experiment. The purpose of this set of simulations was to create the most realistic setup possible to match the SSV Venturi System. The simulations in CFD Simulation Set 1 produced performance curves. In each performance curve, one variable (inlet pressure or scale) was varied while the other were held constant. The results produced when scaling the Venturi System up or down are important to prove scalability. Preliminary Experiments later validated the results. After the effects of scalability were analyzed,

the simulations focused further on the relationship between pump pressure, a potential control parameter in the SSV system.

Because the preliminary experiments did not provide flow rate measurements or entrainment ratios, the CFD Simulation Set 1 uses simulations to analyze the effect of scale and pump pressure on the flow rates and entrainment ratio. The results of CFD Simulation Set 1 will provide a range of appropriate flow rates and entrainment ratios to use when a heat exchanger is added to the model in CFD Simulation Set 2. The results will also provide a realistic entrainment ratio and primary water flow rate for the thermo-economic model provided later in this paper.

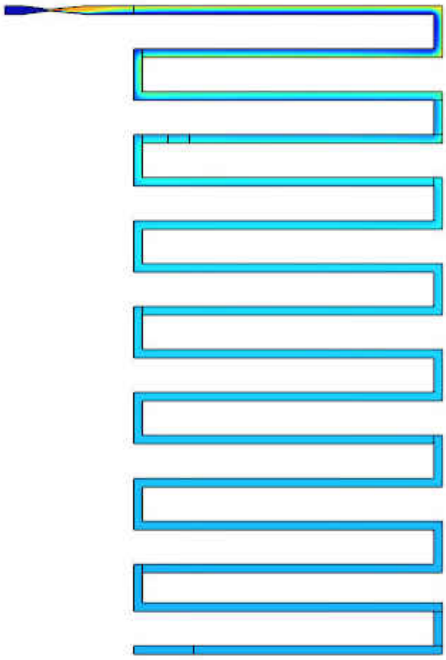

Figure 19: Geometry and Temperature Distribution Example of CFD Simulation Set 2.

CFD Simulation Set 2: Heat Transfer Behavior

The geometry of the 2D model was built to incorporate the Venturi nozzle and a finite length portion of the boiler heat exchanger. In this model, the inlet velocities, not inlet pressure conditions, were used to control the effect of primary flow rate and entrainment ratio on heat exchanger properties. The appropriate primary flow rates and entrainment ratios were provided from CFD Simulation Set 1 results. In the Venturi nozzle, the two faces, primary inlet and vacuum inlet, were set as independent variables to velocity conditions and correlate to a specified entrainment ratio. The discharge was set to an outlet condition at atmospheric pressure. The temperatures of each of the two faces were set as independent variables and varied in the study.

In the heat exchanger, both the external, or ambient, temperature and heat transfer coefficient were specified as independent variables. The ambient temperature was set in accordance with the boiling point temperature inside the boiler. For most tests, the boiling point temperature was set to a constant 40 °C, which aligns with the thermo-economic model. The goal of the 2D simulations was to understand how each independent variable, heat transfer coefficient, primary velocity, and boiling point temperature, affected the efficiency and outlet temperature of the heat exchanger. The initial and final temperatures of the heat exchanger were calculated from a surface average temperature function in the Comsol Multiphysics program. The heat exchanger efficiency is defined below:

$$Heat\ Exchanger\ Efficiency = \frac{T_{in,hx} - T_{f,hx}}{T_{in,hx} - T_{BP}}$$

where, $T_{in,hx}$, $T_{f,hx}$, and T_{BP} are the temperature into the heat exchanger, temperature exiting the heat exchanger, and boiling point or ambient temperature, respectively. Three separate

simulation tests were performed, each involving many simulations, or runs. In tests 1, 2, and 3, the varying parameter was the HTC, inlet primary velocity, and boiling point temperature, respectively. Since the heat transfer coefficient (HTC) is difficult to estimate, determining the effect of HTC on the heat exchanger efficiency helps for subsequent analysis. The value of the HTC was varied from 0 to 25,000 kW/m^2*K. When the vacuum velocity is held constant, varying the Primary inlet velocity directly changed the entrainment ratio. The entrainment ratio has large implication on the thermal efficiency of the Venturi System. The boiling point temperature of the system may vary depending on the design, seawater temperatures, or operating conditions if heat supply is not uniform. The effect on the heat exchanger performance of a varying boiling point temperature is important to analyze. In Test 3, the boiling point temperature ranged from 20°C to 60°C.

B. CFD Simulation Results and Discussion

CFD Simulation Set 1: Venturi Flow Characteristics:

The CFD Simulation Set 1 provides a deeper understanding of the effect of pump pressure, area ratio, and overall scale on the Venturi entrainment ratio, velocities, and achievable vacuum pressures. The scale of the Venturi System did not affect vacuum pressure significantly. The minimum vacuum pressure of the 0.25, 0.5, and 1 in Venturi Systems with inlet pressure of 1.35 bar abs were 0.089 bar abs, 0.095 bar abs, and 0.094 bar abs, respectively. The very slight variation in the vacuum pressures may come from computational inconsistencies or errors that occur when the geometry of the model is changed. When the Venturi System is scaled up, the inlet velocity is scaled proportionally, but the vacuum velocity, and therefore entrainment ratio, is slightly elevated. *Overall, the CFD Simulation Set 1 results prove that the Venturi System can*

be scaled without changing the minimum vacuum pressure achieved. The pump pressure required remains the same, but an increased primary water mass flow rate increases the amount of work required by the pump.

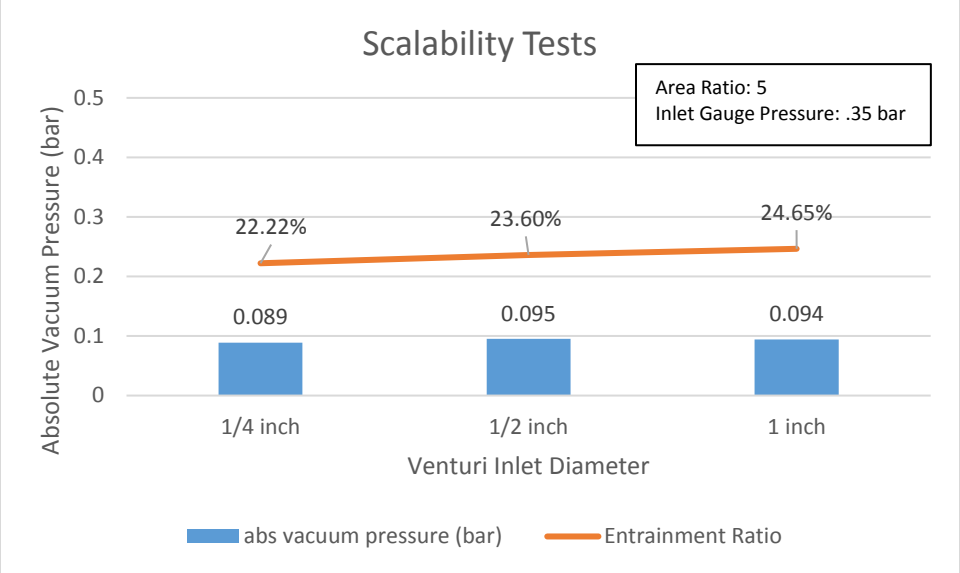

Figure 20: Scalability test, Performance Curve from Simulations.

The inlet pressure, representing the pump pressure required, plays a significant role on the vacuum pressure and inlet velocity, but not on the entrainment ratio. When the inlet pressure of the 0.25 in Venturi System with an Area ratio of 5 was increased from 1.05 bar abs to 1.35 bar abs, the vacuum pressure decreased from 0.879 bar abs to 0.089 bar abs, and the inlet velocity increased from 0.69 m/s to 1.89 m/s. Initially, the entrainment ratio seems constant for the range of inlet pressures, but after further analysis, there was a slight and consistent decrease in entrainment ratio as the inlet pressure was increased. When the same Venturi System inlet

pressure was increased from 1.05 bar abs to 1.35 bar abs, the entrainment ratio decreased from 23.00% to 22.22%. The results can be seen in the performance curves (Figure 40 & Figure 41) in the Appendix. The results show that controlling pump pressure can be used to decrease vacuum pressures in the boiler and increase primary flow rate without significantly changing the entrainment ratio of the Venturi System.

CFD Simulation Set 2: Heat Transfer Beahavior

The CFD Simulation Set 2 provides insight into the sensitivity of Boiler Heat Exchanger performance when the HTC, Primary inlet velocity, entrainment ratio, and boiling point are changed. The Heat Exchanger efficiency was significantly affected by increases in HTC within the range of 0 to 10,000 kW/m^2*K. The Heat exchanger efficiency reached 40% by 10,000 kW/m^2*K, but only increased to 52% by 25,000 kW/m^2*K. Performance curves can be found in the Appendix.

Increasing the Primary inlet velocity had a negative effect on Heat Exchanger efficiency. As velocity was increased, the entrainment ratio decreases, decreasing the resulting temperature after the Primary and Secondary flow mix. Figure 42**Error! Reference source not found.** shows the relationship between initial temperature after mixing and final temperature of the fluid after the section of heat exchanger. When the Primary inlet velocity was increased by a factor of 5 from 1 m/s to 5 m/s, which decreased the entrainment ratio from 10% to 2%, the amount of specific heat transferred decreased by a factor of 10, from 70 kJ/kg to 7 kJ/kg. Both performance curves, Figure 44 and Figure 45, can be seen in the Appendix. The entrainment ratio and Primary inlet velocity play a significant role in the efficiency of the heat exchanger.

As expected, the heat exchanger efficiency was not significantly affected by a change in boiling point temperature. In the range from 20°C to 60°C, the Heat Exchanger Efficiency varied from 28.4% to 30.6%. The relatively constant Heat Exchanger Efficiency is caused by the definition of Heat Exchanger efficiency in this test, and the contribution of boiling point temperature in that definition. However, the total heat transferred in the test was significantly affected by the change in boiling point temperatures. Increasing the boiling point temperature from 20°C to 60°C, decreased the specific heat transferred out of the fluid from 50.4 kJ/kg to 3.1 kJ/kg.

Conclusion of Findings: The SSV system performance is very complicated and changing a single parameter typically affects many operating conditions. It is useful that varying the inlet pressure significantly changes the inlet velocity and vacuum pressure while only affecting the entrainment ratio minimally. The results of CFD Experiment 1 prove that the system can be scaled without greatly affecting performance. The CFD simulation results were constrained by computational limitations.

V. CHAPTER 5:

PRELIMINARY EXPERIMENTS

A. Experimental Methods:

Experimental Venturi Test:

Three Venturi ejectors of various sizes, but same area ratio were obtained and tested to compare performance. The three inlet diameters were 0.25, 0.75, and 1 in. In the test setup, the Venturi ejectors, acting as a vacuum pump, were connected from the secondary inlet to an empty tank. Air, instead of steam, was evacuated from the tank for simplicity. A vacuum gauge was connected to the empty tank for absolute vacuum pressure recordings. The pump chosen for this experiment was a WAYNE 1/2 HP Cast Iron Transfer Utility Pump (120 V, 60 Hz, 8.0 A) The Primary water was pumped in a continuous loop by a circulating pump. After the circulating water pump was turned on, the time and absolute pressure in the tank were recorded in one-minute intervals. The test setup is shown in Figure 21. The purpose of the experiment was to determine the influence of the scale of the Venturi on the minimum vacuum pressure. The results were then compared to those of the CFD simulations.

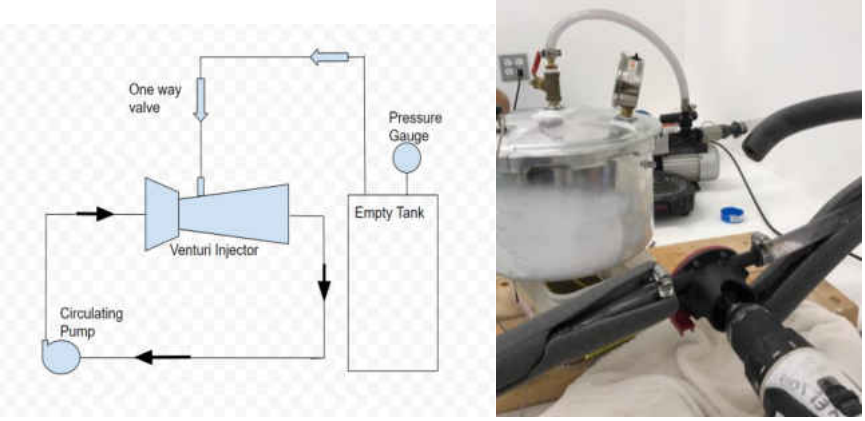

Figure 21: Drawing and Picture of Experimental Venturi Test.

Prototype test:

A prototype test was designed next to test whether the Venturi ejector could sustain low vacuum pressures regardless of steam generation rate, or boiling rate, in the boiler. As more heat is applied to the boiler, the boiling rate increases, and more steam molecules enter the fixed volume boiler. If the molecules are not pumped out of the boiler, the pressure will increase inside the boiler. The Venturi System must have enough force to pump out the steam in the boiler faster than it is generated. The appropriate Venturi nozzle was selected from the results of the Experimental Venturi Test, and a small-scale prototype was built. The prototype consisted of most of the elements in the original, full-scale design: Circulating Pump, Venturi Nozzle, and Boiler Tank. The Venturi ejector chosen was a 0.5 in diameter, plastic nozzle. The experiment used two electric pumps in series. The boiling container used was a Duda Energy 20 Plate Stainless Steel heat exchanger (2x 2.9 x 7.5 in). A flat plate heat exchanger was used for compact design, greater heat transfer surface, and less total volume than a boiler tank. The main focus of

the experiments was to maintain the low vacuum pressure during steam generation. A picture of the system prototype can be seen below.

Initially, the experiment was going to involve heat recuperation, but due to vapor pressure issues, it was very difficult to incorporate into the test. For successful water-ejector operation, the liquid water must be sufficiently cooled before it enters the venture nozzle. To satisfy this condition, the prototype used an open loop design with an ice water bath to maintain low inlet temperatures. The flat plate heat exchanger was still used as the boiler for geometric benefits. The flat plate heat exchanger was partially filled with 100 mL of water. A hot plate was used as the heat source for steam generation. The goal of the prototype experiment is to maintain a stable and low vacuum pressure in the boiler while there is steam generation occurring. Incorporating heat recuperation and a closed loop system into the prototype will require very controlled operating conditions.

B. Experimental Results

The Experimental Venturi Test results are shown in Figure 22. It is seen that the Venturi ejector with larger tube diameter reached the maximum vacuum pressure sooner, though the maximum limit remained relatively constant. For the 1, 0.75, and 0.5 in diameter nozzles, the maximum vacuum pressures were absolute 0.13 bar, 0.13 bar, and 0.17 bar, respectively.

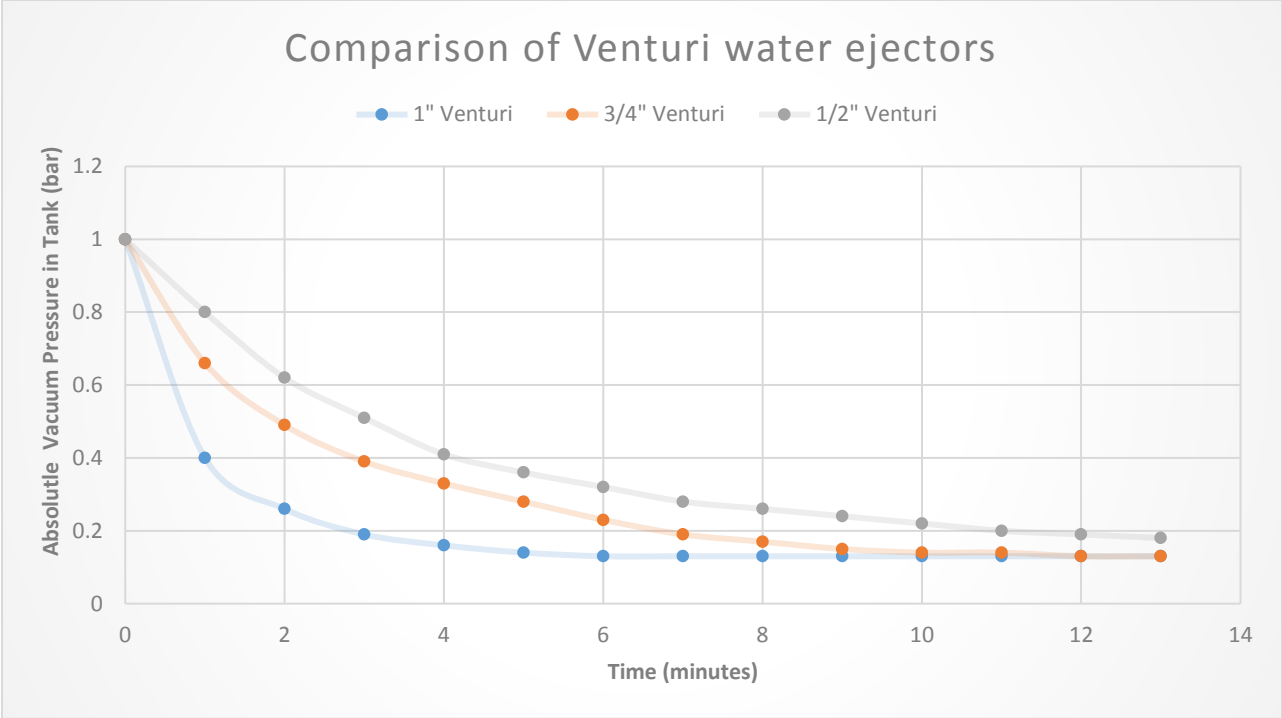

Figure 22: Experimental Venturi Test results comparing the performance of various sized Venturi ejectors generating vacuum pressures within a 1 gallon tank.

The Venturi nozzle chosen for the prototype resulted in a maximum achievable vacuum pressure of 0.07 bar. The 0.07 bar vacuum was achieved in a test where the vacuum gauge was connected directly to the neck of the Venturi nozzle using a Cast Iron Pump. The 0.07 bar vacuum pressure corresponds to a boiling point of 40 °C. It is likely that a lower vacuum pressure is achievable, but without further experimental results, the 40 °C boiling point temperature is appropriate to use in the Thermo-Economic Analysis. The pump performance played a large role in the vacuum pressures achieved.

The prototype test resulted in very stable vacuum pressures in the boiler once an equilibrium was reached. Even while the hot plate was set to “high” and significant boiling was occurring, the

Venturi System was able to outpace the steam generation and maintain a low vacuum pressure in the boiler. The twelve-minute prototype test can be seen in Table 17 in the Appendix. As shown from the table, there were no fluctuations in vacuum pressure and it was clear boiling was occurring at a reduced boiling point temperature. Vacuum pressures did not reach lower levels due to the change from the Cast Iron Pump to the two electric pumps in series. Lower vacuum pressures were achieved with the Cast Iron Pump. It was only after the pump was turned off that the vacuum pressure and temperature gauge increased rapidly. More sophisticated monitoring and control equipment will be necessary for further experimental tests.

The results of the Venturi experimental test of the have impactful implications. If steam evacuation needs to be increased to avoid pressure buildup, the size of the overall Venturi ejector can be modified to solve the issue. If a lower vacuum pressure is required, the overall scale of the Venturi ejector will have no effect, but the Area Ratio of the Venturi ejector can be modified to control the vacuum pressure parameter.

The results of the Prototype test prove the concept that the multifunctional Venturi ejector can act as a vacuum pump for steam production, a compressor for condensation, and a starter for heat recuperation. In addition, boiling does not significantly impact the vacuum pressure in the boiler. However, as steam generation increases dramatically, the simple solution is to add larger size and quantity of Venturi ejectors. It is satisfying to see the small, off-the-shelf Venturi ejector evacuate steam during boiling as quickly as it did in the prototype test.

Conclusion of Findings: The system performance is much more dynamic than originally anticipated. Vapor pressure plays a key factor in design of the system. Vapor pressure issues likely dissuades other thermal technologies (MSF, MED) from utilizing water as the working fluid in Venturi ejector. Experimental results show that the geometric and flow characteristics of the Venturi affect both the maximum achievable vacuum pressure and the steam flow rate. The prototype proved the concept of using a multidimensional Venturi to maintain a low vacuum pressure while evacuating the steam produced in the boiler.

VI. CHAPTER 6:

THERMO-ECONOMIC ANALYSIS

The thermo-economic analysis involved a review of the theoretical formulations and physical principles to properly analyze the system. For this report, an energy and exergy analysis were performed on a theoretical SSV system with a water production capacity of 100 m^3/day. The thermodynamic model was then combined with an economic analysis to create a final Thermo-Economic model of the system. The main goal was to accurately model the performance and cost of each aspect of the system and then estimate the final levelized cost of clean water production for the system.

A. Technical Analysis and Assumptions

Before a thermodynamic model can be created, the technical (non-thermodynamic) parameters must be determined.

Multifunctional Venturi water ejector:

The vacuum pressure in the boiler can be calculated using conservation of mass and the Bernoulli equation. To calculate the vacuum pressure, we use the control volume method to analyze the Venturi nozzle. We analyze two points in the flow through the Venturi nozzle, one at the inlet and one at the throat of the Venturi. The Control Volume setup is shown in Figure 23. For incompressible water flow, the continuity equation becomes:

$$V_1 A_1 = V_2 A_2 = B_1 = B_2 = B$$

Bernoulli's equation can be applied here:

$$(P_1 - P_2) = \frac{1}{2}\rho(V_2^2 - V_1^2)$$

From these two equations, we make two substitutions,

$$V_2^2 = \left(\frac{B}{A_2}\right)^2 \quad \& \quad V_1^2 = \left(\frac{A_2}{A_1}\right)^2 \left(\frac{B}{A_2}\right)^2$$

$$(P_1 - P_2) = \frac{1}{2}\rho\left(1 - \left(\frac{A_2}{A_1}\right)^2\right)\left(\frac{B}{A_2}\right)^2$$

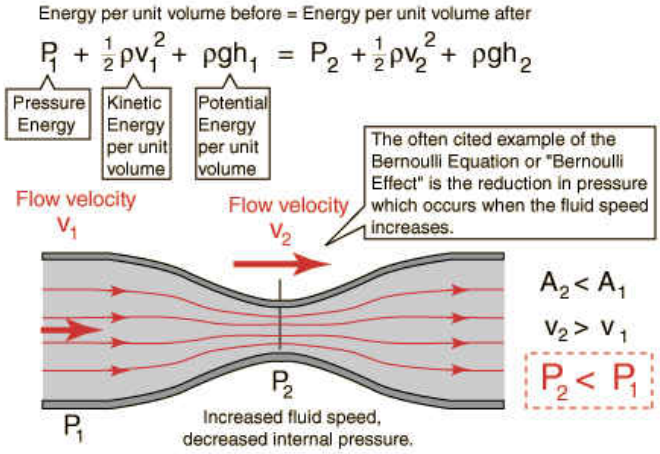

Figure 23: Control Volume Setup and Bernoulli's Equation [56].

Using Equation 5, the throat pressure is determined based on the flow and geometrical characteristics of the system. The results from the theoretical analysis were compared to the results of both the simulations and the experiments.

Flat plate thermal solar collector:

The efficiency of the flat plate solar collector was calculated separately from the entire desalination system. The calculated efficiency was then used in the energy and exergy model for the system. If I represents the solar radiation power density (W/m^2) incident on the aperture plane of the solar collector with a surface area of A (m^2), then the amount of solar radiation received by the collector is:

$$\dot{Q}_{rad} = IA$$

where, $\dot{Q}_{rad}$ is the solar radiation. However, some of the solar rays are reflected and absorbed, and the amount of solar radiation absorbed in the plate is:

$$\dot{Q}_{rad} = I\ (\tau\alpha)\ A$$

where, τ and α represent the rate of transmission of the collector cover and rate of absorption of the collector absorber, respectively. The product of τ and α is approximately 80% of the incoming solar radiation [21]. As the collector absorbs heat, its temperature is getting higher than that of the surrounding and heat is lost to the atmosphere by convection and radiation. The rate of heat loss, $\dot{Q}_L$, depends on the collector overall heat transfer coefficient and the collector temperature.

$$\dot{Q}_L = U_L A * (T_{avg} - T_a)$$

where, U_L, T_{avg}, and T_a are the overall heat transfer coefficient of heat lost by the collector to the environment, average temperature of solar collector, and ambient temperature, respectively. Calculating the total heat loss coefficient can be very complex. The rate of heat loss is dependent on the temperature of the solar collector itself. The heat transferred into the working fluid is calculated as the difference between heat input from solar radiation and heat loss from the collector.

$$\dot{Q}_u = \dot{Q}_{rad} - \dot{Q}_L$$

The above equation calculates the rate of extraction of heat from the collector and may be measured by the amount of heat carried away in the fluid passed through it.

$$\dot{Q}_u = \dot{m}c_p(T_o - T_i)$$

where, $\dot{m}$, c_p, T_o, and T_i are the water mass flow rate through the solar collector, heat capacity of water, temperature of water entering the solar collector, and temperature of water exiting the solar collector, respectively. The above equation provides a somewhat inconvenient solution because it does not account for the temperature of the solar collector. Further analysis shows the useful energy gain from the solar collector. It is convenient to define a quantity that reflects the useful energy gain of a collector to the useful gain if the whole collector surface were at the fluid inlet temperature [21]. This quantity is known as "the collector heat removal factor (F_R) and is expressed as,

$$F_R = \frac{m c_p (T_o - T_i)}{A[I\tau\alpha - U_L(T_i - T_a)]}$$

Using the above equation, the actual useful energy gain is found using an equation generally known as the "Hottel-Whillier-Bliss Equation":

$$Q_u = F_R A[I\tau\alpha - U_L(T_i - T_a)]$$

The above equation is a more appropriate and common representation for solar collector heat input. Thermal Efficiency, η, of flat plate solar collectors are derived from the actual useful energy gain.

$$\eta = \frac{Q_u}{IA}$$

The theoretical thermal efficiency results are shown in a plot below in Figure 24. The theoretical thermal efficiencies were compared at Bean Center with measured efficiencies. The theoretical and measured values are very close and can be seen in Figure 25 [23].

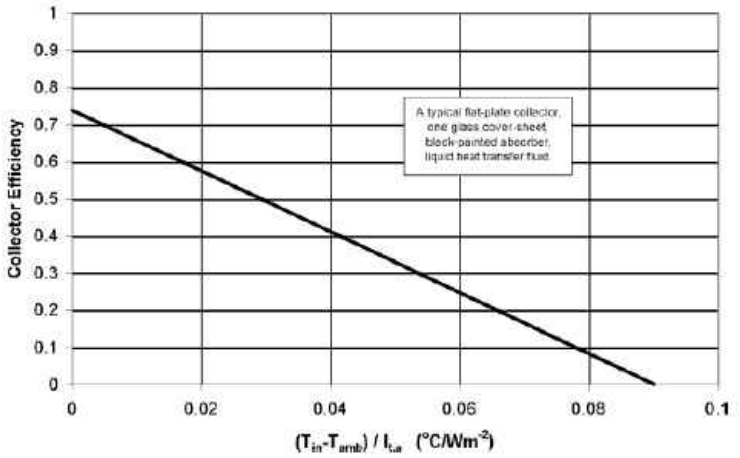

Figure 24: Performance of a typical flat plate thermal collector (ambient temperature 25 ºC) [21].

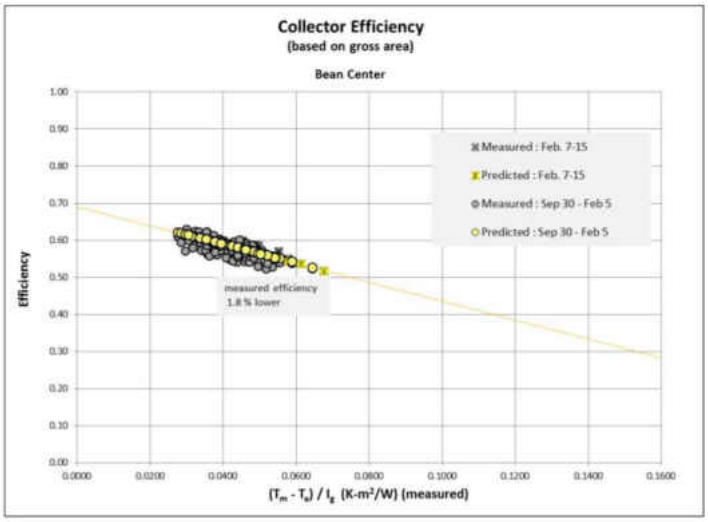

Figure 25: Bean Center – Comparison of measured to predicted collector array efficiency [23].

The actual useful energy gain from the Flat plate solar collector is calculated as:

$$\dot{Q}_u = IA\eta$$

The solar radiation intensity is estimated from the region of California, USA. Using the National Renewable Energy Laboratory (NREL) direct normal solar irradiance maps [22], the annual daily average of solar radiation is estimated as 7.0 kWh/m^2/day. The total land requirement for the solar field is calculated as the total collector surface area, A.

$$A = \frac{\dot{Q}_u}{I\eta}$$

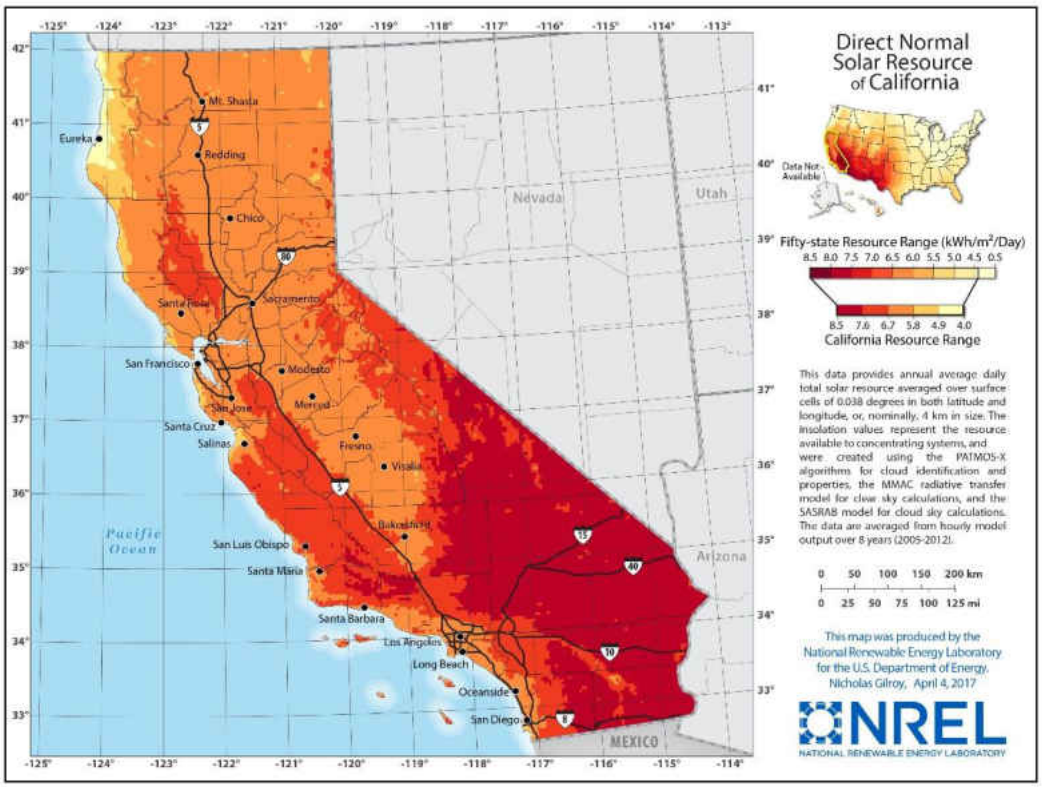

Figure 26: Solar Irradiance map of California in 2017 [22].

Installed-Cost Analysis:

Using NREL report on Flat plate Solar Thermal Collectors, the installation cost of the solar field was estimated. The minimum, average, and maximum installed costs for complete glazed flat plate collector systems are provided in Table 5. A variety of factors contribute to the difference in costs for complete solar hot water systems, including location, system type, and configuration. [23].

Table 5: Unit installation costs of glazed flat plate solar water heating systems [23].

Min ($/m² | $/ft²)		Avg ($/m² | $/ft²)		Max ($/m² | $/ft²)	
$292	$27	$1,538	$143	$3,439	$320

Table 6**Error! Reference source not found.** shows a breakdown of the typical installation costs of a solar thermal system. Solar system component and plumbing costs account for 62% of the total system; the remaining 38% of the costs are associated with engineering design and shipping [3]. The collectors themselves usually cost approximately 20% of the system [23]. The cost structure includes a cost for hot water storage, which may be needed in the SSV system.

Table 6: Solar system cost breakdown [23].

System Component	Percentage	Primary Components
Solar	22%	collectors, roof racking system, pumps, heat exchanger, controller, fluids, storage
Plumbing	40%	pipe, insulation, expansion tanks, valves, vents, and associated appurtenances
Design	38%	shipping, engineering, permitting

B. Thermodynamic Model:

The SSV thermodynamic modeling is described in this section. To accurately model the system, the following assumptions were made:

- The operation is performed at the steady-state.
- Produced freshwater contains no salt.
- The whole desalination system is adiabatic.
- Assumed operating parameters (pressures, temperatures, mass flow rates, salinity) are set to specified values (shown in Table 7) .
- Potential and kinetic energy will be neglected.
- The system is assumed 24-hour operation and water production at rated capacity.
- The average daily solar irradiation is spread over the entire day. A hot water tank is assumed part of the system to retain constant and continuous heat input.

In this section, an energy, mass, and exergy analysis will be performed on the entire system and each subsystem. Expanding the analysis to each subsystem gives further insight into exergy destruction. During the analysis, steam and water tables were used to find enthalpy and temperature values when needed.

The operating parameters and assumptions are shown below:

Table 7: Operating parameter assumptions and constants for Thermo-Economic analysis.

Parameter	Symbol	Value
Operating Assumptions		
Capacity of system	Capacity	100 m^3/day
Boiling Point Temperature	T_{bp}	40 °C
Temperature of seawater into the SSV system	T_{sw}	25 °C
Temperature of Primary into Venturi/out of preheater	T_1	40 °C
Temperature of Primary out of Boiler/into preheater	T_3	42 °C
Entrainment Ratio	ER	10%
Boiler Heat Transfer Coefficient	U_B	4000 W/m^2°C
Preheater Heat Transfer Coefficient	U_{Pre}	1000 W/m^2°C
Velocity	V	1 m/s
Seawater Salinity into system	mfs_{in}	3.5%
Salt mass fraction at brine outlet	mfs_{out}	6%
Primary water pipe radius	r	2.33 inches
Seawater pipe radius	r_{sw}	.7 inches
Constants used in Analysis		
Specific Heat of water	C_P	4.184 kJ/kg°C
Heat of vaporization	h_{fg}	2254 kJ/kg
Specific heat of NaCl	$C_{P,NaCl}$	0.86 kJ/kg°C
Density of water	ρ	1000 kg/m^3

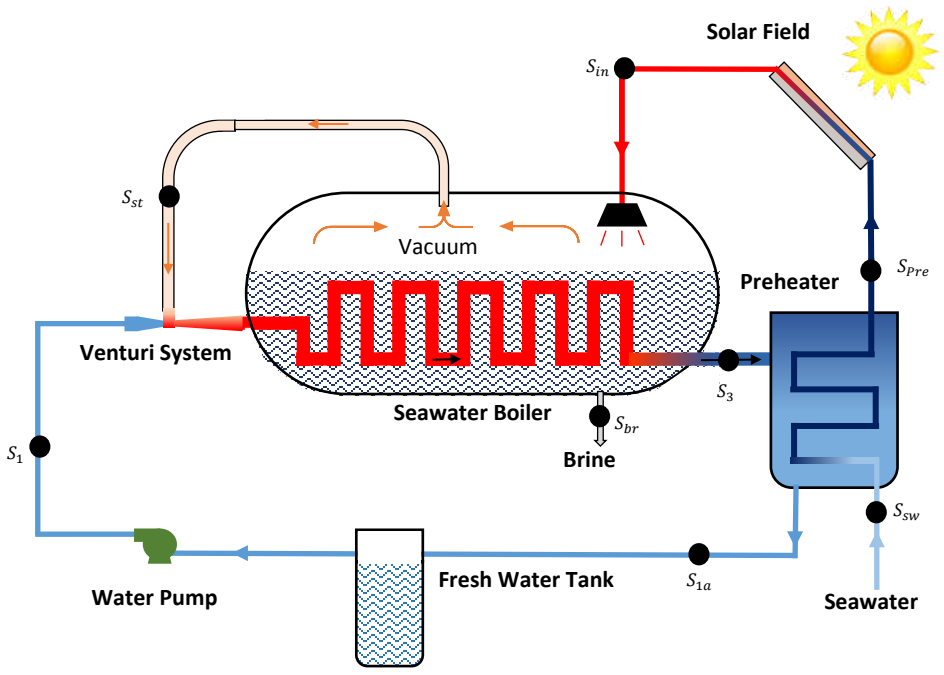

Figure 27: Schematic of Single Stage, Venturi-Driven Desalination.

Mass and Energy Balance:

In a control volume analysis, the steady state equations can be used for mass and energy balance. For the mass and energy analysis, two balancing equations must be equal for the system, as well as for every process:

$$\sum \dot{m}_{in} = \sum \dot{m}_{out}$$

$$\sum H_{in} + Q = \sum H_{out} + W$$

$\sum \dot{m}_{in}$ and $\sum \dot{m}_{out}$ are the summation of mass flow rates into and out of the SSV system, respectively. The heat input, Q, and summation of enthalpy into any control volume, $\sum H_{in}$, must

be equal to the work done by the system, W, the summation of enthalpy out of any control volume, $\sum H_{out}$.

The mass and energy balance for the entire process (black box shown in Figure 28) can be performed as follows:

$$m_{sw} = m_{st}(1 - \frac{mf_{s,in}}{mf_{s,out}})$$

$$m_{sw} = m_{dist} + m_{Br}$$

$$\dot{Q}_{solar} = \sum \dot{H}_{out} - \sum \dot{H}_{in} = (\dot{m}_{dist} * h_{dist}) + (\dot{m}_{br} * h_{br}) - (\dot{m}_{sw} * h_{sw})$$

The product of the mass flow rate of seawater entering the system, $\dot{m}_{sw}$, and the specific enthalpy of the seawater entering the system, h_{sw}, is the enthalpy rate into the SSV system. The enthalpy rate out of the system consists of two flow streams: the distillate outlet and brine outlet. The enthalpy rate of the distillate outlet is the product of the distillate mass flow rate, $\dot{m}_{dist}$, and specific enthalpy of the distillate, h_{dist}. The enthalpy rate of the brine outlet is the product of the brine mass flow rate, $\dot{m}_{Br}$, and specific enthalpy of the brine, h_{br}. The difference between the enthalpy rate into and out of the system is equal to the heat rate required by the solar field, $\dot{Q}_{solar}$.

Pump Work into System: To calculate pump work into the system, the power required to raise the pressure, $(P - P_0)$, of the primary water mass flow rate without steam addition, $\dot{m}_{P1}$, was calculated. The pump efficiency, ϵ, was estimated to be 70%. The pump work into the system will be assumed as power loss of the system.

$$W_{pump} = -\frac{\left(\frac{\dot{m}_{P1}}{\rho} * (P - P_0)\right)}{\epsilon}$$

Note: To determine pump pressure required, the results of the Comsol Multiphysics simulation and approximation of heat exchanger length were used. The pump pressure required was estimated to be 1.6 bar.

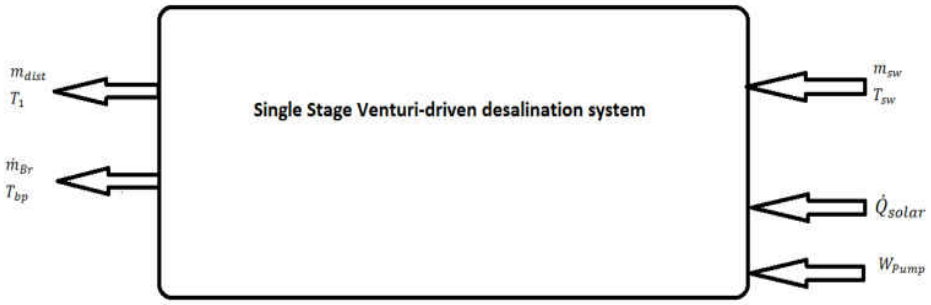

Figure 28: Entire SSV system as a black box.

SSV system is comprised of 5 subsystems: Multfunctional Venturi System, Boiler Heat Exchanger, Solar Collector Field, Preheater Heat Exchanger, and Distillate Outlet. The flow stream properties are calculated below by analyzing each component and can be found in the Thermo-Economic Model Results and Discussion section (Table 10).

Subsystem 1: Multifunctional Venturi System (Figure 29)

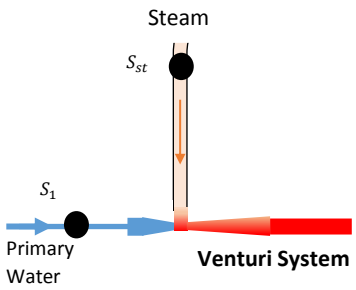

Figure 29: Venturi System Schematic for analysis.

In the Venturi System, we assume the steam and primary water that enter the system also exit the system in the same state and at the same temperature. Mixing will occur in the Venturi System, but condensation will not occur until the flow stream enters the boiler heat exchanger.

$$(\dot{m}_{P1}) + (\dot{m}_{st}) = (\dot{m}_{P2})$$

where $\dot{m}_{st}$ and $\dot{m}_{P2}$ are the mass flow rates of steam and primary water with steam addition, respectively.

Subsystem 2: Boiler Heat Exchanger (Figure 30)

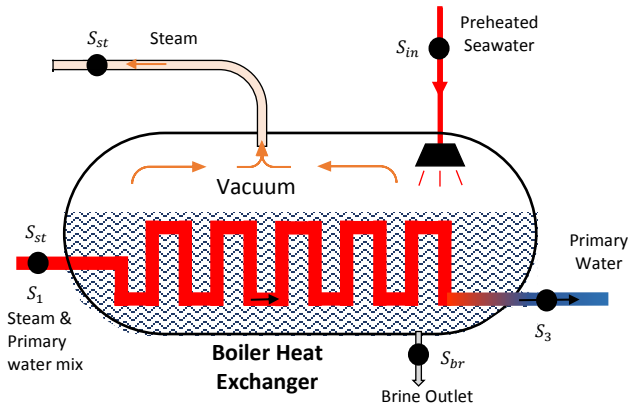

Figure 30: Schematic of Boiler Heat Exchanger from analysis.

The mass and energy balance for the boiler heat exchanger can be calculated as follows:

$$(\dot{m}_{P2}) + (\dot{m}_{sw}) = (\dot{m}_{P2}) + (\dot{m}_{st}) + (\dot{m}_{Br})$$

$$\sum H_{in} + Q_{transf} = \sum H_{Out}$$

$$\dot{Q}_{transf} = \left(C_P * \dot{m}_{P2} * (T_1 - T_3)\right) + \left(h_{fg} * \dot{m}_{st}\right)$$

$$(\dot{m}_{sw} * h_{in}) = (\dot{m}_{st} * h_{st}) + (\dot{m}_{br} * h_{br}) - \dot{Q}_{transf}$$

where, $\dot{Q}_{transf}$, h_{in}, and h_{st} are the heat transferred in the boiler heat exchanger, specific enthalpy of seawater flow stream into the boiler, and specific enthalpy of steam, respectively.

Subsystem 3: Solar collector field (Figure 31)

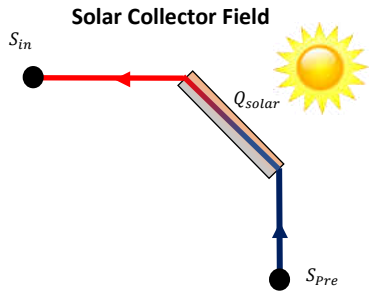

Figure 31: Schematic of Solar Collector Field for analysis.

The mass and energy balance for the solar collector field can be calculated as follows:

$$\dot{m}_{sw} = \dot{m}_{sw}$$

$$\dot{Q}_{solar} = IA\eta = \dot{m}_{sw} C_p (T_{in} - T_{Pre})$$

where T_{in} and T_{Pre} are the temperature of the seawater entering the boiler and the temperature of the preheated seawater entering the solar collector field, respectively.

Subsystem 4: Preheater heat exchanger (Figure 32)

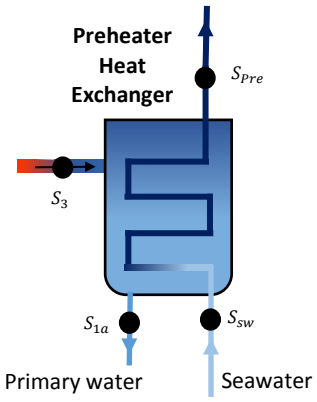

Figure 32: Schematic of Preheater heat exchanger for analysis.

The preheater heat exchanger only transfers heat between the primary water and the inlet seawater. There is no mass transfer. The mass and energy balance for the Preheater heat exchanger can be calculated as follows:

$$\dot{m}_{P2} + \dot{m}_{sw} = \dot{m}_{P2} + \dot{m}_{sw}$$

$$\dot{Q}_{Pre} = \dot{m}_{P2} C_p (T_3 - T_1) = \dot{m}_{sw} C_p (T_{Pre} - T_{sw})$$

where $\dot{Q}_{Pre}$ is the heat transfer rate in the preheater heat exchanger. This inlet represents a heat and mass input into the system.

Subsystem 5: Distillate Outlet (Figure 33)

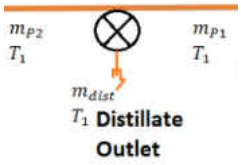

Figure 33: Schematic of Distillate Outlet.

The distillate outlet transfers heat and mass out of the system. The mass and energy balance for the Distillate outlet can be calculated as follows:

$$\dot{m}_{dist} = \dot{m}_{P2} - \dot{m}_{P1}$$

$$\dot{Q}_{out} = \dot{m}_{dist} C_p (T_1 - T_{sw})$$

where $\dot{Q}_{out}$ is heat loss rate due to distillate outlet.

Exergy Analysis

Although the first law is an important tool in evaluating the overall performance of a desalination plant, such analysis dos not take into account the quality of energy transferred. This is an issue of particular importance when both thermal and mechanical energy are employed, as they are in thermal desalination plants. First-law analysis cannot show where the maximum loss of available energy takes place and would lead to the conclusion that the energy loss to the surroundings and the blowdown are the only significant losses. Second law (exergy) analysis is needed to place all

energy interactions on the same basis and to give relevant guidance for process improvement. Exergy is the energy available to be used as work.

The dead state properties are equal to the inlet seawater temperature, T_0, pressure, P_0, specific enthalpy, h_0, concentration, mf_s, and specific entropy, s_0, and are defined as follows:

$$T_0 = 25\ C = 298.15\ K$$

$$P_0 = 101.3\ kPa$$

$$mf_s = .035$$

$$h_0 = mf_s * h_s + mf_w * h_w$$

$$s_0 = mf_s * s_s + mf_w * s_w$$

where mf_w, h_s, h_w, s_s, and s_w are the water mass fraction of flow stream, specific enthalpy of salt at dead state, specific enthalpy of water at dead state, specific entropy of salt at dead state, and specific entropy of water at dead state, respectively. The dead state in an exergy analysis is the state at which no additional energy can be extracted from the fluid or material. The dead state is generally taken to be the environmental steady state conditions.

The steady-state exergy equation is as follows:

$$\dot{E}_{D,tot} = \dot{W}_{pump} + \sum \dot{E}_{in} - \sum \dot{E}_{out}$$

where, $\sum \dot{E}_{in}$, $\sum \dot{E}_{out}$, and $\dot{E}_{D,tot}$ are the total exergy flow rate into the control volume, total exergy flow rate out of the control volume, and exergy destruction in the control volume, respectively. The above equation assumes there is no heat transfer loss to the environment.

The specific exergy of a flow stream, *e,* is expressible in terms of four components:

Physical exergy e^{PH}, kinetic exergy e^{KN}, potential exergy e^{PT}, and chemical exergy e^{CH}

$$e = e^{PH} + e^{PT} + e^{CH}$$

The first three components are evaluated as follows:

$$e^{PH} = (h - h_0) - T_0(s - s_0)$$

$$e^{KN} = \frac{1}{2}v^2$$

$$e^{PT} = gz$$

where g and z are gravitational acceleration and height, respectively.

In this analysis, kinetic, potential, and chemical exergy will be neglected.

Entire Process: The Exergy balance for the entire process (Figure 28) can be performed as follows:

$$\dot{E}_{D,tot} = \dot{W}_{pump} + \sum \dot{E}_{in} - \sum \dot{E}_{out}$$

where,

$$\sum \dot{E}_{in} = \dot{E}_{Q,solar} + \dot{E}_{sw}$$

$$\sum \dot{E}_{out} = \dot{E}_{dist} + \dot{E}_{Br}$$

where $\dot{E}_{Q,solar}$, $\dot{E}_{sw}$, $\dot{E}_{dist}$, and $\dot{E}_{Br}$ are the exergy input from heat transfer in the solar field, exergy flow of seawater into the system, exergy flow of distillate outlet, and exergy flow of brine outlet, respectively. The exergy flow is always in reference to a specific enthalpy and entropy of a restricted *Dead State*. The environment conditions are used as the dead state because that is the state at which no further exergy can be extracted as work. The most appropriate dead state to use is the seawater inlet into the system.

Exergy Inlet: The Exergy entering the system can be broken down into components:

$$\sum \dot{E}_{in} = \dot{E}_{Q,solar} + \dot{E}_{sw}$$

Since $\dot{E}_{sw}$ is defined as the dead state, the exergy rate is equal to zero.

The exergy input from heat transfer is defined as:

$$\dot{E}_{Q,solar} = \left(1 - \frac{T_0}{T}\right) * Q_{solar}$$

where *T* is the temperature at which heat transfer, Q_{solar}, occurs. Since the heat transfer raises the temperature of the seawater, the average seawater temperature in the solar field was used.

Pump Exergy into System: The exergy from work is simply work, W_{pump}. This makes sense because exergy is the energy available to perform work.

Exergy Outlet: The exergy out of the system comes from the pure distillate water leaving the system:

$$\sum \dot{E}_{out} = \dot{E}_{dist} + \dot{E}_{Br}$$

The exergy of the distillate will be saturated water at 40°C and will be compared to the reference dead state.

$$e_{dist} = h_{dist} - h_0 - T_0(s_{dist} - s_0)$$

$$\dot{E}_{dist} = \dot{m}_{dist} e_{dist}$$

where e_{dist} is the specific exergy of the distillate outlet.

The exergy of the Brine will be calculated as pure solid salt. This can change, but I wanted to incorporate the salt flows of the system.

$$e_{br} = h_{Br} - h_0 - T_0(s_{Br} - s_0)$$

$$\dot{E}_{Br} = \dot{m}_{Br} e_{br}$$

where e_{br} is the specific exergy of the brine outlet.

Exergy Efficiency:

The Exergy destruction is equal to:

$$\dot{E}_D = W + \sum \dot{E}_{in} - \sum \dot{E}_{out} = \sum_{i=1}^{j} \dot{E}_{D,i}$$

where, $\dot{E}_{D,i}$ is the exergy destruction in each of the subsystems and $j = 5$.

From the exergy analysis, the exergy efficiency, ε, is defined as follows:

$$\varepsilon = \frac{\sum \dot{E}_{out}}{\sum \dot{E}_{in} + \dot{W}_{pump}}$$

The exergy efficiency is used as the criterion of performance, and the total loss can be broken down in the exergy destruction of each subsystem, or exergy defect. The exergy analysis of each subsystem is carried in a similar process.

Subsystem 1: Multifunctional Venturi System (Figure 29)

The steam and Primary flow stream entering the Venturi System be assumed to exit the Venturi System in the same initial state and temperature. Condensation and mixing will be assumed to occur within the boiler. Therefore, there will be no Exergy destruction in the Venturi System.

$$\dot{E}_1 = \dot{m}_1 e_1 = h_1 - h_0 - T_0(s_1 - s_0)$$

$$\dot{E}_{st} = \dot{m}_{st} e_{st} = h_{st} - h_0 - T_0(s_{st} - s_0)$$

where e_1 and e_{st} are the specific exergy of primary water without steam addition and the specific exergy of steam flow, respectively.

Subsystem 2: Boiler Heat Exchanger (Figure 30)

The exergy destruction for the boiler heat exchanger, $\dot{E}_{D,2}$, can be calculated as follows:

$$\dot{E}_{D,2} = \dot{E}_1 + \dot{E}_{st} + \dot{E}_{in} - \dot{E}_3 - \dot{E}_{st} - \dot{E}_{Br}$$

$$\dot{E}_{in} = \dot{m}_{sw} e_{in} = h_{in} - h_0 - T_0(s_{in} - s_0)$$

$$\dot{E}_3 = \dot{m}_3 e_3 = h_3 - h_0 - T_0(s_3 - s_0)$$

where e_{in} and e_3 are the specific exergy of seawater into the boiler and primary water exiting the boiler.

Subsystem 3: Solar Collector Field (Figure 31)

The exergy destruction for the Solar Collector Field, $E_{D,3}$, can be calculated as follows:

$$E_{D,3} = E_{Q,solar} - (E_{in} - E_{Pre})$$

$$\dot{E}_{Pre} = \dot{m}_{Pre} e_{Pre} = h_{Pre} - h_0 - T_0(s_{Pre} - s_0)$$

where e_{Pre} is the specific exergy of preheated seawater entering the solar field.

Subsystem 4: Preheater heat exchanger (Figure 32)

The exergy destruction for the Preheater heat exchanger, $E_{D,4}$, can be calculated as follows:

$$E_{D,4} = E_{solar} - (E_{in} - E_{Pre})$$

Subsystem 5: Distillate Outlet (Figure 33)

The exergy destruction for the distillate outlet, $E_{D,5}$, can be calculated as follows:

$$E_{D,5} = E_{st} + E_1 - E_2$$

The results of both the energy and exergy analysis can be found in the *Results and Discussion* section of this paper.

C. Economic Model:

Additional assumptions are required for the comprehensive Thermo-Economic Analysis. The analysis in this study assumed a 25-year life of operation for the plant, and that the plant will operate at 100% capacity (100 m^3/day) over the 25-year life. Because the system is designed to be driven mainly by solar energy, approximate values for daily solar insolation, solar thermal efficiency, land cost, and solar collector field cost are estimated. Using the SSV thermo-economic model operating temperatures (Table 10), the solar collector efficiency was estimated to be 70% using Figure 24.

Table 8: Estimates for land and solar parameters used in the economic model.

Solar Insolation	7	kWh/ m^2*day [22]
Solar Thermal input efficiency	70%	[23]
Land Cost Rate	$ 3,020.00	$/acre [13]
Solar Field Cost per acre	500	$/$m^2$ [23]

Capital and operation and maintenance (O&M) costs were also required for a comprehensive economic analysis. Using the average capital and O&M costs of similar technologies (MED & MSF), the costs of the system were accurately estimated [14]. For the average O&M costs, thermal energy and electrical energy were removed using the percentage given in Figure 14.

Table 9: Estimated capital and O&M cost rates for the economic model [14].

	Capital Cost ($/L per day)	O&M ($/m^3)
SSV Desalination	1.4	.05

Note that O&M costs do not include electrical energy or thermal energy costs.

The total cost of the system can be broken down into two types: fixed costs and variable costs. The total cost structure of the SSV system is comprised of three separate cost buckets: Capital costs, $C_{Capital}$, O&M costs, $C_{O\&M}$, and energy costs, C_{Energy}.

Capital Costs:

The Capital Cost is the total investment cost to construct the desalination plant and solar field. The Capital costs includes construction costs, land costs, project financing, project development, and even contingency costs. All capital costs are initial, fixed costs. The total capital cost is approximated using the values in Table 8 and Table 9. In comparison to other thermal desalination systems, the capital cost of solar desalination plants is elevated due to the solar collector field construction.

$$C_{Capital} = C_{desal} + C_{Land} + C_{solar}$$

where C_{desal}, C_{Land}, and C_{solar} are the installation cost of the desalination system, cost of land, and the installation cost of the solar field, respectively.

O&M Costs:

The O&M costs are the total cost of operation and maintenance during the operation of the plant. The O&M includes monitoring, waste discharge, indirect costs, chemicals, labor, and maintenance. The O&M costs will be assumed as variable costs and depend on the amount of clean water produced. The total O&M cost is approximated using the values in Table 9.

Energy costs:

Since the plant is assumed to operate with only solar thermal energy input, the cost of energy only has an electrical energy component for the pump subsystem. Using the pump power and the cost of electricity, the total energy cost was computed.

Discounted Cash Flow Analysis:

To determine the net present value of all cash flows (revenues and costs), each cash flow must be discounted to the present value using a discount or interest rate. This is referred to as a Discounted Cash Flow (DCF) analysis. For this analysis, the construction time period (time from initial investment to the start of commercial operation) will be assumed to last one year, and all Capital costs are allocated at the beginning of the first year (Year 0). Energy and O&M costs will be allocated at the beginning of each year of operation. The present value of each cash flow can be calculated as:

$$PV = \frac{Cash\ Flow}{(1+i)^n}$$

where PV, i, and n are the present value of the cash flow, interest or discount rate, and the number of periods/years between the present and when the cash flow takes place, respectively. The DCF analysis can also be used to determine the Internal Rate of Return (IRR) of a project if

a set price of clean water production is available. IRR is a metric used in capital budgeting to estimate the profitability of potential investments. IRR is a discount rate that makes the net present (NPV) of all cash flows from a particular project equal to zero [50]. For this study, the interest rate on initial investment will be assumed zero. Without determining the financing structure, it would be inappropriate to assume 100% of the investment cost will be in the form of debt financing with a fixed interest rate. The IRR percentage will be the year-over-year ROI of the project for each set price point of clean water production.

Using DCF analysis, cash flow tables were generated for a specified price of water production, and the Internal Rate of Return was calculated. Cash flow tables were made for specified prices, including $\$1.00/m^3$, $\$1.50/m^3$, $\$2.00/m^3$, $\$3.00/m^3$, $\$4.00/m^3$, and $\$5.00/m^3$. Cash flow tables can be seen in the Appendix.

D. Thermo-Economic Model Results and Discussion:

The Thermodynamic model provided the temperature, mass flow rate, enthalpy, and exergy of each flow stream. The properties of each flow stream are shown in Table 10.

Table 10: Flow stream properties solved for using Thermo-Economic Model.

Stream	mass flow rate		Temperature		Enthalpy of stream		Exergy of Stream	
S_1	$\dot{m}_{P1}$	11.57 kg/s	T_1	40 ºC	H_1	1940 kW	E_1	16.49 kW
S_{1a}	$\dot{m}_{P2}$	12.73 kg/s	T_1	40 ºC	H_{1a}	2134 kW	E_{1a}	18.13 kW
S_3	$\dot{m}_{P2}$	12.73 kg/s	T_3	42 ºC	H_3	2240 kW	E_3	23.56 kW
S_{dist}	$\dot{m}_{dist}$	1.16 kg/s	T_1	40 ºC	H_{dist}	194 kW	E_{dist}	1.64 kW
S_{sw}	$\dot{m}_{sw}$	2.78 kg/s	T_{sw}	25 ºC	H_{sw}	283 kW	E_{sw}	0.00 kW
S_{Pre}	$\dot{m}_{sw}$	2.78 kg/s	T_{Pre}	34 ºC	H_{Pre}	390 kW	E_{Pre}	1.65 kW
S_{in}	$\dot{m}_{sw}$	2.78 kg/s	T_{in}	49 ºC	H_{in}	599 kW	E_{in}	10.72 kW
S_{st}	$\dot{m}_{sw}$	1.16 kg/s	T_{BP}	40 ºC	H_{st}	2574 kW	E_{st}	135.0 kW
S_{br}	$\dot{m}_{br}$	1.62 kg/s	T_{BP}	40 ºC	H_{br}	258 kW	E_{br}	2.29 kW

The results of the Thermo-economic model can be seen in Table 11. The model is a representation of a theoretical SSV plant with a capacity of 100 m^3/day. The heat recuperation makes up the vast majority of the heat input required to generate steam. The heat transferred in the boiler encompasses 90.6% (2,678 kW) of the heat required alone. Adding the heat recuperated in the Preheater, the total heat recuperated is 94.3% (2,785 kW) of the heat input required to sustain 100 m^3/day of water production. The remaining heat input (169 kW) is added via the Solar Collector Field. Changes in the entrainment ratio and operating temperatures greatly affects the energy and mass balance of the system.

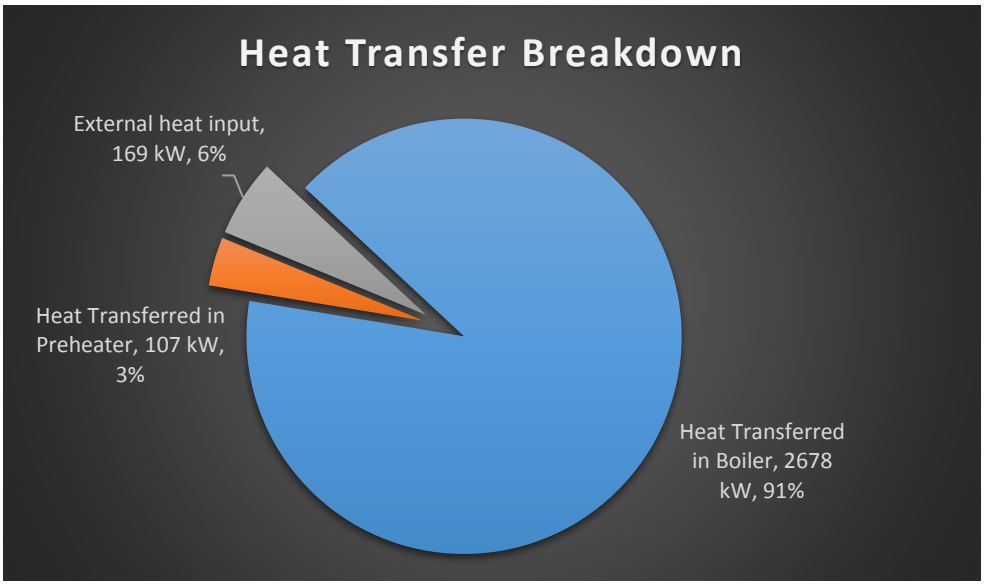

Figure 34: Heat transfer breakdown.

The energy and mass balance indicate high thermal efficiency. The performance ratio, which is the amount of water produced per kg of steam, is 15.4. The performance ratio is directly calculated from the thermal energy requirement. From a thermodynamic standpoint, the SSV system significantly outperforms MSF and MED plants. The results in Table 11 can be compared to other mainstream desalination technologies in Table 1 and mainstream solar desalination technologies in Table 3.

The electrical energy requirements are much lower than other thermal desalination technologies. The SSV system requires only one circulating pump to circulate the primary water cycle and generate a vacuum in the boiler. The same circulating pump provides the motive force to deliver seawater at atmospheric pressure through the preheater, solar field, and into the boiler held at

vacuum pressures. Typically, both MSF and MED require a large number of pumping units, including pumps for seawater intake, distillate product, brine blowdown, and chemical doings.

Table 11: Results from energy and mass balance.

Energy Calculations & Results	
Heat Transfer in Boiler	2678 kW
Heat Transfer in Preheater	107 kW
Heat loss	169 kW
Heat Input by Solar Field	169 kW
Pump Work	0.97 kW
Thermal Efficiency	94.3%
Thermal Energy Requirement	40.6 kWh/m3
Electrical Energy Requirement	0.23 kWh/m3
Performance Ratio	15.4

Table 12: Results from exergy analysis.

Exergy Calculations and Results	
Exergy of Solar Heat Transfer	9.10 kW
Pump Work/Exergy	0.97 kW
Exergy Destruction	6.13 kW
Exergy Efficiency	39%

Table 13: Exergy destruction in each subsystem.

Exergy Breakdown from subsystems:	
Exergy Destruction in Boiler	1.35 kW
Exergy Destruction in Preheater	3.78 kW
Exergy Destruction in Solar Field	0.03 kW
Pump Work/Energy	0.97 kW
Total Exergy Destruction	**6.12 kW**

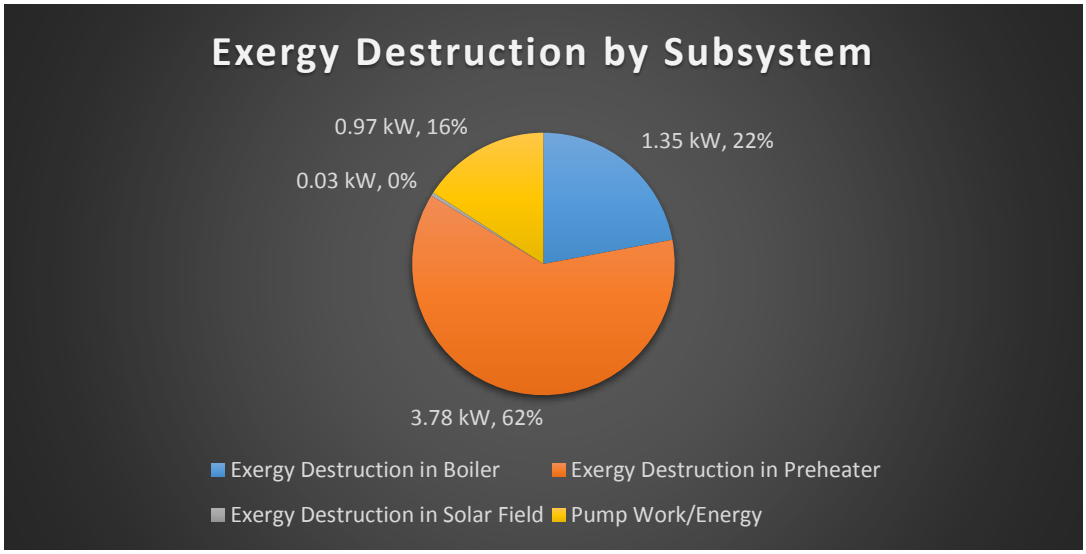

Figure 35: Pie chart of exergy destruction in each subsystem.

The exergy analysis results can be used as a theoretical baseline that will need to be validated by experimental results from a pilot plant. In the SSV system, most of the exergy destruction occurred in the boiler and preheater.

The low operating temperatures reduce the exergy destruction during heat transfer. The brine heater, or boiler, used in MSF usually heats the incoming seawater well above 100 °C. In comparison, the incoming seawater used for heating enters the boiler at 49 °C, shown in Table 10. As seen in Table 12 the exergy efficiency of the SSV system is higher than both MSF and MED.

Thermo-economic Model:

The results of Thermo-Economic Analysis show that the SSV system has high thermal efficiency (comparable to MSF and MED) and very low electrical and thermal energy requirements. Ultimately, SSV desalination achieved a levelized cost estimate of \$0.67/m^3 for the theoretical 100 m^3/day system. It should be mentioned that the unit cost of electricity varies in the study of desalination systems. In Hoseyn Sayyaadi *et al.* [2], the unit cost of electricity used in the model was \$0.03/kWh. In this study, the cost of electricity used was \$0.10/kWh, the average overall cost of electricity in the United States in December 2017 [54]. The low electricity requirements of the SSV system should not be overlooked. When desalination studies use higher, more accurate prices for electricity, the estimated cost of desalination raises significantly. The results of the Thermo-Economic Analysis can be seen below:

Table 14: Levelized unit cost of each cost component for SSV System.

Levelized Costs (\$/m^3)	
Capital Costs	0.61
O&M Costs	0.05
Energy Costs	0.02
Total Levelized Cost	**0.67**

Since the system was analyzed with solar energy as its heat input source, the cost of energy or heat input comes in the form of the capital cost of the solar field. Therefore, the majority of the unit levelized system cost is derived from capital or installation costs. The Capital and O&M costs were calculated using cost rates from actual MSF and MED projects in the Middle East and North Africa. Estimating the Capital and O&M costs using alternative methods, such as component costs, could lead to high error if the cost of some components are missed or a reputable reference source is not found. However, there are many reasons to believe the cost to build and operate an SSV plant would be far less than that of MSF or MED. First, the number of pumps and separate piping systems is greater in MSF and MED. As stated, both MSF and MED require many pumping units, including pumps for seawater intake, distillate product, brine blowdown, and chemical doings. The SSV system has one, single stage of steam generation. This reduces the size and complexity of the plant greatly. Second, the SSV system is designed to operate on 100% heat input from Flat plate solar collectors, which are more costly than conventional heat sources, such as steam or fossil fuels. There are many potential cost saving strategies, including developing a lower-cost alternative solar thermal collector technology or using a hybrid heat input system that utilizes geothermal energy, fossil fuels, or power plant and process plant waste heat. Lastly, the operating and top brine temperature of the SSV system is much lower than that of both MSF and MED. The top brine temperature (TBT) is approximately 40 °C and the max seawater temperature leaving the solar collector field is 49 °C. Most of the SSV system remains around 40 °C. In comparison, the TBT of MED is around 70 °C, and the max seawater temperature of MSF is above 100 °C [3]. The lower temperatures have two benefits: cheaper materials with lower temperature ratings can be used and corrosion issues and

costs will be decreased. Overall, there are many reasons to believe both the installation and O&M costs can be less than the cost ratings used in this study.

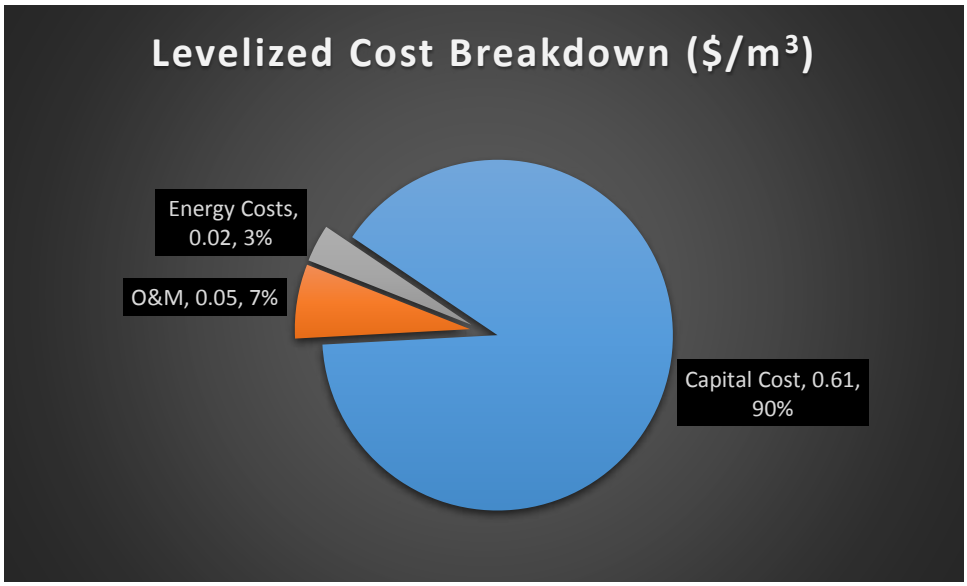

Figure 36: Pie chart of levelized unit cost breakdown.

A main advantage, and a disadvantage of the SSV system is that it is designed to operate solely on solar thermal energy. Unfortunately, the current cost of solar thermal collectors, even cheaper flat plate solar collectors, far exceed the cost of heat input by steam, which is commonly used by other thermal desalination systems. The solar thermal system required for the proposed 100 m^3/day plant is rated at 169 kW, requires 0.2 acres, and has a total installation, or capital, cost of $414,673.

Table 15 is a scenario analysis of the levelized cost of water while varying both Useful Life and Solar Field cost rate. All the cells highlighted in green are scenarios in which the levelized cost of water production is under \$0.50/m^3. In the Thermo-economic model, the levelized cost of the Solar Field alone is \$0.45/m^3 or \$0.055/kWh. Steam, on the other hand, with an estimated cost of \$2 per ton, equates to less than one-tenth the levelized cost of the Solar Field, or \$0.0035/kWh. The model assumes a useful life of 25 years. Since most of the cost associated with the SSV system are upfront, fixed capital costs, the unit cost of the technology is highly dependent on the useful life. If the useful life was increased to 30 years, the unit cost of solar thermal energy input drops to \$0.0093/kWh. A sensitivity analysis for the levelized cost of the Solar Field can be seen in the Appendix (Figure 48). It is worth noting that although the cost of steam may be less costly than solar field heat input, the use of steam requires the desalination system be built in combination with a power plant, greatly limiting the number of potential applications and flexibility of use.

Table 15: Scenario analysis for the LCOW.

Levelized cost with various Useful Life and Solar Field Cost							
	Useful Life = 25 years						
Solar Field Cost=\$500/m^2	\$0.67 /m3	15 years	20 years	25 years	30 years	35 years	40 years
	\$25 /m2	\$0.36 /m3	\$0.29 /m3	\$0.24 /m3	\$0.21 /m3	\$0.19 /m3	\$0.18 /m3
	\$50 /m2	\$0.40 /m3	\$0.31 /m3	\$0.27 /m3	\$0.23 /m3	\$0.21 /m3	\$0.19 /m3
	\$100 /m2	\$0.47 /m3	\$0.37 /m3	\$0.31 /m3	\$0.27 /m3	\$0.24 /m3	\$0.22 /m3
	\$250 /m2	\$0.70 /m3	\$0.54 /m3	\$0.45 /m3	\$0.38 /m3	\$0.34 /m3	\$0.31 /m3
	\$500 /m2	\$1.08 /m3	\$0.83 /m3	\$0.67 /m3	\$0.57 /m3	\$0.50 /m3	\$0.45 /m3
	\$750 /m2	\$1.46 /m3	\$1.11 /m3	\$0.90 /m3	\$0.76 /m3	\$0.66 /m3	\$0.59 /m3
	\$1000 /m2	\$1.84 /m3	\$1.39 /m3	\$1.13 /m3	\$0.95 /m3	\$0.83 /m3	\$0.73 /m3
	\$1500 /m2	\$2.59 /m3	\$1.96 /m3	\$1.58 /m3	\$1.33 /m3	\$1.15 /m3	\$1.02 /m3

Using the Discounted Cash Flow (DCF) analysis, a more realistic picture can be made for the investment potential for an SSV plant. As stated, a major disadvantage of the technology is that 90% of the total cost comes from fixed capital costs. The results of the DCF analysis include the effect of the time value of money, and upfront costs will have more of an impact than costs incurred later in the life of the project. The Cash Flow tables in the Appendix demonstrate the effect of water prices on the IRR of the project. Figure 37 presents the potential rate of return of the 100 m^3/day SSV plant based on the Thermo-Economic model results. The initial investment for the 100 m^3/day SSV project is estimated at $552,135. For comparison, the average returns of the S&P 500 index are approximately 10%, which is less than the 12% IRR of the SSV project at a water price of \$2.00/m^3. In cities such as San Marcos, TX, White House, TN, Laurel, MD, Lakeland, FL, and Lubbock, TX, the utility cost of water is currently around \$7.50/kgal, or \$2/m^3. The average 2016 water escalation rate in the United States was 4.1%. In some areas, such as the Northeast, the average water escalation rate was 8.6% [53].

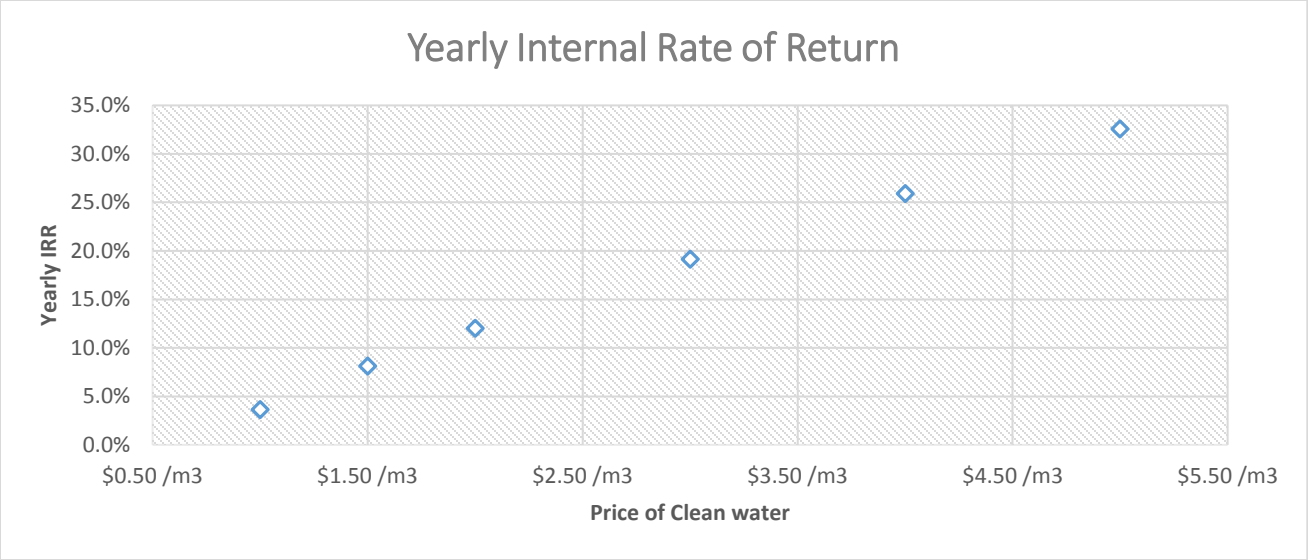

Figure 37: Yearly internal rate of return of a 100 m^3/day SSV plant.

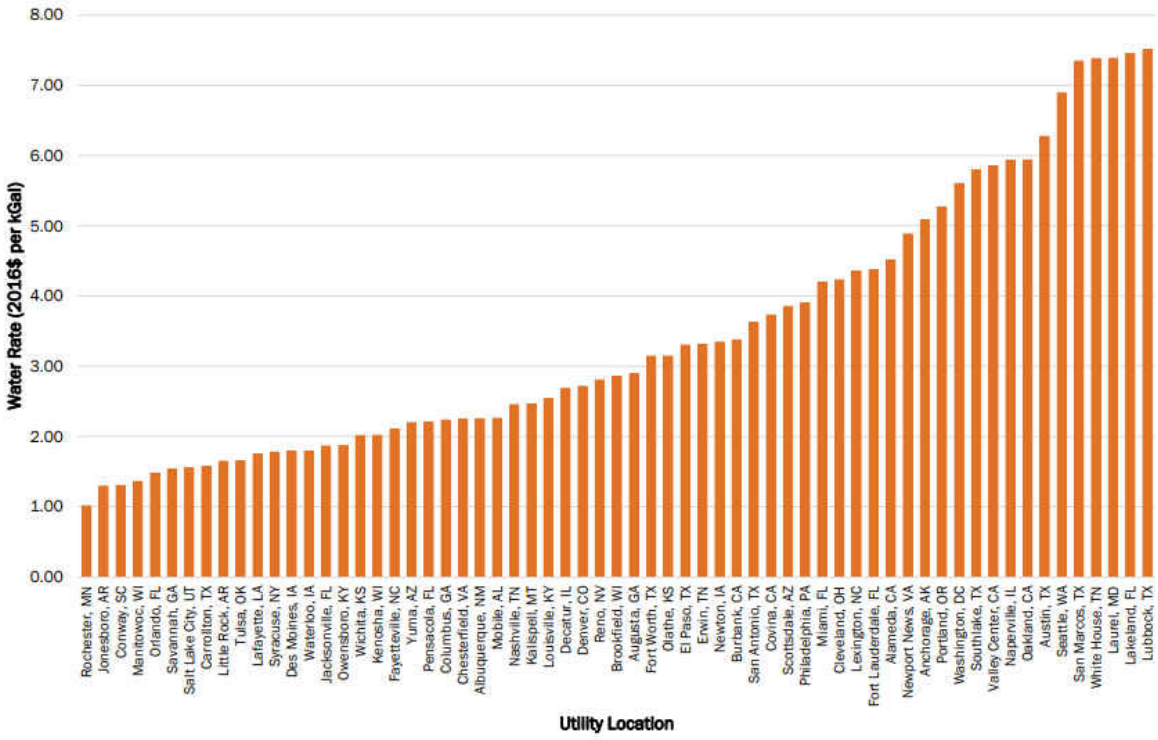

Figure 38: 2016 Utility water rates in selected cities in the United States [53].

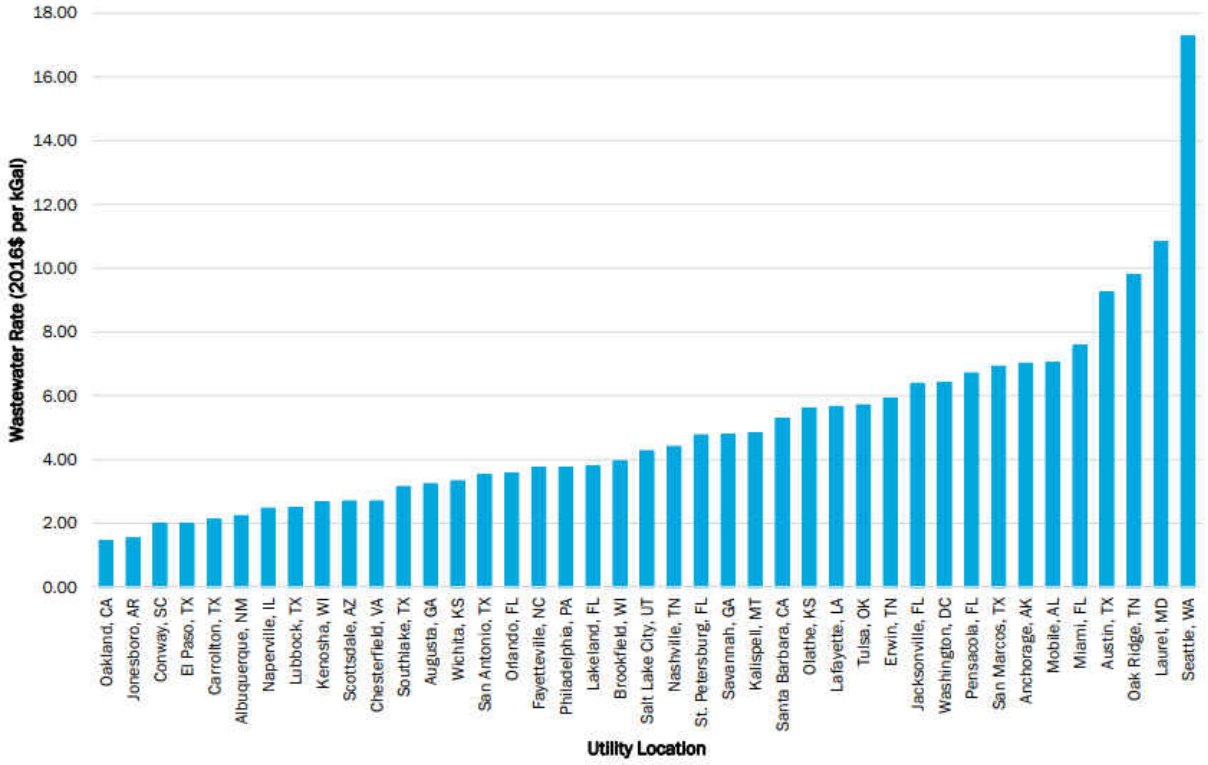

Figure 39: 2016 Utility wastewater rates in selected cities in the United States [53].

Conclusion of Findings: Using referenced U-factor measurements were much more accurate than using heat transfer equations to calculate the overall U-factor in the boiler Heat Exchanger. The heat transfer equations become very complex when accounting for boiling and condensation. The solar irradiance rate used in the model is an average for some areas in California, which a suitor for desalination plants. Compared to other thermal desalination technologies, the thermal ($40.6 kWh/m^3$) and electrical ($.23 kWh/m^3$) energy requirements are significantly below the averages of other thermal desalination technologies. The low thermal energy requirements led to a calculated performance ratio of 15.4. The exergy efficiency of the system was calculated as

39%, which is relatively high and can be attributed to the low temperature of heat transfer in the system.

The anticipated Capital and O&M costs of the system are expected to be much lower than both MSF and MED, but to be provide an economic factor, the average MED costs were used in the model. Land costs are extremely variable and change drastically depending on where the system is developed. However, land costs make up a small percentage of the total cost of the system. The levelized cost of the solar collector field ($0.055/kWh) is over double the cost of steam heat input ($0.0035/kWh) used in other thermal desalination systems. However, there are clear benefits to using renewable energy sources and because the cost of solar thermal energy is a fixed cost, increasing the useful life of the proposed plant can decrease the cost below that of steam heat input. A main advantage found by the Thermo-Economic analysis is that the electrical energy costs are greatly reduced. If higher, more accurate electricity costs were used in other thermal desalination studies, the resulting cost of the system would increase greatly.

VII. CHAPTER 7:

CONCLUSION

A. Primary contributions of this study:

This paper introduces the concept of Single-Stage Venturi-driven Desalination, a single stage, thermal desalination system using a multifunctional Venturi water ejector to create a simple system and reduce the cost of desalinated water. The system requires only low-grade solar heat (< 60 ºC) mainly to supplement the heat loss during operation. As compared to the conventional methods of solar desalination, such as MSF, MED, and RO, the proposed system has the following intellectual novelties: **First,** the novel multifunctional water ejector integrates a vacuum pump for steam production, a compressor for condensation, and a starter for heat recuperation. **Second**, only residential-grade solar water heating is needed for the heat demand which greatly reduces the production cost of desalination, as compared to those systems using concentrated solar power (CSP). **Third**, the proposed system is operated standalone based solely on solar energy.

The SSV system relies on the efficient performance of the Venturi water-ejector system. The Venturi System was studied using a CFD simulations and experimental testing. The experimental results demonstrated that the multifunctional Venturi water ejector could simultaneously act as a vacuum pump for steam production, a compressor for condensation, and a starter for heat recuperation. During experimental tests, the Venturi System achieved a vacuum pressure of .07 bar, equivalent to a boiling point temperature of 40°C, during boiling. The experimental results came from off-the-shelf Venturi nozzles. With high-performance, custom-built Venturi nozzles, it is anticipated that low vacuum pressures and higher entrainment ratios are possible. The CFD

simulations produced performance curves for Venturi flow characteristics (CFD Experiment 1) and heat exchanger behavior (CFD Experiment 2) with a portion of heat exchanger added to the model. The CFD Experiment 1 results concluded that the performance of the Venturi System was not negatively affected by scaling up the system, a conclusion validated by Preliminary Experiment results. It also concluded that pump pressure can be used as a control parameter to control vacuum pressure and primary flow rate without effecting entrainment ratio. The CFD Experiment 2 results determined the effect of Primary inlet pressures, Heat Transfer Coefficient, and Boiling point temperature on heat exchanger properties like temperatures, and heat exchanger efficiency.

A Thermo-Economic analysis, using results from the CFD simulations and experimental tests as operating parameters, was created as a baseline estimate for the thermodynamic and economic performance of the SSV system. The rated capacity of the theoretical SSV plant was 100 m^3/day. The results of the thermodynamic aspect of the study determined the thermal (40.6 kWh/m^3) and electrical (.23 kWh/m^3) energy requirements, performance ratio (15.4), and exergy efficiency (39%). The exergy destruction came mostly from the Preheater (62%) and Boiler (22%). Adding an economic analysis to the model, the costs of the system were estimated. The cost breakdown was divided into three categories, Capital costs, O&M costs, and energy costs that were levelized and accounted for 90%, 7%, and 3% of the entire system cost, respectively. The high capital fixed costs of the SSV system make the levelized cost highly sensitive to the useful life of the system (Figure 48). *The estimated levelized cost the SSV system was calculated to $0.67/$m^3$* (without time value of money). Comparing the estimated levelized cost to other solar desalination technologies in Table 3, the baseline SSV system cost is lower than any solar

thermal desalination technology and falls within \$0.01/m^3 of the RO/Solar Pond cost estimates. A Discounted Cash Flow analysis was performed to calculate the IRR of an SSV project for different price points of clean water. The upfront cost for a 100 m^3/day SSV plant is estimated as \$552,135. For a water rate of \$2.00/m^3, the IRR of the SSV project will be above 12%, outpacing the average S&P 500 returns [50]. The results of the economic analysis were compared to the 2017 cost of water and wastewater in selected US cities prepared by the Department of Energy. The estimated levelized cost of \$0.67/m^3 falls below the Utility water rates in 35 out of the 61 US cites studied. As traditional water sources are depleted or degraded, the cost of water will continue to rise in the US as evidenced by the average water escalation rate of 4.1% [53].
The results of this paper propose and support a novel desalination system that can be a cost-competitive alternative to current solar desalination technologies. Due to the low cost of the system, coupled with the zero carbon emissions and high efficiencies, the SSV system is a great candidate for clean water production in both urban and rural systems. In cities, the SSV system can be utilized on the tops of large buildings or, at larger scales, in the center of large communities. Industrial customers can own and operate their own, on site, system with ease. Rural areas have the excess space for large solar fields and low land costs to make the SSV system very economical.

Unlike the complex MSF, MED, and RO designs, the system can be modular and portable, does not require high grade heat from power plants or fossil fuels, and can potentially achieve a true Zero Liquid Discharge. These attributes make the technology ideal for emergency situations, such as hurricanes, droughts, or attacks, where the modular system can be deployed quickly, and deliver clean water to areas while being removed from the power grid.

B. Widening the scope of research performed in this paper:

CFD Simulations:

The model of the multifunctional Venturi ejector provided quick analysis of performance when parameters were changed. To provide more value, a 3D model with additional components should be built. The boiler should be added to the model to determine how the steam flow rate is affected in each test simulation. Additionally, adding a constraint to avoid negative pressure readings will increase the usefulness of the model.

In general, a more comprehensive model of the system will provide a quick method of analysis when the system has changes made to it. To incorporate more of the subsystems and a multiphase model of the boiler and Venturi nozzle, the model will become extremely complex and will require both a skilled CFD professional and high-performance computer.

Experimental testing:

The system is very dynamic, and the prototype quickly gains complexity when adding more components. Sensors and tight system parameters are necessary to control the system. Funding for a higher-grade pump, Venturi ejector, and larger scale components will greatly improve results and analysis. Using the current prototype design, it will be useful to develop a fully-functioning pilot plant to elevate maturity of project and start commercialization of technology. The goal is to incorporate more aspects into the system and sustain a rated capacity of 100 m^3/day at the current cost estimate of \$0.67/m^3.

Currently, this project has submitted a proposal for funding to the Department of Energy (DOE) in the Office of Energy Efficiency and Renewable Energy (EERE). The funding opportunity number is DE-FOA-0001778. In collaboration with Idaho National Laboratory, Old Dominion University will use any EERE funding to demonstrate the innovative desalination system. Normally, an exergy analysis will be performed on an existing desalination system as an analysis tool. In this study, a theoretical exergy and energy analysis was performed as a baseline for the performance of a novel technology, SSV desalination. In the future, the baseline results should be compared to experimental results of a pilot or operational SSV desalination plant.

Thermo-Economic Analysis:

A more comprehensive prototype will provide greater insights into the various costs of the system. Also, as the computational model integrates more subsystems, the results can be compared the baseline results calculated in the Thermo-Economic Analysis. A vital aspect of the analysis is the heat transfer coefficients used in the model. The referenced heat transfer coefficients in the boiler can range greatly from 1000-15000 $kW/m^2°C$, and until experimental results are found, the estimate may have a large error.

Other subsystem costs, such as thermal storage and municipality pipelines, will likely be added. Some desalination project cost models include municipality pipeline costs, and some do not. At this point, thermal storage may provide benefit to the system, but until a pilot plant is built, it is not necessary in the calculations.

C. Future Research:

There is significant room to add to the foundational research performed in this study. On all fronts, (CFD Simulations, Experimental testing, and Thermo-Economic Analysis) additional studies can help validate and also improve the results of this paper.

The performance of the system is highly dependent on high heat transfer efficiency in the boiler. Strategies to optimize the heat transfer within the boiler to minimize the size of the boiler and system overall will have a large impact in the success of the technology. Below are specific areas of research that can greatly improve the design, performance, and validity of SSV desalination.

Low-Cost, Low-Grade Solar Systems:

Future research should consider solar systems that can produce low-grade heat very cheaply. Cheap low-grade heat is the key to the low-cost of clean water using the system. Low-cost, efficient solar systems will also reduce the land requirement of the system, opening up new applications for portable and modular systems that can be deployed quickly. The current cost rate of Flat plate solar collector systems ($\$500/m^2$) drastically increases the cost of the system. Research should pursue other potential sources of cheap low-grade heat, such as non-concentrated solar systems, geothermal sources, and process waste heat, that can be integrated with system to produce clean water.

CFD simulations:

The computational model needs to be more inclusive of other subsystems to provide great value and results. Next steps involve integrating more aspects of the system to see if modeling results agree with theoretical and experimental.

Zero Liquid Discharge:

The question still remains whether it is possible or practical to run the SSV system at saturated salt concentration. Operating in such a condition will allow salt to accumulate at the bottom of the boiler and be removed periodically. This is a true Zero Liquid discharge solution. Corrosion and boiling point elevation are the main concerns. The boiling point temperature may need to be depressed further to make the solution possible.

Advanced Venturi System designs:

New innovations to the multifunctional Venturi water-ejector, specifically used for this system, will provide better operation of the system. It may be possible to construct a variable-sized water ejector, which allows the total size and area ratio to be manipulated. If the total size and area ratio can be manipulated during operation, a sophisticated control system can be created to dynamically control parameters such as entrainment ratio and vacuum pressure in the boiler. Incorporating a variable speed pump, it is possible to control additional parameters like pump pressure, primary water velocity, electrical energy consumption, and efficiency.

Greenhouse Insulation system:

A low-profile greenhouse, encapsulating the system, has been theorized to eliminate heat loss through walls from the system. In many hot, arid regions, a standard greenhouse can reach temperatures of over 140°F. If the greenhouse and surrounding environment can act as a heat source, rather than a heat sink, insulating the system may not be necessary, further reducing costs. Instead, adding more heat transfer surface between the environment and system through radiators and fins may increase the system efficiency. Since the high cost of the SSV system is mainly attributed to the high cost of thermal solar energy, any reduction in energy required can have large cost savings.

Ending Remarks

This paper introduces a novel desalination technology, SSV desalination. SSV desalination is a carbon-free and cost competitive solution to the evolving issue of water scarcity. This paper provides a baseline performance for SSV desalination but does not provide any optimization of operating parameters or system configuration. It is encouraged to further analyze the system and develop strategies to further reduce cost, enhance performance, and increase the number of applications of the system. Going forward, there are many different areas of research that can improve upon the results within this paper and increase the technological readiness level of the SSV desalination technology.

"Success is not final, failure is not fatal: it is the courage to continue that counts."

-Winston Churchill

References

[1] - M. Al-Shammiri, M. S. (1999). Multi-effect distillation plants: state of the art. *Desalination, 126*, 45-59.

[2] - Hoseyn Sayyaadi, A. S. (2010). Thermoeconomic optimization of multi effect distillation desalination systems. *Applied Energy, 87*, 1122-1133.

[3] - Kalogirou, S. A. (2005). Seawater Desalination using renewable energy sources. *Progress in Energy and Combustion Sciences, 31*, 242-281.

[8] - H. Sharon, K. S. R. (2015). A review of solar energy driven desalinationn technologies. *Renewable and Sustainable Energy Reviews, 41*, 1080-1118.

[9] - M. Shatat, S. B. R. (2012). Water Desalination Technologies Utilizing Conventional and Renwable Energy Sources. *International Journal of Low-Carbon Technologies, 9*.

[10] - Ali Al-Karaghouli, L. L. K. (2013). Energy consumption and water production cost of conventional and renewable-energy-powered desalination processes. *Renewable and Sustainable Energy Reviews, 24*, 343-356.

[12] - Noreddine Ghaffour, T. M. M., Gary L. Amy. (2013). Technical Review and Evaluation of the Economics of Water Desalination: Current and Future Challenges for Better Water Supply Sustainability. *Desalination, 309*, 197-207.

[13] - Agriculture, A.-T. H. P. o. (2017). Farmland Value Guide. Retrieved from agweb.com/land/farmland-value-guide/

[14] - Solutions, A. W. (2016). *Desalination Technologies and Economics: Capex, OPEX, & Technological Game Changers to Come*. Retrieved from

[17] - P.G. Youssef, R. K. A.-D., S.M. Mahmoud. (2014). Comparative Analysis of Desalination Technologies. *Energy Procedia, 61*, 2604-2607.

[21] - Struckmann, F. (2008). Analysis of a Flate-Plate Solar Collector. *Heat and Mass Transport*.

[22] - Laboratory, N. R. E. (April 4, 2017). *Solar Maps*. Retrieved from https://www.nrel.gov/gis/solar.html

[23] - NREL. High Performance Flate Plate Solar Thermal Collector Evaluation.

[24] - C. Mustacchi, V. V. (1981). Solar Desalination - Design, Performances, Economics. *Sogesta*.

[25] - JA Eibling, S. T., GOG Lof. (1971). Solar Stills for community use - digest of technology. *Solar Energy*.

[26] - Daniels, F. (1974). Use of the sun's energy [Press release]

[27] - Tata, A. (1980). Solar Assisted Desalination Pilot Plant. *Snia Techint SpA*.

[28] - S.M.A. Moustafa, D. I. J., H.I. El-Mansey. (1985). Performance of a self-regulating solar multistage flash desalination system. *Solar Energy, 35*(4), 333-340.

[29] - Kalogirou, S. (1995). *The application of solar desalination for water purification in cyprus.* (Ph.D), University of South Wales,

[30] - Eduardo Zarza, J. I. A., Javier Leon. (1991). Solar Thermal desalination project at the Plataforma Solar de Almeria. *Solar Energy Materials, 24*, 608-622.

[31] - El-Nashar, A. M. (1992). Optimizing the Operating Parameters of a Solar Desalination Plant. *Solar Energy, 48*(4), 207-213.

[32] - Ali M. El-Nashar, A. A. A.-B. (1998). Exergy losses in multiple-effect stack seawater desalination plant. *Desalination, 116*, 11-24.

[33] - Kalogirou, S. A. (2003). Solar Thermal Collectors and applications. *Progress in Energy and Combustion Sciences, 30*, 231-295.

[34] - Aly, S. E. (1984). Energy Savings In Distillation Plants by using Vapor Thermo-Compression. *Desalination, 9*, 37-56.

[35] - M.A. Darwish, N. M. A.-N. (1987). Energy Consumption and Costs of Different Desalting Systems. *Desalination, 64*, 83-96.

[36] - O.A. Hamed, K. A. A. (1994). An assessmenet of a ejectocompression desalination process. *Desalination, 96*, 103-111.

[38] - Karthick Palani, S. P. (2013). A numerical analysis of novel liquid-gas Jet Ejector. *Journal of Engineering Research and Applications (IJERA), 3*(4), 1644-1654.

[39] - Kalogirou, S. (1996). Survery of Solar Desalination Systems and System Selection. *Pergamon*.

[40] - Galvan, R. M. M. (1979). Solar Multistage Flash Evaporation (SMSF) as a solar energy application on desalination processes. *Desalination, 31*, 545-554.

[43] - Armstrong, M. T. A. H. E. S. F. P. R. (2011). A comprehensive techno-economical review of indirect solar desalination. *Renewable and Sustainable Energy Reviews, 15*, 4187-4199.

[44] - El-Nashar, A. M. (2001). Congeneration for power and desalination - state of the art review. *Desalination, 134*, 7-28.

[47] - Goosen, N. G. J. B. H. M. M. F. A. (2015). Renewable energy-driven desalination technologies: A comprehensive review on challenges and potential applications of integrated systems. *Desalination, 156*, 94.

[49] - Data, G. W. I. D. (2017). *IDA Desalination Yearbook*. Retrieved from

[50] - Investopedia. Retrieved from https://www.investopedia.com/terms/d/dcf.asp

[52] - Toolbox, E. Water - Saturation Pressure. Retrieved from https://www.engineeringtoolbox.com/water-vapor-saturation-pressure-d_599.html

[53] - Energy, O. o. E. E. a. R. (2017). *Water and Wastewaster Annual Price Escalation for Selected Cities across the United States*. Retrieved from

[54] - (EIA), U. S. E. I. A. (2018). *Electric Power Monthly with Data for December 2017*. Retrieved from

[55] - (EERE), O. o. E. E. a. R. E. (2017). *Funding Opportunity Announcement: Solar Desalination (DE-FOA-0001778)*. Department of Energy.

[56] - Hyperphysics. Bernoulli Equation. Retrieved from http://hyperphysics.phy-astr.gsu.edu/hbase/pber.html

[57] - IEEE. Ejectors and Eductors Information. Retrieved from https://www.globalspec.com/learnmore/manufacturing_process_equipment/fluid_processing_equipment/eductors

Appendix

Table 16: Vapor pressure table for liquid water [52].

Temperature	Water saturation pressure		
[°C]	[kPa], [100*bar]	[atm]	[psi]
0.01	0.61165	0.0060	0.088712
2	0.70599	0.0070	0.10240
4	0.81355	0.0080	0.11800
10	1.2282	0.0121	0.17814
14	1.5990	0.0158	0.23192
18	2.0647	0.0204	0.29946
20	2.3393	0.0231	0.33929
25	3.1699	0.0313	0.45976
30	4.2470	0.0419	0.61598
34	5.3251	0.0526	0.77234
40	7.3849	0.0729	1.0711
44	9.1124	0.0899	1.3216
50	12.352	0.122	1.7915
54	15.022	0.148	2.1788
60	19.946	0.197	2.8929
70	31.201	0.308	4.5253
80	47.414	0.468	6.8768
90	70.182	0.693	10.179
96	87.771	0.866	12.730
100	**101.42**	**1.001**	**14.710**
110	143.38	1.42	20.796
120	198.67	1.96	28.815
130	270.28	2.67	39.201
140	361.54	3.57	52.437
150	476.16	4.70	69.061
160	618.23	6.10	89.667
180	1002.8	9.90	145.44
200	1554.9	15.35	225.52
220	2319.6	22.89	336.43
240	3346.9	33.03	485.43
260	4692.3	46.31	680.56
280	6416.6	63.33	930.65
300	8587.9	84.76	1245.6
320	11284	111.4	1636.6
340	14601	144.1	2117.7
360	18666	184.2	2707.3
370	21044	207.7	3052.2

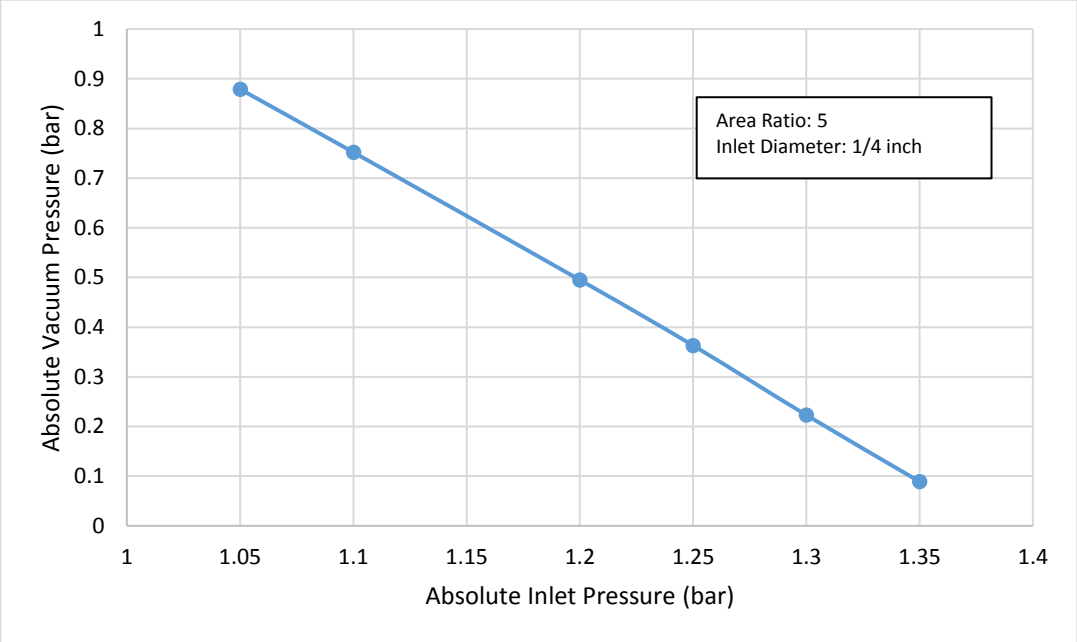

Figure 40: Inlet pressure vs. vacuum pressure, performance curve from CFD Simulation Set 1.

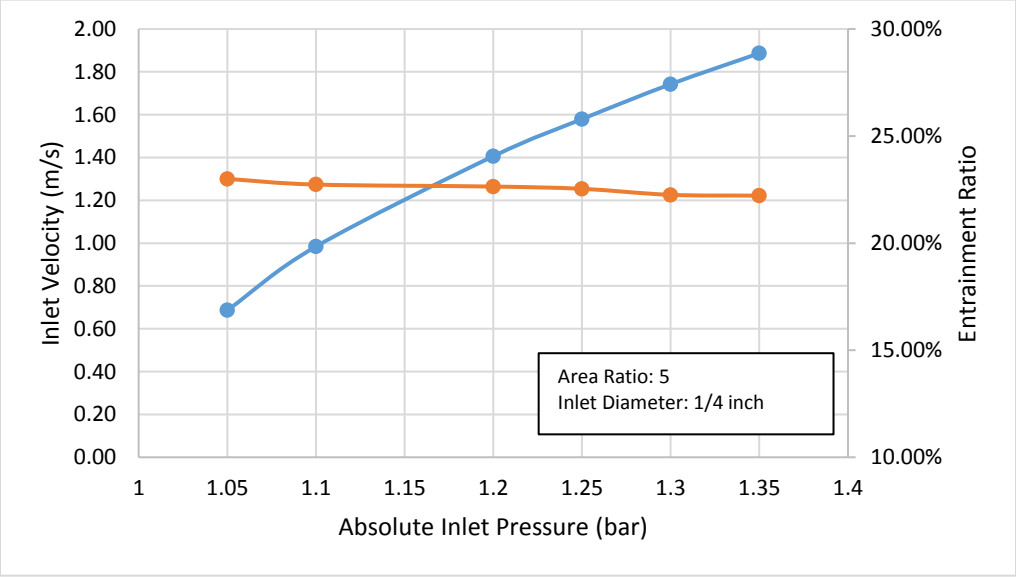

Figure 41: Effect of inlet pressure on entrainment ratio and inlet velocity, performance curve from CFD Simulation Set 1.

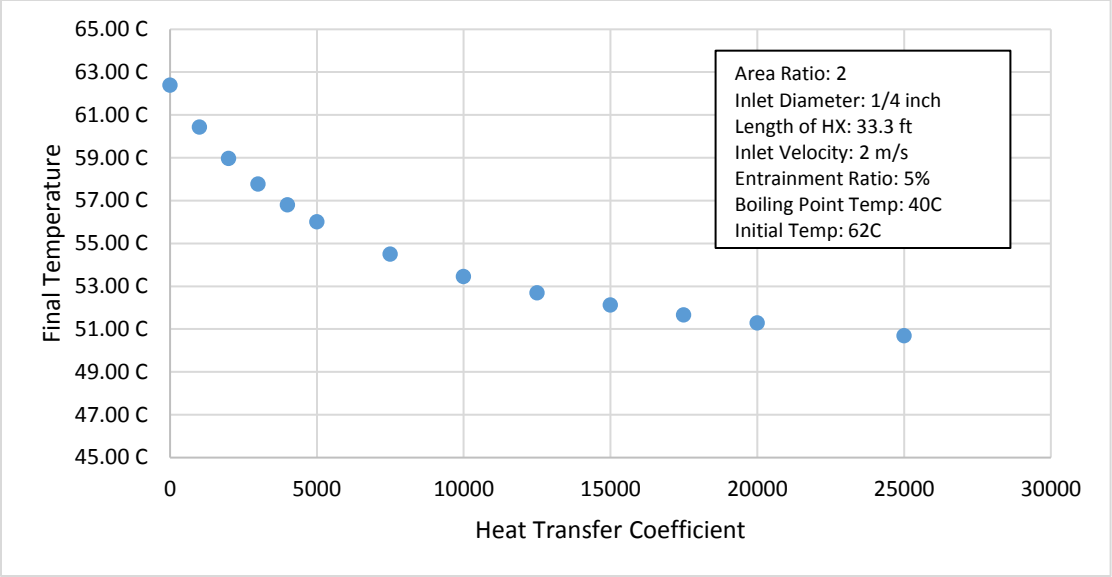

Figure 42: Final temperature vs heat transfer coefficient, performance curve from CFD Simulation Set 2.

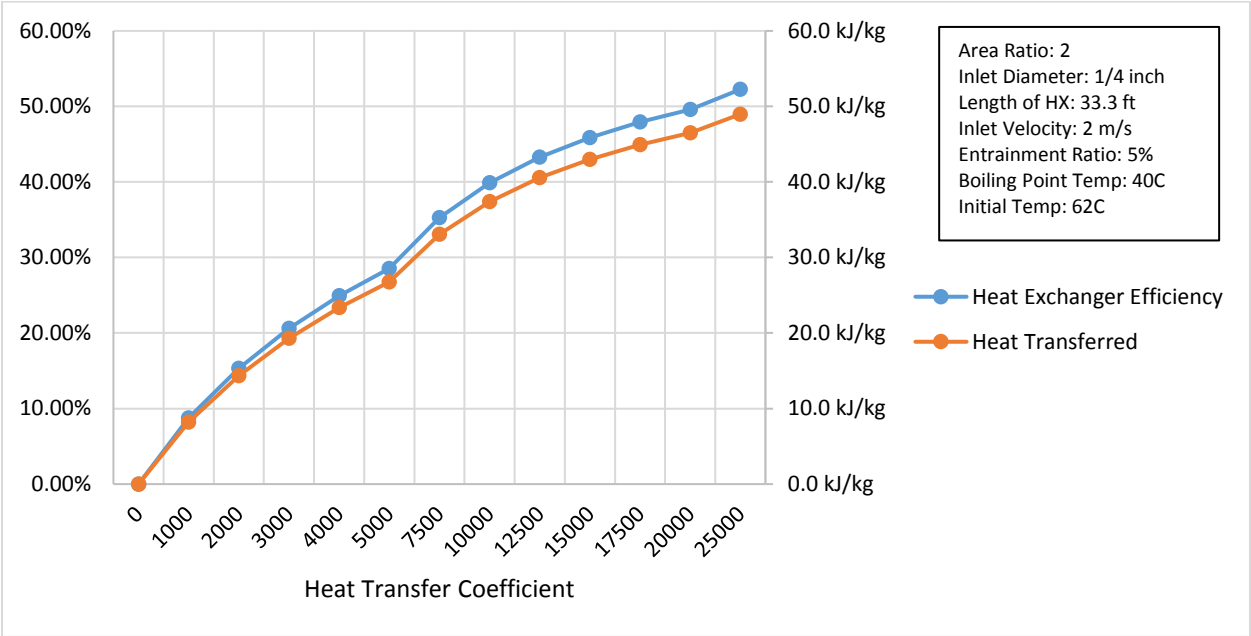

Figure 43: Heat transfer coefficient effect on heat exchanger behavior, performance curve from CFD Simulation Set 2.

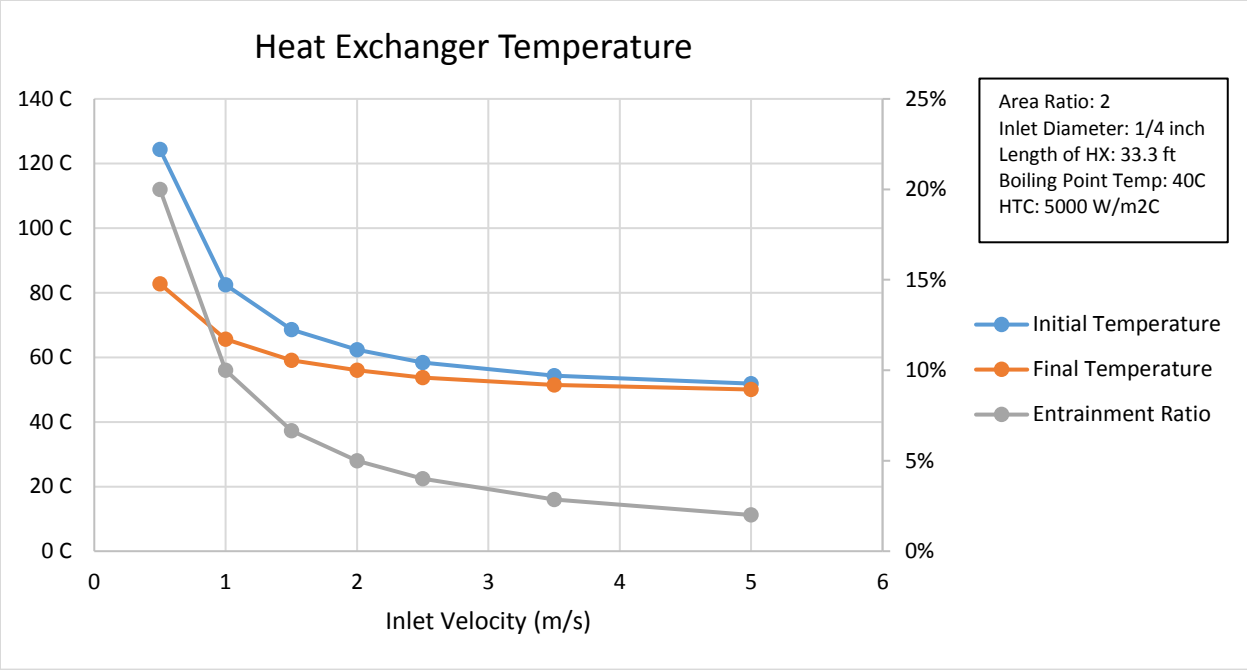

Figure 44: Inlet velocity vs heat exchanger temperatures, performance curve from CFD Simulation Set 2.

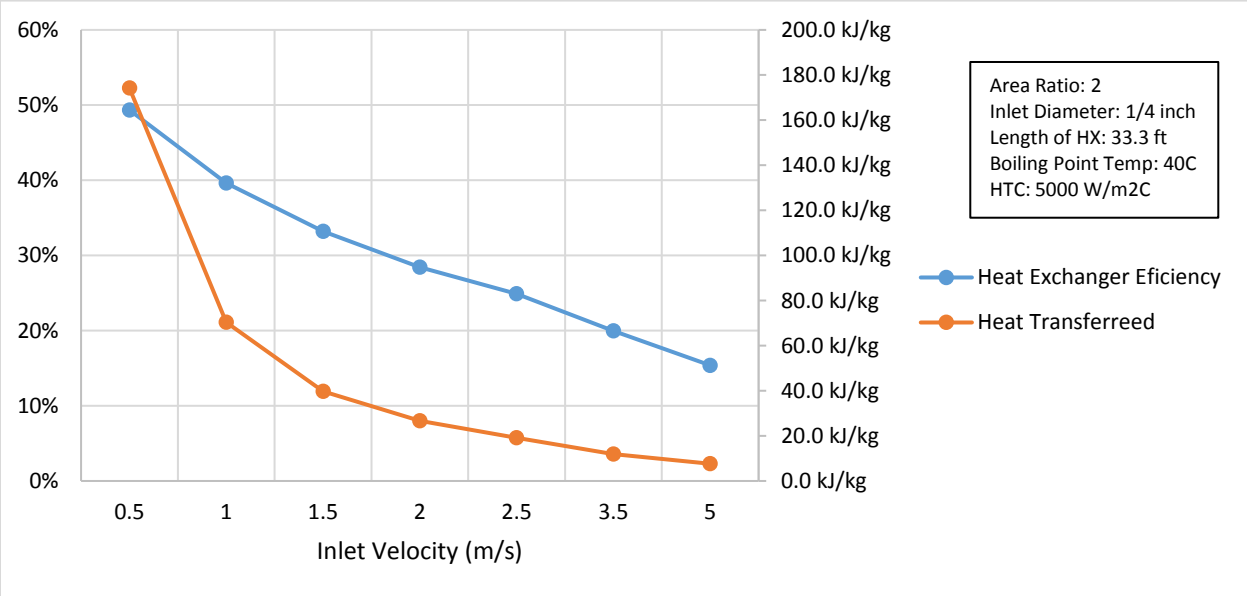

Figure 45: Primary inlet velocity effect on heat exchanger behavior, performance curve from CFD Simulation Set 2.

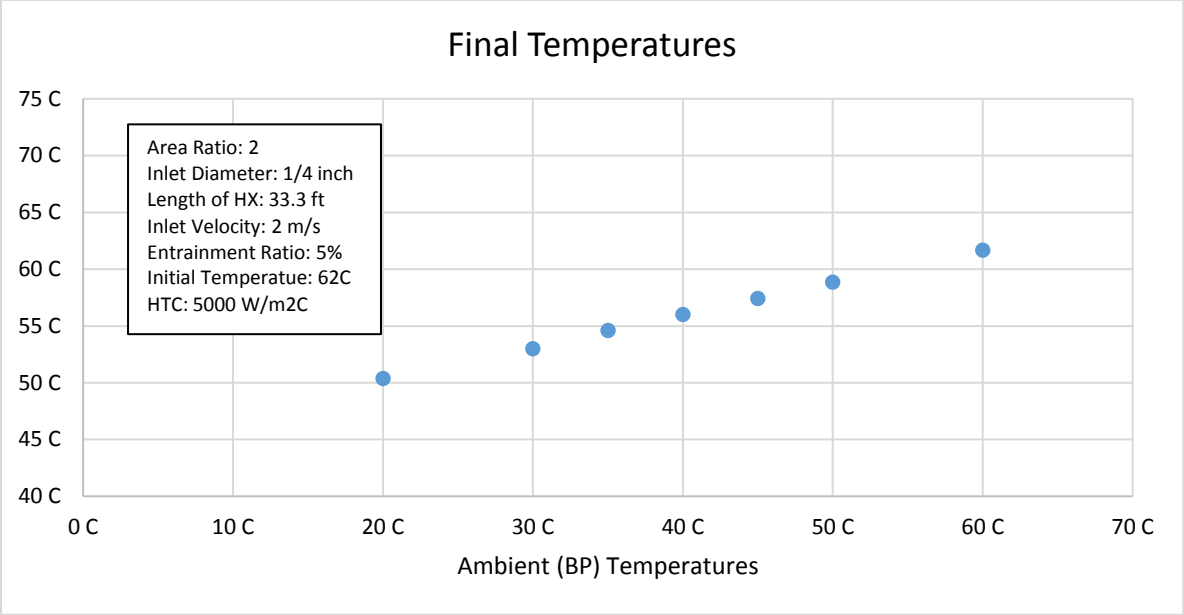

Figure 46: Boiling point temperature vs heat exchanger final temperatures, performance curve from CFD Simulation Set 2.

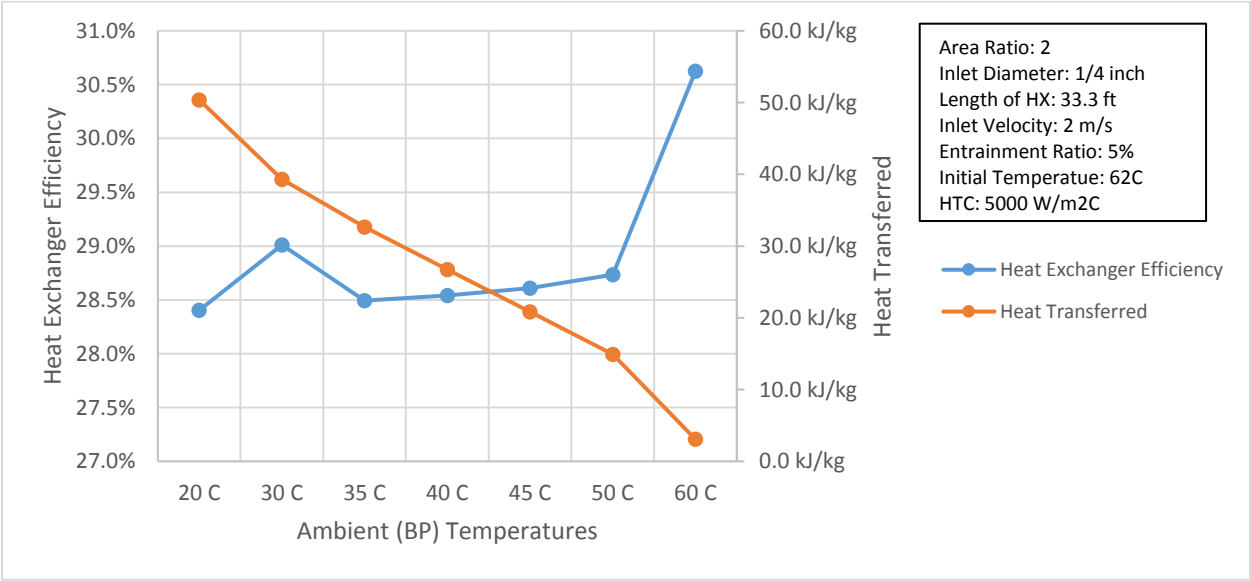

Figure 47: boiling point Temperature effect on heat exchanger behavior, performance curve from CFD Simulation Set 2.

Table 17: Prototype test demonstrating the vacuum pressure can be maintained during boiling.

Time	HX Temp (F)	Vacuum Pressure (Bar)	Note 1
1	112	0.35	Heater On
2	114	0.35	
3	140	0.35	
4	160	0.35	
5:30	172	0.3	
6	174	0.3	
7	175	0.35	
8	170	0.35	
9	170	0.35	
10	170	0.35	Pump Off
13	185	0.5	

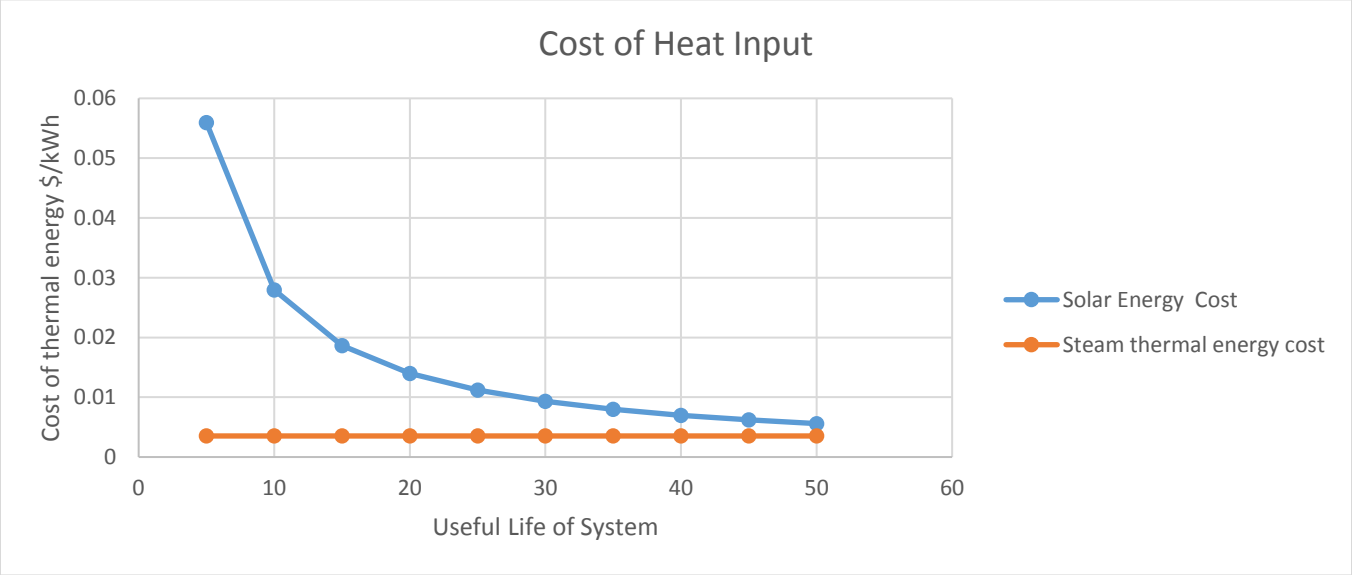

Figure 48: Sensitivity analysis of the unit cost of solar thermal collector field.

Table 18: Table of cash flows for 100 m^3/day SSV project with water price at \$1.00/m^3.

Price of clean water \$1.00 /m3 IRR 3.6%

	Year										
	0	1	2	3	4	5	6	7	8	9	10
CAPEX (Investment)Cost	\$552135										
O&M Cost		\$1686	\$1686	\$1686	\$1686	\$1686	\$1686	\$1686	\$1686	\$1686	\$1686
Energy Cost		\$850	\$850	\$850	\$850	\$850	\$850	\$850	\$850	\$850	\$850
Total Cost	\$552135	\$2537	\$2537	\$2537	\$2537	\$2537	\$2537	\$2537	\$2537	\$2537	\$2537
Total Revenue		\$36500	\$36500	\$36500	\$36500	\$36500	\$36500	\$36500	\$36500	\$36500	\$36500
Net Income each year	-\$552135	\$33963	\$33963	\$33963	\$33963	\$33963	\$33963	\$33963	\$33963	\$33963	\$33963
Net Project Income	\$296,952										
Net ROI	54%										

Year														
11	12	13	14	15	16	17	18	19	20	21	22	23	24	25
\$1686	\$1686	\$1686	\$1686	\$1686	\$1686	\$1686	\$1686	\$1686	\$1686	\$1686	\$1686	\$1686	\$1686	\$1686
\$850	\$850	\$850	\$850	\$850	\$850	\$850	\$850	\$850	\$850	\$850	\$850	\$850	\$850	\$850
\$2537	\$2537	\$2537	\$2537	\$2537	\$2537	\$2537	\$2537	\$2537	\$2537	\$2537	\$2537	\$2537	\$2537	\$2537
\$36500	\$36500	\$36500	\$36500	\$36500	\$36500	\$36500	\$36500	\$36500	\$36500	\$36500	\$36500	\$36500	\$36500	\$36500
\$33963	\$33963	\$33963	\$33963	\$33963	\$33963	\$33963	\$33963	\$33963	\$33963	\$33963	\$33963	\$33963	\$33963	\$33963

Table 19: Table of cash flows for 100 m^3/day SSV project with water price at \$1.50/m^3.

Price of Clean Water \$1.50 /m3 IRR 8.1%

	Year										
	0	1	2	3	4	5	6	7	8	9	10
CAPEX Cost	\$552135										
O&M Cost		\$1686	\$1686	\$1686	\$1686	\$1686	\$1686	\$1686	\$1686	\$1686	\$1686
Energy Cost		\$850	\$850	\$850	\$850	\$850	\$850	\$850	\$850	\$850	\$850
Total Cost	\$552135	\$2537	\$2537	\$2537	\$2537	\$2537	\$2537	\$2537	\$2537	\$2537	\$2537
Total Revenue		\$54750	\$54750	\$54750	\$54750	\$54750	\$54750	\$54750	\$54750	\$54750	\$54750
Net Income each year	-\$552135	\$52213	\$52213	\$52213	\$52213	\$52213	\$52213	\$52213	\$52213	\$52213	\$52213
Net Project Income	\$753,202										
Net ROI	136%										

Year														
11	12	13	14	15	16	17	18	19	20	21	22	23	24	25
$1686	$1686	$1686	$1686	$1686	$1686	$1686	$1686	$1686	$1686	$1686	$1686	$1686	$1686	$1686
$850	$850	$850	$850	$850	$850	$850	$850	$850	$850	$850	$850	$850	$850	$850
$2537	$2537	$2537	$2537	$2537	$2537	$2537	$2537	$2537	$2537	$2537	$2537	$2537	$2537	$2537
$54750	$54750	$54750	$54750	$54750	$54750	$54750	$54750	$54750	$54750	$54750	$54750	$54750	$54750	$54750
$52213	$52213	$52213	$52213	$52213	$52213	$52213	$52213	$52213	$52213	$52213	$52213	$52213	$52213	$52213

Table 20: Table of cash flows for 100 m^3/day SSV project with water price at \$2.00/m^3.

Price of Clean Water $2.00 /m3 IRR 12.0%

	Year										
	0	1	2	3	4	5	6	7	8	9	10
CAPEX Cost	$552135										
O&M Cost		$1686	$1686	$1686	$1686	$1686	$1686	$1686	$1686	$1686	$1686
Energy Cost		$850	$850	$850	$850	$850	$850	$850	$850	$850	$850
Total Cost	$552135	$2537	$2537	$2537	$2537	$2537	$2537	$2537	$2537	$2537	$2537
Total Revenue		$73000	$73000	$73000	$73000	$73000	$73000	$73000	$73000	$73000	$73000
Net Income each year	-$552135	$70463	$70463	$70463	$70463	$70463	$70463	$70463	$70463	$70463	$70463
Net Project Income	$1,209,452										
Net ROI	219%										

Year														
11	12	13	14	15	16	17	18	19	20	21	22	23	24	25
$1686	$1686	$1686	$1686	$1686	$1686	$1686	$1686	$1686	$1686	$1686	$1686	$1686	$1686	$1686
$850	$850	$850	$850	$850	$850	$850	$850	$850	$850	$850	$850	$850	$850	$850
$2537	$2537	$2537	$2537	$2537	$2537	$2537	$2537	$2537	$2537	$2537	$2537	$2537	$2537	$2537
$73000	$73000	$73000	$73000	$73000	$73000	$73000	$73000	$73000	$73000	$73000	$73000	$73000	$73000	$73000
$70463	$70463	$70463	$70463	$70463	$70463	$70463	$70463	$70463	$70463	$70463	$70463	$70463	$70463	$70463

Table 21: Table of cash flows for 100 m^3/day SSV project with water price at \$3.00/m^3.

Price of Clean Water \$3.00 /m3 IRR 19.1%

	Year										
	0	1	2	3	4	5	6	7	8	9	10
CAPEX Cost	\$552135										
O&M Cost		\$1686	\$1686	\$1686	\$1686	\$1686	\$1686	\$1686	\$1686	\$1686	\$1686
Energy Cost		\$850	\$850	\$850	\$850	\$850	\$850	\$850	\$850	\$850	\$850
Total Cost	\$552135	\$2537	\$2537	\$2537	\$2537	\$2537	\$2537	\$2537	\$2537	\$2537	\$2537
Total Revenue		\$109500	\$109500	\$109500	\$109500	\$109500	\$109500	\$109500	\$109500	\$109500	\$109500
Net Income each year	-\$552135	\$106963	\$106963	\$106963	\$106963	\$106963	\$106963	\$106963	\$106963	\$106963	\$106963
Net Project Income	\$2,121,952										
Net ROI	384%										

Year														
11	12	13	14	15	16	17	18	19	20	21	22	23	24	25
\$1686	\$1686	\$1686	\$1686	\$1686	\$1686	\$1686	\$1686	\$1686	\$1686	\$1686	\$1686	\$1686	\$1686	\$1686
\$850	\$850	\$850	\$850	\$850	\$850	\$850	\$850	\$850	\$850	\$850	\$850	\$850	\$850	\$850
\$2537	\$2537	\$2537	\$2537	\$2537	\$2537	\$2537	\$2537	\$2537	\$2537	\$2537	\$2537	\$2537	\$2537	\$2537
\$109500	\$109500	\$109500	\$109500	\$109500	\$109500	\$109500	\$109500	\$109500	\$109500	\$109500	\$109500	\$109500	\$109500	\$109500
\$106963	\$106963	\$106963	\$106963	\$106963	\$106963	\$106963	\$106963	\$106963	\$106963	\$106963	\$106963	\$106963	\$106963	\$106963

Table 22: Table of cash flows for 100 m^3/day SSV project with water price at \$4.00/m^3.

Price of Clean Water \$4.00 /m3 IRR 25.9%

	Year										
	0	1	2	3	4	5	6	7	8	9	10
CAPEX Cost	\$552135										
O&M Cost		\$1686	\$1686	\$1686	\$1686	\$1686	\$1686	\$1686	\$1686	\$1686	\$1686
Energy Cost		\$850	\$850	\$850	\$850	\$850	\$850	\$850	\$850	\$850	\$850
Total Cost	\$552135	\$2537	\$2537	\$2537	\$2537	\$2537	\$2537	\$2537	\$2537	\$2537	\$2537
Total Revenue		\$146000	\$146000	\$146000	\$146000	\$146000	\$146000	\$146000	\$146000	\$146000	\$146000
Net Income each year	-\$552135	\$143463	\$143463	\$143463	\$143463	\$143463	\$143463	\$143463	\$143463	\$143463	\$143463
Net Project Income	\$3,034,452										
Net ROI	550%										

Year														
11	12	13	14	15	16	17	18	19	20	21	22	23	24	25
$1686	$1686	$1686	$1686	$1686	$1686	$1686	$1686	$1686	$1686	$1686	$1686	$1686	$1686	$1686
$850	$850	$850	$850	$850	$850	$850	$850	$850	$850	$850	$850	$850	$850	$850
$2537	$2537	$2537	$2537	$2537	$2537	$2537	$2537	$2537	$2537	$2537	$2537	$2537	$2537	$2537
$146000	$146000	$146000	$146000	$146000	$146000	$146000	$146000	$146000	$146000	$146000	$146000	$146000	$146000	$146000
$143463	$143463	$143463	$143463	$143463	$143463	$143463	$143463	$143463	$143463	$143463	$143463	$143463	$143463	$143463

Table 23: Table of cash flows for 100 m^3/day SSV project with water price at \$5.00/m^3.

Price of Clean Water $5.00 /m3 IRR 32.6%

	Year										
	0	1	2	3	4	5	6	7	8	9	10
CAPEX Cost	$552135										
O&M Cost		$1686	$1686	$1686	$1686	$1686	$1686	$1686	$1686	$1686	$1686
Energy Cost		$850	$850	$850	$850	$850	$850	$850	$850	$850	$850
Total Cost	$552135	$2537	$2537	$2537	$2537	$2537	$2537	$2537	$2537	$2537	$2537
Total Revenue		$182500	$182500	$182500	$182500	$182500	$182500	$182500	$182500	$182500	$182500
Net Income each year	-$552135	$179963	$179963	$179963	$179963	$179963	$179963	$179963	$179963	$179963	$179963
Net Project Income	$3946952										
Net ROI	715%										

Year														
11	12	13	14	15	16	17	18	19	20	21	22	23	24	25
$1686	$1686	$1686	$1686	$1686	$1686	$1686	$1686	$1686	$1686	$1686	$1686	$1686	$1686	$1686
$850	$850	$850	$850	$850	$850	$850	$850	$850	$850	$850	$850	$850	$850	$850
$2537	$2537	$2537	$2537	$2537	$2537	$2537	$2537	$2537	$2537	$2537	$2537	$2537	$2537	$2537
$182500	$182500	$182500	$182500	$182500	$182500	$182500	$182500	$182500	$182500	$182500	$182500	$182500	$182500	$182500
$179963	$179963	$179963	$179963	$179963	$179963	$179963	$179963	$179963	$179963	$179963	$179963	$179963	$179963	$179963

ASSOCIATE
Capital Projects & Infrastructure
Advisory Services
PricewaterhouseCoopers LLP
Philadelphia, PA
732.570.2552 mobile

EMAIL ADDRESS
Brandon.Proetto@pwc.com

EDUCATION
Rutgers University
B.S., Mechanical Engineering (2015)

Old Dominion University
M.S. Mechanical Engineering (2018)

EMPLOYMENT HISTORY
Jan. 2018 - present
PricewaterhouseCoopers, LLP
Experienced Associate, Capital Projects & Infrastructure

Oct 2017- Jan 2018
Consolidated Edison
Associate Engineer, Transmission Planning

Nov. 2015 – Oct. 2017
Dominion Energy
Engineer, Electric Transmission

Brandon's CV

Brandon Proetto is an Associate in PwC's Capital Projects and Infrastructure (CP&I) practice based in the Greater Philadelphia market. The CP&I practice provides specialized consulting services to private and public clients, both in the US as well as globally, who are undertaking large scale programs and portfolios related to capital assets.

Previously, Mr. Proetto worked as an Engineer in the Power and Utilities industry for Dominion Energy and Con Edison. At Dominion Energy, he gained extensive experience in work and asset management in Electric Transmission. He also participated in engineering design change packages and capital projects at an 1800MW Nuclear facility. With on-site experience at Surry Nuclear Power Station, Brandon has demonstrated a strong operational acumen in the Nuclear industry. At Con Edison, Brandon helped operate a compliance program for the Transmission Planning department.

Mr. Proetto is finishing a M.S. degree in Mechanical Engineering at Old Dominion University. His research is in the water desalination industry, and he has a thorough knowledge of thermal desalination technologies (MSF, MED, and VC). The topic of his thesis is a Thermo-Economic analysis of a novel thermal desalination technology.

Selected Project Experience

I. Power and Utilities

Dominion Energy

Capital Equipment Upgrades
Assisted with the replacement of eight high-voltage power transformers at a nuclear power facility. Facilitated meetings with multiple crafts to enhance transparency and adhere to project schedule. Coordinated procedure development and equipment testing prior to startup. Communicated with Electric Transmission and Nuclear Operations organizations to ensure both organizational and plant standards were met.

Work and Asset Management
Employed SAP, Maximo, and P6 Primavera to manage the daily work orders and maintenance activities at a nuclear facility and within a substation service territory. Represented the Control Operations department at POD and other scheduling meetings to establish weekly schedules and plant probabilistic risk assessment (PRA). Analyzed and

trended operating conditions of power transformers, circuit breakers, current and voltage transformers, disconnect switches, and other Electric Transmission assets to predict potential failures and abide with NRC & INPO regulations.

Root Cause Analysis & Design Change Packages
Led a team on a Root Cause Analysis (RCA) and developed a new transformer maintenance strategy. Produced Design Change Packages (DCP) for the replacement of a GSU Transformer bushing turret and upgrade of six transformer multi-gas analyzers. Developed budget, project scope, and schedule for design changes and presented work plan to station management.

Con Edison

NERC Compliance Program
Developed work plans with subject matter experts to remain in compliance with the United State NERC Standards and prevent fines up to $1,000,000 per day per violation. Researched new requirements to provide Con Edison feedback and insight to regulators. Helped maintained NERC compliance information database for internal and external audits.

Nuclear Power Plant Construction Project

Risk Management Oversight Program
Implementing a Risk Management Program for the oversight organization of a $15 billion dollar nuclear power plant construction project. Used industry expertise and PwC Project Governance Framework to develop a Risk Register, Risk Breakdown Structure, and Risk Reporting Criteria to manage project cost recovery and facilitate transparency to stakeholders.

General Rate Case for Power and Gas Utility

Gas Distribution Rate Case Support
Supporting the production of Client's Gas Distribution General Rate Case. Reconciling and analyzing data from multiple sources for continuity and accuracy. Developing work-papers to support the year-by-year cost changes, unit costs, unit volumes, and total costs for each Capital and Expense cost category.